

The Design and Development of the Electro-optic Hybrid System for Measuring Atmospheric Turbulence Under Low SNR Conditions

Chunyan Zhou

M.S. Electrical Engineering, Oregon Graduate Institute of Science & Technology, 1994

M.S. Optics, Nankai University, P.R.China, 1988

B.S. Physics, Nankai University, P. R. China, 1985

A dissertation submitted to the faculty of the
Oregon Graduate Institute of Science & Technology
in partial fulfillment of the
requirements for the degree of Doctor of Philosophy
in
Electrical Engineering
January, 1996

The dissertation "The Design and Development of the Electro-optic Hybrid System for Measuring Atmospheric Turbulence Under Low SNR Conditions" by Chunyan Zhou has been examined and approved by the following examination committee:

J. Fred Holmes, Professor and Thesis Advisor

V. S. Rao Gudimetla, Assistant Professor

Anthony E. Bell, Associate Professor

M. A. K. Khalil, Professor,
Department of Physics, Portland State University

DEDICATION

To

My Parents and Grandparents

ACKNOWLEDGEMENTS

I wish to express my sincere thanks to my advisor, Dr. J. Fred Holmes, for his guidance, instruction, and encouragement during this research. I am also very grateful to my thesis examination committee members, Dr. V. S. Rao Gudimentla, Dr. Anthony Bell, and Dr. M.A.K. Khalil, for reviewing my dissertation and providing many valuable suggestions. Furthermore, I particularly wish to thank Senior Engineer, John Hunt, for his skillful technical support in the design and development of the electronic circuits. Moreover, I would like to thank Doug Davis and the other staff members in the machine shop for the instruction required to build the mechanical parts of my experimental system; I really enjoyed working in the machine shop. My thanks also go to my fellow students Dr. Badih Rask and Dr. Feng Chen for their help and friendship during my stay at OGI. I would also like to thank the students, staff, and faculty members of the EEAP department for making OGI such a wonderful research environment. Finally, I would like to thank my parents and grandparents for their love and encouragement and my husband, Yongyan Wang, for his enormous help in conducting the field experiments and in writing this Ph.D. dissertation.

TABLE OF CONTENTS

DEDICATION	iii
ACKNOWLEDGEMENTS	iv
TABLE OF CONTENTS	v
LIST OF FIGURES	iix
LIST OF TABLES	x
ABSTRACT.....	xi
CHAPTER 1: Introduction	1
1.1 Overview of atmospheric turbulence measurement methods	2
1.1.1 Temperature sensor method.....	2
1.1.2 Sodar method	3
1.1.3 Radar method	5
1.1.4 Optical remote sensing method.....	6
1.2 OGI Atmospheric Turbulence Research	8
CHAPTER 2: Background.....	11
2.1 Introduction	11
2.2 Characterization and representation of the atmospheric turbulence	11
2.2.1 Refractive index structure function $D_n(r)$	12
2.2.2 Refractive index structure constant C_n^2	13
2.2.3 Variance of log amplitude function σ_χ^2	14
2.3 Laser propagation in atmosphere	15
2.3.1 Beam wander	15
2.3.2 Beam intensity fluctuations (scintillations)	16
2.3.3 Turbulence-induced beam spreading	18
2.4 Pseudo-Random Code (PRC) sequence	20
2.4.1 The PRC primitive polynomial	20
2.4.2 PRC properties	21
2.4.3 The comparison of the PRC-decoding methods	24
2.5 Fiber optics.....	26
2.5.1 Fiber characteristics	27
2.5.2 Fiber types.....	28
2.5.3 Fundamental fiber-optic system design	30
2.5.4 Light source selection	30
2.5.5 Optical fiber selection	31
2.5.6 Optical detector selection.....	32
CHAPTER 3: Theory.....	35
3.1 Introduction	35
3.2 Problem formulation and analysis.....	37
3.2.1 Laser propagation in the atmosphere	37
3.2.2 Optical processing and optical spatial filtering.....	40
3.2.3 Signal processing	47
3.3 Numerical experiments and results	50
3.3.1 The effects of the optical spatial filter	50
3.3.2 The effect of the filter size, u_0	53
3.3.3 The effect of the target distance, z_0	56
3.3.4 The effect of the laser beam size a_0	58
3.3.5 The effect of the wavelength, λ	60
CHAPTER 4: Experimental System.....	62

4.1 Introduction	62
4.2 Transmitting subsystem	62
4.2.1 Laser source and laser controller	64
4.2.2 PRC Generators	66
4.2.3 511 PRC generator	66
4.2.4 The Modified Wavetek PRC generator	68
4.2.5 Fiber-optical transmitter system	69
4.2.6 Shutter	70
4.3 Receiving subsystem	71
4.3.1 Telescope	72
4.3.2 Fiber-optic receiver	72
4.3.3 Field-of-View (FOV)	73
4.3.4 Optical spatial filter	74
4.3.5 Photodetectors and Wavelength Filters	76
4.4 Data processing subsystem	78
4.4.1 Analog circuit	78
4.4.2 A/D board	79
4.4.3 Computer software processing	80
4.5 Calibrating subsystem	81
CHAPTER 5: Experimental Results	82
5.1 Introduction	82
5.2 Range resolution	82
5.2.1 Single-hard-target range resolution	83
5.2.2 Multiple-screen-targets range resolution	85
5.3 Turbulence Strength Measurements	89
5.3.1 Turbulence measurement in cases of high SNR	89
5.3.2 Turbulence measurements in the cases of low SNR	91
5.4 Target speckle image reduction	94
CHAPTER 6: Summary and Conclusion	95
REFERENCES	97
Appendix A	103
A.1 Intensity distribution	103
Appendix B	109
B.1 The schematic diagrams of electric circuits	109
B.1.1 Schematic of the 511 PRC generator	110
B.1.2 Schematic of the auxiliary circuit of Wavetek PRC generator	111
B.1.3 Schematic of the shutter control circuit	112
B.1.4 Schematic of the PMT circuit	113
B.1.5 Schematic of the analog circuit	114
Appendix C	115
C.1 Programs	115
C.1.1 The program for range finding (prctds3.for)	115
C.1.1.1 Main Program	115
C.1.1.2 prctds3.par	121
C.1.2 The program of calibrating two channels (calib.for)	122
C.1.2.1 main program	122
C.1.2.2 calib.par	126
C.1.3 The program of recording two channel data (records4.for)	126

C.1.3.1 main program	126
C.1.3.2 records4.par	133
C.1.4 Subroutines	133
C.1.4.1 highv.for	133
C.1.4.2 adin.for	134
C.1.4.3 seedat.for	136
C.1.4.4 set.for	137
C.1.4.5 plot.for	139
C.1.4.6 takead.for	140
C.1.4.7 fft.for	142
C.1.5 The PRC delay time versus digital code number for 511-PRC generator	143
C.1.6 Program for the data processing (p4.c)	144
C.1.7 Program for numerical simulation (intensity.f)	149
Appendix D	153
D.1 Experimental procedure	153
VITA	156

LIST OF FIGURES

Figure 2-1: Laser beam is deflected by turbulence cells that are larger than the beam diameter	16
Figure 2-2: Strong turbulence leads to the internal breaking up of the focused laser beam into smaller, individual patches [Weichel, 1990a].....	17
Figure 2-3: (a) Feedback shift register corresponding to x^4+x+1 , and (b) the shift register specifies a recurrence relation.....	21
Figure 2-4: Correlation function of $PRC(t)* PRC'(t+\tau)$, with pulse width T.....	23
Figure 2-5: Fiber structure	27
Figure 2-6: The digital BL (bandwidth-length) system design grid (described as: region and optical source/fiber pair). I: SLED (Surface-emitting LED) with step-index multimode fiber; II: LED or laser diode with step-index or graded-index multimode fiber; III: laser diode or ELED (Edge-emitting LED) with step-index multimode fiber; IV: laser diode or ELED with graded-index multimode fiber; V: laser diode with graded-index multimode fiber; VI: laser diode with single-mode fiber; VII: laser diode with step-index multimode fiber [Sunak, 1990].	33
Figure 3-1: System diagram of the proposed experimental system.....	36
Figure 3-2: Laser beam propagation in the atmosphere.....	37
Figure 3-3: Optical Processing.....	40
Figure 3-4: Optical spatial filter.....	46
Figure 3-5: Signal Processing	47
Figure 3-6: The normalized intensities versus the turbulence strength. $I_0(t_0)$ is the received intensity without the optical spatial filter, while $I_f(t_0)$ is the received intensity with the optical spatial filter (simulation results).....	52
Figure 3-7: The effect of filter size on the turbulence strength measurement (simulation results).....	54
Figure 3-8: The effect of the target distance on the turbulence strength measurement (simulation results)	57
Figure 3-9: The effect of the laser beam size on the turbulence strength measurement (simulation results)	59
Figure 3-10: The effect of the laser wavelength on the turbulence strength measurement. (simulation results).	61
Figure 4-1: The experimental system diagram.	63
Figure 4-2: The transmitting subsystem.	64
Figure 4-3: The receiving subsystem	71
Figure 4-4: Field of view of the system	73
Figure 4-5: The calibrating subsystem.....	81
Figure 5-1: The single-hard-target range resolution result, laser intensity in channel 1 and channel 2 (11/23/93) (a) Scotch light hard target, (b) Sand-blasted aluminium hard target.....	84

Figure 5-2: Experiment results for screen target range resolving (2/2/95) data set 1	87
Figure 5-3: Experiment results for screen target range resolving (2/2/95) data set 2.....	88
Figure 5-4: Turbulence measurement under high SNR situations. Solid line is the theoretical curve, dos are the experimental results (9/7/94)	90
Figure 5-5: Turbulence measurement under low SNR situations. Solid line is the theoretical curve, dos are the experimental results.....	92
Figure 5-6: Modified receiver system. The de-magnification lens L_4 is inserted between telescope and the receiving fiber.....	94
Figure B-1: The schematic of the 511 PRC generator	110
Figure B-2: The schematic of the auxiliary circuit of Wavetek PRC generator	111
Figure B-3: The schematic of the shutter control circuit	112
Figure B-4: The schematic of the Photomultiplier Tube circuit	113
Figure B-5: The schematic of the analog circuit.....	114

LIST OF TABLES

Table 3-1: The simulation parameters for intensity versus turbulence strength.	51
Table 3-2: Simulation conditions for the effect of the filter size.	55
Table 3-3: Simulation conditions for the effect of the target distance.	56
Table 3-4: Simulation conditions for the effect of laser beam size.....	58
Table 3-5: Simulation conditions for effect of the laser wavelength.	60
Table 4-1: TOLD9150 specifications.	65
Table 4-2: TOLD9150 peak wavelength versus temperature	66
Table 4-3: The characteristics of R446 NOTE: ENI refers to the amount of input light in Watts to produce a SNR of unity in the output of a PMT.....	76

ABSTRACT

The Design and Development of the Electro-optic Hybrid System for Measuring Atmospheric Turbulence Under Low SNR Conditions

Chunyan Zhou

Oregon Graduate Institute of Science & Technology, 1996

Supervising Professor: Dr. J. Fred Holmes

A major problem in atmospheric optics applications is optical-system-performance degradation caused by atmospheric turbulence. Obviously, accurate estimation of the turbulence level along the propagation path plays an important role in the prediction and improvement of atmospheric optical system performance. The objectives of our research are the following: (1) Developing an optical spatial filtering method to measure the strength of the turbulence; (2) Designing and developing an electro-optical system to measure the turbulence profile based on the method developed; (3) Applying the resultant electro-optical system to measure the turbulence strength in a low signal-to-noise ratio environment.

Even though a variety of turbulence measurement techniques have been developed, scientists are still seeking more effective methods which can measure the turbulence profile conveniently and accurately. In this project, we develop a new single-ended atmospheric-turbulence remote-sensing method. The first key technique of this method is the optical spatial filtering technique. By blocking the target-induced speckle field, the high-pass optical spatial-filter extracts the turbulence-induced part of the reflected signals from the received laser intensities. As a result, we can use the received signals to estimate the turbulence strength along the laser propagation path. The second key technique is the pseudo-random-code (PRC) modulation method, where transmitted laser signals are mod-

ulated by the PRC and the received backscattered signals are demodulated by cross-correlation with the delayed PRC signal. This technique is essential to accomplish range-resolved turbulence detection under low SNR conditions. By coding and decoding the laser signal, the technique can estimate the range-resolved turbulence strength. Additionally, the PRC technique is capable of suppressing the background signal level in the detected signals by increasing the PRC code length. Therefore, the method is superior to the conventional turbulence measurement method in terms of range-resolved turbulence detection and low SNR signal measurement.

In this research, we theoretically analyze the proposed method and practically establish the experimental system. The theoretical analysis shows that the filtered laser intensity can be related with the turbulence strength within certain limits of turbulence level. This linear-dynamic range is determined by the spatial filter size, the laser beam size, and the laser propagation distance. But it is not affected by the coherence of the laser source. The developed experimental system is an electro-optic hybrid turbulence detecting system, which consists of an optical subsystem, an electrical subsystem, a fiber-optical subsystem, and a computer control subsystem. Because the compact experimental system is highly stable and fully automated, it can achieve reliable real-time turbulence detection. The system has made range resolve measurements of the backscattered intensity and measured the turbulence strength under both high and low SNR conditions. Experimental results in both range resolution and turbulence measurement verify that the developed method and the experimental system can successfully detect the strength of turbulence under low SNR conditions.

CHAPTER 1

Introduction

A major problem in atmospheric optics application is the optical-system-performance degradation caused by atmospheric turbulence. The atmospheric turbulence, resulting from air temperature fluctuations, creates spatial and temporal variations of the refractive index. When a laser beam propagates in a turbulent medium, degradations of the beam behavior, such as phase distortion, intensity fluctuations (scintillations), and random changes in the beam direction (beam wander), will occur. Obviously, accurate estimation of the turbulence level along the propagation path plays an important role in the prediction and improvement of atmospheric optical system performance. Even though a variety of turbulence measurement techniques have been developed, scientists are still seeking effective methods which can measure the turbulence profile conveniently and accurately.

The objectives of our research are the followings: (1) proposing an optical spatial filtering method to measure the strength of the turbulence; (2) designing and developing an electro-optical system to measure the turbulence profile based on the method developed; (3) applying the resultant electro-optical system to measure the turbulence strength in a low signal-to-noise ratio environment.

Before discussing the principles, configuration, and results of this research in detail, it is necessary to review the development and techniques of current atmospheric turbulence detection systems.

1.1 Overview of atmospheric turbulence measurement methods

Many approaches have been implemented to measure the strength of the atmospheric turbulence. By convention, the strength of turbulence is characterized by the structure constant of the refractive-index fluctuations, C_n^2 [Tatarskii, 1961a] (detail definition of C_n^2 is in section 2.2.2 on page 13). The available turbulence measurement methods can be categorized as a temperature sensor method, an acoustic sounder method (Sodar), a Radar method, and an optical remote sensing method.

1.1.1 Temperature sensor method

The temperature sensor method is an in-situ measuring method. It determines C_n^2 by using a single or an array of small fast thermometers to acquire the temperature spatial fluctuation (C_T^2), which is defined as

$$C_T^2 = \langle [T(\mathbf{r}_1 + \mathbf{r}) - T(\mathbf{r}_1)]^2 \rangle \cdot |\mathbf{r}|^{-\frac{2}{3}} \quad (1.1)$$

where T represents the temperature, \mathbf{r}_1 and $\mathbf{r}_1 + \mathbf{r}$ are the locations where the temperature data are monitored. Because air temperature fluctuation results in atmospheric turbulence by changing the spatial variation of the atmospheric density, the strength of turbulence C_n^2 is proportional to the temperature structure parameter C_T^2 . Consequently, the strength of

the turbulence can be measured by observing the in-situ temperature fluctuation C_T^2 .

Typically, these temperature sensors are fine-wire, platinum or tungsten probes. One or more of these probe pairs are separated horizontally, so that the temperature difference of these sensor pair represents the value of C_T^2 . Also, C_T^2 can be measured by a single sensor [Walters, 1995], where a higher-order structure function was used to extract C_n^2 profiles from a vertical sequence of temperature data collected by a single probe on a meteorological balloon. Furthermore, temperature probes are mounted on different objects to measure C_n^2 at different spacial locations. For example, the measurement of local C_n^2 profile requires the sensor to be mounted on a tower [Gossard, et. al, 1985]. Moreover, the detection of a high altitude C_n^2 profile requires the sensor to be mounted on aircraft [Lawrence, 1970], [Ochs, 1970], or balloon borne [Bufton, 1972], [Azouit, 1980], [Beland, 1993], [Walters, 1995].

Although a temperature sensor method gives the exact temperature variation information at a certain altitude, it lacks spatial coverage and temporal continuity. In addition, because of the expense and difficulty of launching balloons and aircraft, this method has been used infrequently.

1.1.2 Sodar method

The Sodar (sound detection and ranging) is a ground-based remote sensing method for detecting the vertical profiles of wind and turbulence from near ground up to several hundred meters. Its principle is based on the fact that C_n^2 of the acoustic wave is closely related to sound speed variation and air temperature fluctuation. When short pulses of acoustic waves are emitted as a collimated beam into the atmosphere, a small fraction of the transmitted energy is backscattered by the irregularity in the atmospheric

velocity and temperature. Since the reflected acoustic power can be used to measure the C_T^2 profile, the Sodar method is effective in determining the turbulence profile in the acoustic wave propagation and reflection path [Little, 1969].

The theory and experiment of Sodar have been investigated by many scientists [Gilman, 1946], [Little, 1969], [McAllister, 1968], [Brown 1978],[Gossard, 1985], [Vogt, 1995]. For example, Beran et al [1973], used an acoustic sounder to quantitatively measure the C_T^2 at a height of about 100 m. Later, Fukushima et al.[1975] used the same method to measure acoustic C_T^2 profiles to a height of about 1 km, but no in-situ instrumentation was used. Shortly after the preceding work, Asimakopoulis et al. [1976] reported the first good agreement between acoustic measurement results and in situ temperature sensor values. Up to now, the research on Sodar is still a very active field relating to atmospheric turbulence profile probing.

Compared with the temperature sensor method, the Sodar method has many advantages. Not only it is mobile and easy to install, but also it can operate unattended for a long period of time with low cost. In addition, the Sodar method is better than the Radar method in lower atmosphere detection, because the interaction of sound waves with the lower atmosphere is much stronger than for most parts of the electromagnetic spectrum. Hence, a Sodar provides the most complete picture of the C_n^2 spatial structure in the planetary boundary layer of the earth (roughly the lower 1 km of the atmosphere) [Clifford, 1978a].

The Sodar technique, however, has a number of serious limitations. First of all, because of the strong atmospheric absorption of acoustic energy, the effective range of the method is within several hundred meters. Secondly, the method can only measure the vertical profiles of turbulence. The reason for this limitation is that ground reflections can

enter through antenna side lobes and mask the weak atmospheric signal, unless the propagation direction is nearly vertical. Finally, the Sodar method is hindered by other limitations such as volume averaging, spatial and temporal separation of sampling volume, and slow propagation of sound. These drawbacks limit the Sodar method's applications.

1.1.3 Radar method

Similar to the Sodar method, the Radar measurement method uses the reflective wave signal to detect the turbulence profile. Their major difference is that the Radar method uses a radio wave, while the Sodar method employs an acoustic wave. Since the fluctuation of the radio wave reflective index is dominated by atmospheric temperature and humidity fluctuations, C_T^2 can be evaluated by the reflected radio wave, when the humidity profile is known.

The Radar method was first used to identify strong atmospheric turbulent layers in the 1960's [Atlas, 1966], [Lane, 1967], [Hardy, 1969]. One of the earliest studies used the Radar method to measure C_n^2 vertical profiles [Kropfli et al., 1968]. The results verified the relationship between radar reflectiveness and C_n^2 in the atmospheric. Since then, numerous similar radar methods have been proposed to determine the atmospheric C_n^2 profile [VanZandt, 1978], [Gage, 1978], [Chadwick, 1980], [Balsley, 1981], [Good, 1982] and [Gossard, 1984].

The major advantage of the Radar technique is its long detecting range. Because radio wave absorption by the atmosphere is much smaller than for an acoustic wave, the radio wave's travel distance and the radar sensor's response distance are much longer than those of acoustic sensors. Consequently, the Radar method is able to measure atmospheric turbulence up to 20 km altitude. However, the radar receiver has the same ground clutter

problem as the acoustic sensors. Thus, they can only determine the turbulence vertical profile. Another drawback of the Radar method is that both turbulence strength and humidity affects the strength of the reflective radar wave. Therefore, the Radar method requires the measurement of the humidity vertical profile. Both the vertical limitation and the inconvenience make the radar technique less attractive.

1.1.4 Optical remote sensing method

Most of the optical-turbulence-measurement methods are line-of-sight methods, where the light source and the light receiver are on the opposite ends of the light propagation path. Because the scintillation at the receiver is determined by the turbulence along the propagation path, the turbulence profile can be identified by the scintillation at the receiver. The optical remote sensing method is more powerful than the Sodar and the Radar methods in its capability for measuring both vertical and horizontal turbulence strength. However, as a powerful laser source is seldom available, the detecting range of the optical method is shorter than the detecting range of the Sodar and Radar methods, when a laser is the optical source. Another drawback is that the vertical C_n^2 profile has poor spatial resolution when star light is used as the optical source (stellar scintillation) [Hanson, et.al, 1994], because only the receiving signal can be modulated.

One optical method relies on a spatial filtering technique [Lee, 1974]. This method uses an optical filter, which consists of clear stripes alternating with opaque strips, to spatially modulate the receiving apertures and sometimes the transmitting apertures as well. When the transmitter source is a natural source, such as the sun, or the stars, they can not be modulated by a spatial filter. On the other hand, when the transmitter source is an artificial source, like a laser, they can be modulated. One function of the spatial filter tech-

nique is to provide a spatial resolution along the propagation path. Another function of the filter technique is to detect wind speed and turbulence strength simultaneously. In summary, the spatial filtering technique is very effective in probing the wind speed and turbulence strength in the line-of-sight approaches.

The optical spatial filter technique at first used stellar scintillations to measure atmospheric turbulence. The reason is that the twinkling of stars and the motion of stellar images produce information about the turbulence strength and the wind speed in the upper atmosphere [Mikesell, 1951], [Protheroe, 1964]. The earliest work in C_n^2 probing is that of Townsend's [Townsend et al., 1965], who used spatially filtered star scintillations to infer the velocity and temperature profile of a 10 km turbulence layer. Later a number of theoretical studies and experiments were reported [Peskov, 1968], [Fried 1969], [Strohbehm 1970], [Shen 1970], [Vernin 1973], [Ochs, 1976], [Rocca, 1974], and [Clifford, 1987b].

The application of the spatial filter technique to measure horizontal path turbulence profiles was originally proposed by Lee [Lee, 1974]. The method spatially filtered the optical transmitter and receiver to measure the cross-wind velocity and the strength of refractive turbulence in the propagation path. Its greatest advantage is the high horizontal resolution. Following Lee's pioneer work, scientists continued to improve the spatial filtering method to get better spatial resolution [Wang, 1974]. For example, Churnside et al [1988] improved the turbulence measurement spatial resolution by applying both a spatial and a temporal filter to a receiver, and a spatial filter to an incoherent optical source. Recently, an interesting report by Hanson et al. [1994] used the unfiltered light source and a double filtered receiver to measure the refractive turbulence strength. This system has the advantage of being able to use a natural light source, such as the sun or a planet, to gain a high detecting spatial resolution.

The above discussed methods are line-of-sight methods. They require the source and detector to be separated by the propagation path. However, this condition does not prevail in most of the field measurements, where it is impossible to put a source or a detector at opposite ends of the path. Hence, it is necessary to put a light source and a receiver at the same end. The relevant research has been conducted by the Oregon Graduate Institute research group. Their approach and experiment results are discussed below.

1.2 OGI Atmospheric Turbulence Research

Since the mid 1970's, the Oregon Graduate Institute of Science and Technology's (OGI) laser remote sensing research group has carried out original research in the statistical properties of a laser beam propagating in the atmosphere [Lee, et.al., 1976], [Holmes, et.al., 1980], [Holmes, et.al, 1987], [Draper, et.al, 1989], [Holmes, 1991], [Gudimetla, et. al, 1992], [Holmes and Rask, 1995]. In the mid eighties, Dr. J. Fred Holmes proposed a single-ended optical system that employed an optical spatial filter technique to scale the path-averaged-strength of atmospheric turbulence. Following this idea, the method was perfected by the work of Libo Sun [1988] and Don Martens [1991]. The early stage of this research concentrated on the statistical effects of a high-pass optical spatial filter on the received laser intensity for both the line-of-sight and the single-ended systems [Sun 1988]. Following the theory, the research group also developed an optical system to evaluate the turbulence strength through the mean received beam intensity. Both the theoretical analysis and the experimental results show that the log scale of the mean-output-intensity is linearly related to the log scale of the path-integrated-turbulence within certain turbulence levels. Therefore, in the linear response range, the turbulence strength can be scaled by the normalized receiving laser intensity. In addition, the experimental results

also illustrate that the optical spatial filter method works effectively in both line-of-sight and single-ended systems.

Later, the research group continued to make progress in measuring the turbulence strength under the condition of low signal-to-noise ratio (SNR) [Martens, 1991]. As a first improvement, the laser source of a single-ended optical-spatial-filter system is modulated by a pseudo-random code (PRC) sequence. The second improvement is in the data processing, where the received signal is cross-correlated with a circularly-shifted pseudo-random code. By modifying both the laser source modulation and receiving subsystems, the new system is able to achieve the theory-predicted linear relationship between the received laser intensity and the atmospheric turbulence strength under poor SNR conditions.

The previous approaches on the turbulence measurement have several limitations. First, the methods can not measure the turbulence range profile. Second, the approaches have a slow PRC demodulated process. Therefore, they can not realize real-time detection. Finally, the methods are very sensitive to the alignments of the transmitting and receiving system. Since the transmitter and receiver are not on the same optical axis, it is difficult to obtain reliable experimental results.

In this dissertation, we propose a new single-ended turbulence detection system to measure turbulence range profiles under low SNR conditions. This thesis is divided into six chapters. The first chapter reviews the turbulence detection methods and compares their advantages and shortcomings concisely. The second chapter presents the theoretical background of the atmospheric turbulence characterization, the phenomena regarding the laser propagation in turbulence media, characteristics and functions of the PRC sequence, and the fundamental concepts used in the fiber-optic system design. Chapter 3 formulates

the relationship between the received laser intensity and the turbulence variations. It also discusses the principals used for designing the experimental system. Chapter 4 describes in detail about each sub-system of the developed experimental system. Chapter 5 describes and discusses the experimental results in terms of range finding and turbulence measurement in both high and low SNR. Chapter 6 summarizes the entire thesis research and derives the conclusions from the research.

CHAPTER 2

Background

2.1 Introduction

This chapter presents the theoretical background related to this dissertation in four sections. The first section describes the theory related with the atmospheric turbulence characteristics and their representation methods. The second section discusses the three fundamental phenomena regarding laser beam propagation in atmospheric turbulence. In the third section, we introduce the characteristics of the pseudo-random-code (PRC) sequence and emphasize the advantages of PRC coding technique in measuring low SNR signal. Finally, the fourth section provides the fundamental knowledge used in the fiber-optic system design. Clearly, the above four sections serves as the theoretical basis of this dissertation.

2.2 Characterization and representation of the atmospheric turbulence

Atmospheric turbulence refers to the fluctuations of the temperature which result in the fluctuations of the refractive index in the atmosphere. The variation of the refractive index will affect the performance of laser beam propagation in a turbulence medium.

Even before the first working laser was announced in 1960, much of the necessary theoretical work and some of the experimental work regarding wave propagation in a random medium had already been done, primarily in Russia. The two pioneering monographs in this field by Chernov [1960] and Tatarskii [1961b] were both published in Russia before 1960 and translated in the United States in 1960 and 1961. Since then, many theoretical and experimental works have been implemented in the understanding and utilization of the atmospheric turbulence.

The atmospheric turbulence characterization can be both described theoretically and experimentally. They are introduced below.

2.2.1 Refractive index structure function $D_n(\mathbf{r})$

Because atmospheric turbulence is a random process, a statistical quantity, $D_n(\mathbf{r})$, called the refractive index structure function, describes the spatial variation level of the refractive index from point \mathbf{r}_2 ($\mathbf{r}_2 = \mathbf{r}_1 + \mathbf{r}$) to point \mathbf{r}_1 . The definition of $D_n(\mathbf{r})$ is given by

$$D_n(r) = \langle [n(\mathbf{r}_2) - n(\mathbf{r}_1)]^2 \rangle \quad (2-1)$$

In the definition formulation (see equation 2-1), n is the atmospheric refractive index, which is a function of optical wavelength λ (in μm), atmospheric pressure P (in millibar), and atmospheric temperature T (in Kelvin). Their relationship is shown in equation 2-2.

$$n = 1 + 77.6 \times 10^{-6} \left(1 + 7.52 \times 10^{-3} \lambda^{-2} \right) (P/T) \quad (2-2)$$

Because the atmospheric pressure variations are relatively small and rapidly dispersed, the reflective index is little affected by atmospheric pressure. On the contrary, the solar heating of the earth's surface and wind shear create strong temperature variation. Therefore, the atmospheric index of refraction is primarily due to atmospheric temperature fluctuations. As a result, the refractive index structure function, $D_n(r)$, is mainly related to the atmospheric temperature variation.

2.2.2 Refractive index structure constant C_n^2

It was pointed out by Tatarskii [1961c] that $D_n(r)$ can be determined by the refractive index structure constant C_n^2 and the space displacement vector \mathbf{r} between points \mathbf{r}_1 and \mathbf{r}_2 by equation 2-3, in the Kolmogorov's refractive index spectral density model.

$$D_n(r) = C_n^2 r^{\frac{2}{3}} \quad l_0 \ll r \ll L_0$$

where $r = |\mathbf{r}_2 - \mathbf{r}_1|$ (2-3)

where l_0 is the inner scale of the turbulence and L_0 is the outer scale of turbulence. Equation 2-3 shows that $D_n(r)$ is only associated with the distance between the two interested points and is not related with the observation location.

It should be noted that the structure constant C_n^2 is not really a constant, but a function of both time and space. It is a coefficient to describe the strength of the refractive index turbulence. Obviously, in order to determine its value, we must carefully consider the experimental conditions and the appropriate averaging time.

2.2.3 Variance of log amplitude function σ_χ^2

The variance of the log-amplitude of the transmitting wave, denoted by σ_χ^2 , can be used to scale the turbulence strength at weak turbulence conditions, where small perturbation theory is used to describe the field of the optical wave. The log-amplitude argument χ is defined as [Tatarskii, 1961]

$$\chi = \ln\left(\frac{A}{A_0}\right) \equiv \frac{A_1}{A_0} \quad (2-4)$$

where A is the wave amplitude from a point source, A_0 is the unperturbed amplitude and A_1 is the first order small perturbational amplitude. If the turbulence inner size (l_0) is much shorter than the Fresnel zone scale size ($\sqrt{\lambda L}$), σ_χ^2 is directly associated with the wave propagation length (L) and refractive index constant (C_n^2), as shown in equation 2-5.

$$\sigma_\chi^2 \propto C_n^2 k^{\frac{7}{6}} L^{\frac{11}{6}} \quad (2-5)$$

The validation of the above formula will break down for long paths and strong turbulence, because higher order terms in the scattered field will take effect.

From the above discussion, we can get the following conclusions: 1) $D_n(r)$ is the general definition of spatial refractive index fluctuation. 2) C_n^2 is an index of turbulence strength, which is only determined by the scale of turbulence and not related with any other factors. 3) σ_χ^2 is a practical turbulence strength index. Even though it is a function of wave length (λ), wave propagation path length (L), and structure constant C_n^2 , it can be measured directly in the experiment by evaluating the variance of the wave amplitude.

4) the σ_χ^2 is proportional to C_n^2 when λ and L are constant. Therefore, they are interchangeable as measures of optical turbulence. For the simplicity reason, we use σ_χ^2 to represent the turbulence strength in our experiment.

2.3 Laser propagation in atmosphere

When a laser beam passes through air, the random fluctuations in the air temperature produce small refractive index inhomogeneities that effect the beam in the following different ways: beam wander, intensity scintillation, and beam spread. Consider, for example, an initially well-defined phase front propagating through a region of atmospheric turbulence. Because of random fluctuations in phase velocity, the initially well defined phase front will become distorted. This alters and redirects the flow of laser energy in the medium. As the distorted phase front propagates through the atmosphere, the direction and intensity of the beam randomly change. The random change in direction is called beam wander, and the intensity fluctuation is called scintillation. The beam is also found to be larger in size than the dimensions predicted by diffraction theory and this phenomena is called the “beam spread”.

2.3.1 Beam wander

The “beam wander”, also called “spot dancing”, describes the rapid displacement of the beam's spot on a target with distance L from the laser source. This effect is due to the interaction of the laser beam with the turbulent cells which have larger scale sizes than the beam diameter as shown in Figure 2-1. The beam wander parameter (σ_r^2) can be determined by C_n^2 , the beam spot size (w), and L as shown in equation 2-6 [Chiba, 1971].

$$\sigma_r^2 = 1.90 C_n^2 (2w)^{-1/3} L^3 \quad (2-6)$$

Beam wander has been measured under various conditions of transmitter configurations and turbulence strengths. The results show that beam wander is nearly independent of wavelength and very sensitive to the variations of both C_n^2 and L [Weichel, 1990a]. For example, for a path length of approximately 1km, the standard deviation σ_r^2 may vary from 0.5 mm (weak turbulence) to 30 mm (strong turbulence) for a 6 cm diameter beam. Obviously, beam wander becomes a major problem when a laser beam must remain on a specific target-point for a certain period of time.

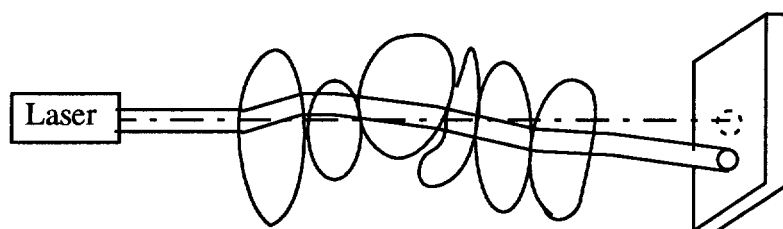


Figure 2-1: Laser beam is deflected by turbulence cells that are larger than the beam diameter

2.3.2 Beam intensity fluctuations (scintillations)

Beam Intensity fluctuations are primarily produced by turbulent cells that are smaller than the beam diameter. The movement of small index-of-refraction inhomogeneities through the path of a beam causes random deflection and interference between different portions of the wave-front, which can lead to an internal breaking up of the beam spot into small speckles. Figure 2-2 shows a typical instantaneous intensity distribution of a focused laser beam [Dunphy, 1974]. The dominant size of the speckle is approximately $\sqrt{\lambda L}$ [Weichel, 1990a], where L is the distance from the laser to the observation target.

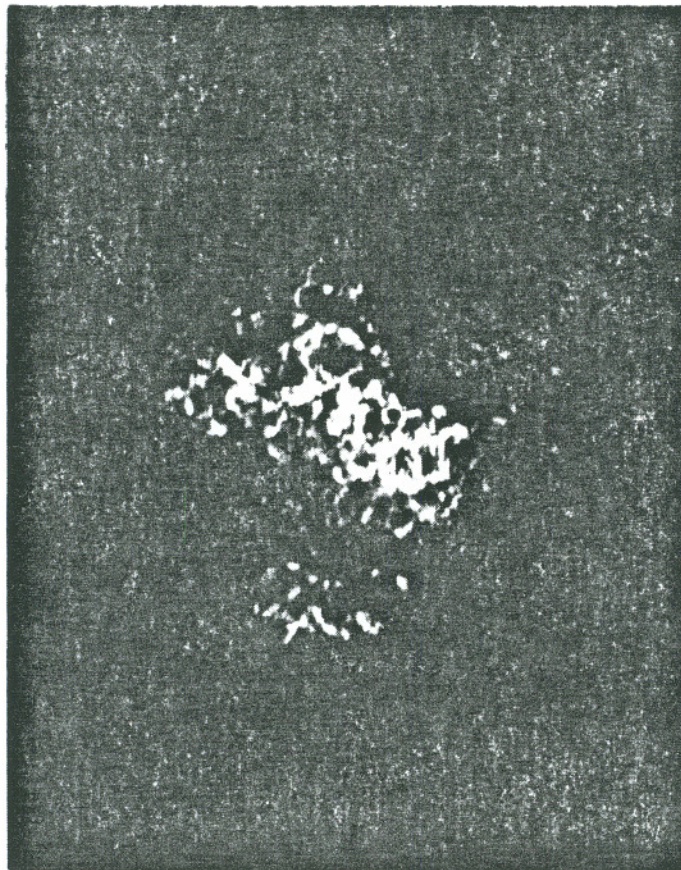


Figure 2-2: Strong turbulence leads to the internal breaking up of the focused laser beam into smaller, individual patches [Weichel, 1990a]

Because of the constantly changing pattern, a small detector placed in the beam will measure intensity fluctuations or scintillation. The frequency of the intensity fluctuation recorded at a fixed point within the beam usually varies between 1 Hz and several kHz [Weichel, 1990a].

In the single-ended detection scheme, beam intensity fluctuation are also caused by the interference of the beam scattered from a rough diffuse target. The rough surface of the target is a collection of independent scatterers that create an optical path difference greater than the wavelength of the incident light to form a speckle field. Therefore, the received intensity fluctuations in the single-ended detection scheme are caused both by the scattering from the diffusion target and small turbulent cells in the atmosphere.

2.3.3 Turbulence-induced beam spreading

In addition to the internal breaking up discussed in the previous section, the beam will also spread in size beyond the dimension predicted from diffraction theory. This effect is called beam spread. Sometimes, it is also referred as beam breathing.

The spot size increase due to the atmospheric turbulence is significant. According to the diffraction theory, a focussed beam from a uniformly illuminated circular aperture of diameter d produces a radiation pattern in the focal plane whose diameter is $D = \lambda f/d$, where f is the focal length of the optical system and λ is the wavelength of the beam. The presence of atmospheric turbulence, however, prevents us from achieving diffraction-limited focal spot sizes. In practice, the observed spot sizes are often twice as large as the spot sizes predicted by diffraction-limited focal spot sizes [Weichel 1990b]

In the far field, the turbulence-induced beam spread has been shown by Yura [1971] to be

$$a_t \approx 2L / (k\rho_0)$$

$$\text{and } \rho_0 = \left(0.545k^2 C_n^2 L \right)^{-3/5} \quad (2-7)$$

where L is the propagation path length, a_t is the beam radius where the relative mean irradiance is decayed to its $1/e$ value, and ρ_0 is a measure of the lateral coherence length of a spherical wave propagating through a homogeneous turbulent medium. The expression for ρ_0 in equation 2-7 is valid only in the range of $z_c \ll L \ll z_i$ [Lutomirski, 1971], where

$$z_c = \left[0.4k^2 C_n^2 \left(\frac{L_0}{2\pi} \right)^{5/3} \right]^{-1} \quad \text{and} \quad z_i = \left[0.4k^2 C_n^2 l_0^{5/3} \right]^{-1} \quad (2-8)$$

The range z_c is the distance from which the average field is decayed by e^{-1} , and z_i is the distance where the transverse coherence length of the field equals the inner scale of turbulence (l_0). L_0 is the outer scale length of turbulence. According to Equation 2-7, the turbulence-induced beam spread a_t is wavelength dependent (see Equation 2-9)

$$a_t = 2.01 \lambda^{-1/5} C_n^{6/5} L^{8/5} \quad (2-9)$$

Equation 2-9 shows that the dependence of turbulence-induced beam spread on wavelength is small, being proportional to $\lambda^{-1/5}$. This is an important result because it implies an optimum wavelength for propagation in a turbulent atmosphere for a given aperture diameter, since beam spread due to diffraction is proportional to the wavelength.

2.4 Pseudo-Random Code (PRC) sequence

The Pseudo-Random Code (PRC) modulation technique has been widely used in the telecommunication industry to execute range finding, scrambling, fault detection, synchronization, etc. [MacWilliams and Sloane, 1976]. PRC sequences (which are also called pseudo-noise(PN) sequences, maximal-length shift-register sequences, or m-sequence) are combinations of certain binary sequences with length L , where $L = 2^m - 1$ and m is a positive integer referred to the degree of the constructive polynomial. In our research, PRC modulation is used to accomplish range finding.

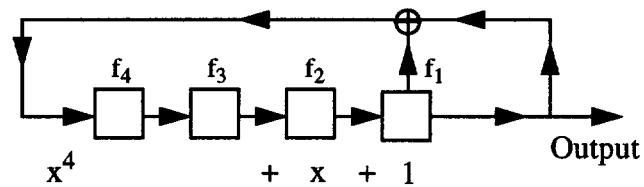
2.4.1 The PRC primitive polynomial

A primitive polynomial $h(x)$ of degree m is a fundamental structure of PRC codes. For example, when the degree of the primitive polynomial m equals 4, $h(x) = x^4 + x + 1$ [MacWilliams and Sloane, 1976], where $h(x)$ specifies the feedback shift register as illustrated in figure 2-3.

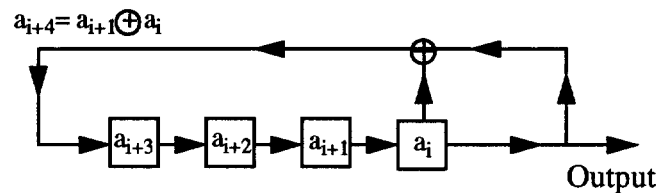
In figure 2-3, $f_1, f_2, f_3,$ and f_4 are the four registers with values of either 0 or 1. Suppose the registers contain $a_{i+3}, a_{i+2}, a_{i+1}, a_i$ at time i , when time increases one step to $i+1$, the value of the four register right shift by one to the next register. Then, the value of a_i at time step i is the output signal. The new register values are given by

$$a_{i+4} = a_{i+1} \oplus a_i, \quad a_{i+3}, a_{i+2}, a_{i+1}$$

Therefore, the PRC output signal is the sequence of $a_i, a_{i+1}, a_{i+2},$ etc. Note that “ \oplus ” represents the Exclusive-OR operation.



(a)



(b)

Figure 2-3: (a) Feedback shift register corresponding to x^4+x+1 , and (b) the shift register specifies a recurrence relation

The PRC sequence is a periodic signal. Since each of the m registers contains 0 or 1, there are 2^m possible states for the shift register. However, the all zero state has no practical meaning. Therefore, the maximum code period length L is 2^m-1 .

2.4.2 PRC properties

The most important property of the PRC is that its periodic auto-correlation function has no side lobes. Therefore, the PRC is capable of range resolution.

Consider a PRC sequence containing only 0 and 1. We can generate a new series of PRC (PRC') by replacing 0's by -1's and keeping 1 unchanged, i.e.,

$$PRC'(t) = 2 \times PRC(t) - 1.$$

The normalized auto-correlation function, $\rho(n)$, of PRC' is represented by

$$\begin{aligned} \rho(0) &= 1 & \rho(i) &= -\frac{1}{L} \\ \text{for} & & & 1 \leq i \leq L-1 \end{aligned} \tag{2-10}$$

Equation. 2-10 shows that the normalized auto-correlation function has maximum value 1 at zero shift, and $-1/L$ elsewhere. As the code length gets longer, the value of $-1/L$ can become very small. This means that the auto-correlation of PRC'(t) has also no practical side lobe. Consequently, the only contribution to the auto-correlation is contained in the main lobe. Therefore, PRC coding technique can be used for range finding with correlation type signal processing.

Consider another situation where the correlation function is between PRC and PRC'. This corresponds to the situation using PRC'(t) to decode the signal modulated by PRC(t). The correlation function of PRC(t) and PRC'(t) equals $(L+1)/2$ for zero time shift. Otherwise, it is zero

$$\begin{aligned} \rho(0) &= \frac{L+1}{2} & \rho(i) &= 0 \\ \text{for} & & & 1 \leq i \leq L-1 \end{aligned} \tag{2-11}$$

Compared with the previous situation where the side lobe is $-1/L$, the side lobe in Equation 2-11 is zero. Obviously, the correlation between PRC(t) and PRC'(t) has smaller range cross-talk than the auto-correlation of PRC'(t) with itself. Therefore, the new coding method is more powerful with short code lengths than the previous coding method. However, the drawback of the laser coding method is that its peak value is about

half of that of the $PRC'(t)$ auto-correlation function. Even though $PRC(t)*PRC'(t)$ coding has a lower peak value, we still choose it in our research because of its side lobe advantages.

In practical applications, we must consider the PRC pulse period, denoted by T . In this situation, equation 2-11 can be modified into equation 2-12. Figure 2-4 illustrates its normalized correlation function.

$$\langle PRC(t) PRC'(t+\tau) \rangle = \begin{cases} 1 - \frac{|\tau|}{T} & \text{for } |\tau| \leq T \\ 0 & \text{elsewhere} \end{cases}$$

(2-12)

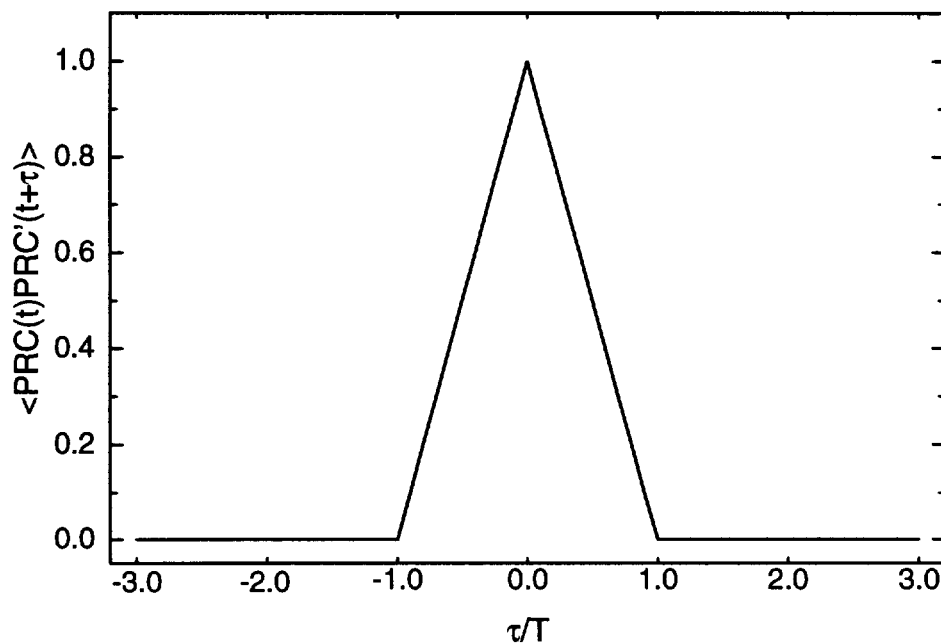


Figure 2-4: Correlation function of $PRC(t)* PRC'(t+\tau)$, with pulse width T .

In Figure 2-4, the x-axis denotes the ratio of time t and pulse width T , the y-axis is the correlation function of $PRC(t)$ and $PRC'(t)$. From Figure 2-4, we can see that the correlation function has a triangular shape with a spread of $\pm T$. Therefore, the range resolution is defined as $2cT$, where c is the speed of light.

2.4.3 The comparison of the PRC-decoding methods

There are two different approaches to decode the PRC modulated signal. One is $PRC' \times PRC$ cross-correlation method. Another is $PRC \times PRC$ cross-correlation method. The former approach can suppress the background signal more than the latter one. This can be proved by comparing the signal and background noise level of the two decoding techniques.

When using $PRC'(t)$ to decode the $PRC(t)$ modulated signal, the received signal is expressed as [Nagasawa, et al., 1990]:

$$y_i = \sum_{j=0}^N P_0 a_{i-j} G_j + P_{bi} ; \quad N \geq L \quad (2-13)$$

In the equation, N is the number of PRC codes used, L stands for the PRC code length, P_0 denotes the transmitted power, a_{i-j} (1, 0) is the Pseudo-Random modulation code corresponding to PRC, P_{bi} represents the background noise power, G_j denotes the response function of the overall system to the signal to the transmitted power, and "i" indicates the number of time steps. Its decoded signal, S_k , can be evaluated by

$$S_k = \sum_{i=0}^{L-1} y_i a'_{i-k} \quad (2-14)$$

where a'_{i-k} (1, -1) is the Pseudo-Random modulation code corresponding to PRC'. Substituting equation 2-13 into equation 2-14, we can obtain the formula of the received decoded signal

$$S_k = P_0 \sum_{j=0}^N \phi_{aa'}(j-k) G_j + \sum_{i=0}^{L-1} a'_{i-k} P_{b_i} \quad (2-15)$$

where $\phi_{aa'}(j-k)$ is the cross-correlation function of a_i and a'_i . Because a_i and b_i are independent signals, and

$$\sum_{i=0}^{L-1} a'_{i-k} = 1 \quad (2-16)$$

the ensemble average of the last term in Equation 2-15 becomes,

$$\left\langle \sum_{i=0}^{L-1} a'_{i-l} b_i \right\rangle = \left\langle \left(\sum_{i=0}^{L-1} a'_{i-l} \right) \right\rangle \langle P_{b_i} \rangle = \langle P_{b_i} \rangle \quad (2-17)$$

where $\langle P_{b_i} \rangle$ is ensemble average of P_{b_i} . By taking the ensemble average of S_k and using equation 2-11 to represent $\phi_{aa'}(j-k)$, the average received signal is given by

$$\langle S_k \rangle \Big|_{prc' \times prc} = \frac{L+1}{2} P_0 G_k + \langle P_{b_i} \rangle \quad (2-18)$$

In Equation 2-18, $P_0 G_k (L+1)/2$ is the signal power and $\langle P_{b_i} \rangle$ is the background noise level.

When using PRC(t) to decode the PRC(t) modulated signal, the summation of the PRC(t) code is given by

$$\sum_{i=0}^{L-1} a_{i-k} = \frac{L+1}{2} \quad (2-19)$$

Following the same procedure as for the PRC' decoding, the expected value of S_k is expressed as

$$\langle S_k \rangle \Big|_{prc \times prc} = \frac{L+1}{2} P_0 G_k + \frac{L+1}{2} \langle P_{bi} \rangle \quad (2-20)$$

In Equation 2-20, the first term is the corresponding signal power. It equals the power of the PRC'(t) decoding case. However, the background signal level increases by a factor of $(L+1)/2$ compared with the background noise of the PRC'(t) decoding approach.

By comparing equation 2-18 and equation 2-20, we see that the background signal level of PRC'xPRC approach is lower than that of PRCxPRC approach. This difference becomes more obvious for larger L . Therefore, we choose the PRC'xPRC decoding approach in our experiment, since we must discriminate between the actual signal and the background. Moreover, when the background signal is strong, we can increase the PRC code length, L , to enhance the signal and increase the ratio of the signal over the background noise.

2.5 Fiber optics

The developments of a small attenuation glass fiber and an efficient semiconductor laser source have dramatically changed optical-communications. In our research, we use a laser diode and an optical fiber to set up a fiber-optical transmitting and receiving system. By using fiber to connect the electro-optic receiver and laser transmitter with the

telescope, the system becomes more flexible. For instance, the telescope can be located outside the lab, while keeping the diode laser and detector inside the lab, where it is easy to keep a stable thermal environment. In the future, our experimental system can be more compact and portable.

2.5.1 Fiber characteristics

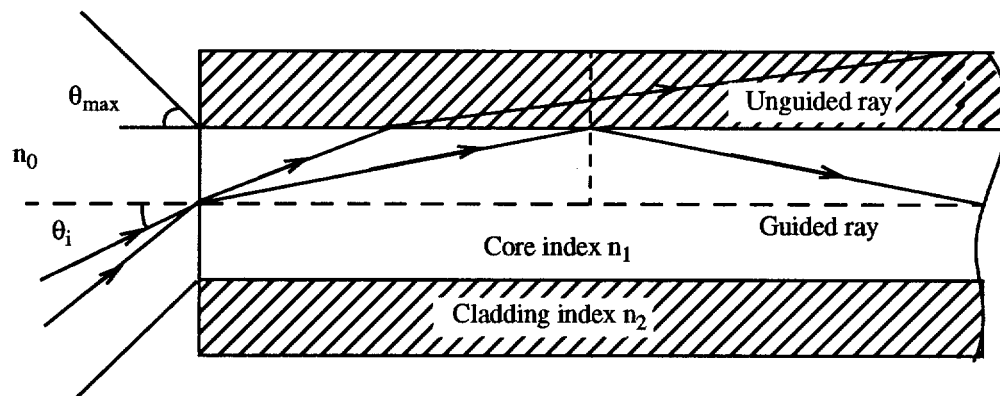


Figure 2-5: Fiber structure

The two important parameters used to describe fiber characteristics are bandwidth-length ($B \cdot L$) product (BL product) and numerical aperture (NA). The BL product describes the fiber's information carrying capacity. B is the transmitting bit rate and L denotes the fiber length between the transmitter and receiver. In practice, the BL product of a fiber-optic system can range from a few megabits per second x kilometers [$(Mb/s) \cdot km$] to many hundreds of gigabits per second x kilometers [$(Gb/s) \cdot km$].

NA depicts the acceptance cone within which all bound rays are contained, defined by the following equation

$$NA = n_0 \sin(\theta_i|_{max}) \quad (2-21)$$

In the equation, n_0 is the air refractive index and θ_i is the angle between the incoming ray and the fiber axis (see Figure 2-5). The $\sin(\theta_i|_{max})$ is determined by the refractive index of fiber core (n_1) and refractive index in the fiber cladding (n_2)

$$\sin(\theta_i|_{max}) = (n_1^2 - n_2^2)^{1/2} \quad (2-22)$$

NA is a convenient measure of the ability of an optical fiber to capture light from the light source. Higher NA implies the fiber can accept light from a wide-angle source, such as a light-emitting diode (LED), with less coupling loss. Generally, a higher NA indicates a higher source-to-fiber coupling efficiency.

2.5.2 Fiber types

Optical fibers are classified into single-mode fiber and multimode fiber, based on the number of optical modes which propagate in the fiber at the wavelength of operation. The concept of optical mode refers to a specific solution of the electromagnetic wave equation that satisfies the appropriate boundary conditions, and has the property that its spatial distribution does not change with propagation [Quinn, 1989]. Practically, the number of modes which can be supported by the fiber depends on the size and dopant level of the fiber.

Single-mode fibers allow only fundamental modes to transmit through the fiber. They have a small core size (typical value $8 \mu m$) and low dopant level (typical value range 0.3 to 0.4 percent index elevation over the cladding index). As a result, higher order

modes cannot meet the boundary condition and become radiative. They will soon be lost through the cladding. The corresponding cut-off wavelength of the single-mode fiber is given by the following equation [Quinn, 1989].

$$\lambda_c = \left(\frac{2\pi a}{2.405} \right) (n_1^2 - n_2^2)^{1/2} \quad (2-23)$$

where a is the core radius, and n_1 and n_2 are the refractive index of the core and cladding, respectively. According to Eq. 2-22, we can choose the proper core size to obtain the required cut-off wavelength. Any wave with λ shorter than λ_c will not be transmitted through the fiber.

Multimode fibers, on the other hand, allow more than one mode to propagate through the fiber at the operating wavelength. In a multimode fiber, the core size (ranging from 35 to 1000 μm), NA (ranging from 0.2 to 0.29) and dopant level are much higher than those of single-mode fibers. Consequently, there are many optical modes which satisfy the boundary condition at the fiber-cladding interface. Therefore, multimode fibers can carry as many as a few hundreds of optical modes simultaneously.

Single-mode and multimode fibers have different applications due to their different characteristics. Single-mode fibers have higher information carrying capacity than multimode fibers because intermodal dispersion is absent [Quinn 1989]. Obviously, when the energy of the injected pulse is transported by a single mode, the pulse broadening caused by the interference of the different transmission modes, which is the primary factor in the bandwidth limit for the multimode fibers, can be negligible. Therefore, single-mode fibers have higher bandwidth and lower attenuation than multimode fibers. However, single-mode fiber require a higher costly light source and more expensive fiber-fiber, light-fiber coupling instrument than multimode fiber. The reason is that single-mode fibers

have small core sizes and multimode fibers have relatively large diameters. In order to reduce the coupling loss due to misalignment, more delicate instruments are needed for single-mode fiber coupling. In addition, the different sizes of single-mode and multimode fibers make the single-mode fiber more difficult to operate. Apparently, single-mode fibers are frequently used in the long BL product situation where high system performance is more important than the economy concern. On the contrary, the multimode fiber is more frequently used in the low BL product situation, where it can reach the application specifications without expensive cost.

2.5.3 Fundamental fiber-optic system design

The fiber-optic system design includes the selection of the light source, fiber, and light detector, according to the system's performance specifications. Practically, the system fundamental performance is represented in terms of the system bit rate (B) and the system fiber length (L). The transmission bit rate B specifies the system frequency response. L depicts the system attenuation limits. Consequently, the light source, fiber, and light detector configurations are designed to match the B and L requirement. Other than B and L criteria, several limiting factors should also be considered in the fiber-optic system design. They include modulation format, system sensitivity (fidelity), cost, reliability, and ability to upgrade.

2.5.4 Light source selection

The selection of a light source depends on the requirement of its output power, source-fiber coupling efficiency, frequency response, and transmission wavelength spectrum. The combination of these factors must meet the system's B and L criteria.

For fiber-optic communication systems, the available light sources are LEDs and laser diodes. Their different characteristics determine their various applications. Compared with LEDs, laser diodes are superior in terms of higher output power, higher source-fiber coupling efficiency, faster rise time, and higher frequency response. On the other hand, the diode laser has a high chip-processing and packaging complexity, higher cost, poorer reliability and sensitivity. Considering the above factors, LEDs are often chosen for lower BL applications, while laser diodes are used to upgrade the system when higher technological performance is demanded and cost factors become less important. For example, a laser diode is the better choice over an LED for launching a light source into a single-mode fiber. The selected laser source of our experimental system is the laser diode. Detail discussions of the selected light source described in Section 4.2.1.

2.5.5 Optical fiber selection

The fiber selection is based on the system requirements and the following fiber features. They are fiber dispersion, source-fiber coupling efficiency, fiber extrinsic losses, ease of installation and operation, cost, and thermal stability. The first step in fiber selection is making a decision on the single-mode fiber or multimode fiber choice, and the second step is choosing the fiber features for the selected type of fiber. As discussed before, multi-mode fibers have a large core size (up to $2000\ \mu\text{m}$), higher Numerical Aperture (NA) (0.2 to 0.29), and lower cost than that of single-mode fibers. Because of the larger core size and higher NA, multi-mode fibers are able to reduce the laser-fiber coupling loss to match broad application requirements. On the contrary, single-mode fibers have better performance than multi-mode fibers in terms of higher information carrying capacity, lower transmission loss, and no modal correlation. Therefore, single-mode fibers are extremely suitable for the high BL product applications, while multimode fibers are better

for low BL product situations. After a single-mode fiber or multimode fiber has been selected, the second step is to choose the fiber with proper features, such as operating wavelength, NA, fiber core size, and attenuation factor. These factors rely on laser-fiber coupling and fiber-fiber coupling considerations.

The following example exemplifies the light source and fiber pair selection in the digital fiber optical system design using the light fiber design grid (see Figure 2-6). In the figure, the fiber link length (L) is divided into eight convenient sections, spanning from 1 m to more than 100 km. Similarly, the system transmission B has been divided from less than 10 kb/s to more than 1 Gb/s. Once the designed system BL product is known, the designer can identify the corresponding range on the BL grid and choose the light source and fiber type referring to the suggestion by the grid. The figure illustrates that multimode fibers are commonly the first choice in the low BL product application. Therefore, in our experimental system, we use a multi-mode fiber. Detailed discussions are presented in Sections 4.2.5 and 4.3.2.

2.5.6 Optical detector selection

The laser detector selection is based on the detector's characteristics, including receiver sensitivity, receiver gain, wavelength responsibility, response speed, and the active detector diameter. Among them, the key parameter is the receiver sensitivity, which determines the minimum incident optical power required at the receiver to satisfy the specified value of bit error rate for digital systems, or SNR for analog systems.

The available fiber-optic detectors are APD (Avalanche photodiode) and PIN photodiodes. APD offers high sensitivity and wide receiving dynamic range through controlling of the avalanche gain. However, it has a temperature sensitive gain and high dark

		L ₁	L ₂	L ₃	L ₄	L ₅	L ₆	L ₇	L ₈
B \ L		1-10m	10-100m	100-1000m	1-3km	3-10km	10-50km	50-100km	>100km
B ₁	<10Kb/s								
B ₂	10-100Kb/s			I				VII	
B ₃	100-1000Kb/s								V
B ₄	1-10Mb/s						V		
B ₅	10-50Mb/s								
B ₆	50-500Mb/s				II				
B ₇	500-1000Mb/s							VI	
B ₈	>1Gb/s	III	IV						

Figure 2-6: The digital BL (bandwidth-length) system design grid (described as: region and optical source/fiber pair). I: SLED (Surface-emitting LED) with step-index multimode fiber; II: LED or laser diode with step-index or graded-index multimode fiber; III: laser diode or ELED (Edge-emitting LED) with step-index multimode fiber; IV: laser diode or ELED with graded-index multimode fiber; V: laser diode with graded-index multimode fiber; VI: laser diode with single-mode fiber; VII: laser diode with step-index multimode fiber [Sunak, 1990].

current and noise at long-wavelengths (1.3-1.55 μm). In addition, it requires a high bias supply voltage and costs more than PIN diodes. On the other hand, PIN photodiodes have lower sensitivity, narrower dynamic range, less thermal sensitive gain, weaker dark current, and lower noise at long wavelengths. Also, they don't need a high bias power supply and are therefore cheaper to operate. Unfortunately, neither the APD or PIN can reach larger than 10^3 gain which is required according to our experimental conditions.

In our experimental system, we use a PMT (Photo Multiplier Tube) as the photo-detector. Even though the PMT is not as compact as both the APD and PIN diodes and requires high voltage power supply (higher than 500 Volts), its gain can reach up to 10^7 to meet the need of weak signal detection. Its performance is discussed in Section 4.3.5.

CHAPTER 3

Theory

3.1 Introduction

Accurate atmospheric turbulence measurements are difficult to accomplish by the conventional line-of-sight method, because it is inconvenient to install a laser source and a detector at opposite ends of the propagation path. A better approach is to use a single-ended detection system, in which the laser source and detector are at the same end of the transmission path. However, in order to obtain single-ended measurements, we face the following three challenges. The first challenge is to detect a poor SNR signal. Since the backscattered signals from most of the natural sources, such as aerosols, are very weak, the low SNR makes the detection very difficult. The second difficulty is to measure the turbulence range resolution along the laser propagation path. The conventional range detecting method, such as the optical-spatial-filtering technique used in the line-of-sight application, becomes ineffective in the signal-ended detection. We must develop a new approach. The third challenge is to separate the target-induced speckle field and the turbulence-induced field. Clearly, the solution to the above challenges depends on a innovative approach.

This dissertation propose a single-ended-turbulence measurement system. Our approach includes: (1) using a pseudo-random-code (PRC) to modulate laser source; (2)

employing an optical high-pass spatial filter to block the target-induced speckle field; and (3) decoding the received laser signals to recover low SNR range bin signals. The system diagram is shown in Figure 3-1.

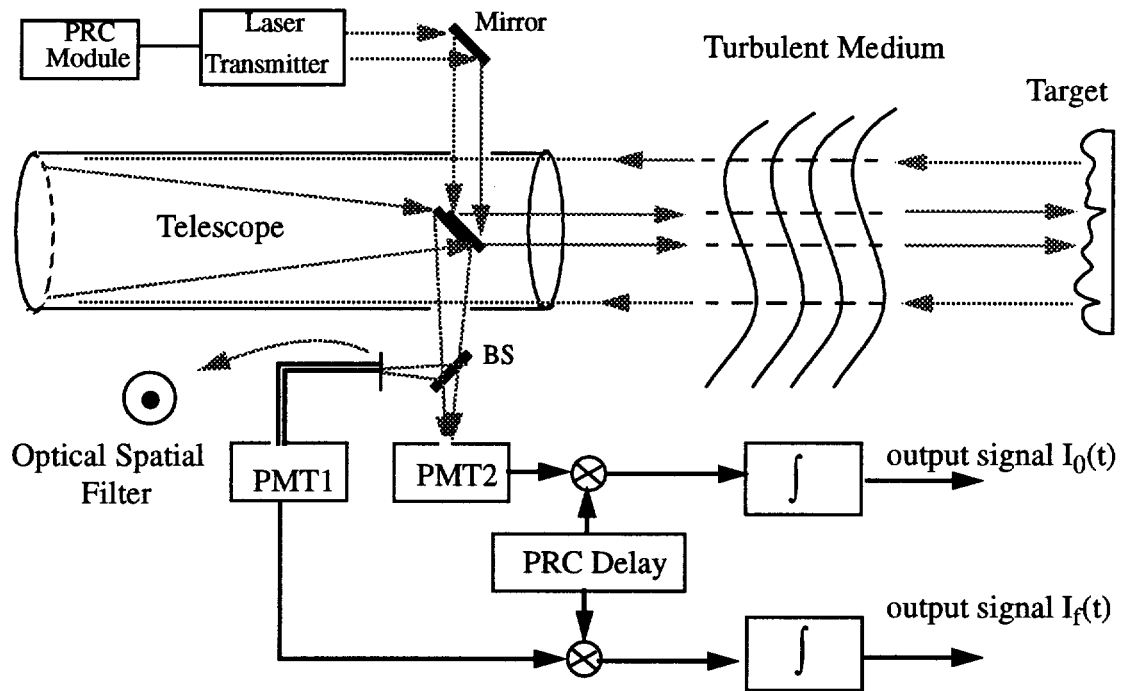


Figure 3-1: System diagram of the proposed experimental system

The figure shows that the PRC-modulated laser beam is first transmitted into the atmosphere. After passing through turbulence, it is backscattered by targets, such as a hard target, a screen target, or aerosols. Then, the backscattered signal is collected by a telescope receiver at the same end as the transmitter. The received laser beam is then divided into two channels (the reflecting channel and the transmitting channel) by a beam splitter (BS). In the reflecting channel, the signal is optically spatial filtered, and then focused onto a photo-multiplier-tube (PMT). In the transmitting channel, the signal is directly focused into a PMT. The output signals from two PMTs are both multiplied by

For a single-ended system, the laser propagation includes the laser beam transmission, the target reflection, and the backscattered laser beam transmission. The conceptual diagram is illustrated in Figure 3-2. In the figure, \mathbf{r} , \mathbf{p} , and \mathbf{q} are the coordinates of the source, target, and receiver respectively. z represents the distance between the source and target.

First, we suppose the transmitting laser is a monochromatic source, with wave-number k . The PRC modulated field distribution $U(\mathbf{r}, t, k)$, at point \mathbf{r} and time t , is calculated as

$$U(\mathbf{r}, t, k) = U_0 \exp\left(-\frac{r^2}{2\alpha_0^2} - \frac{ikr^2}{2F}\right) (PRC(t))^{1/2} \quad (3-1)$$

where U_0 is the transmitting wave amplitude, α_0 denotes the characteristic beam radius, F represents the beam focal length, and $PRC(t)$ ($[0,1]$) is the code modulating function.

The laser transmission follows the extended Huygens-Fresnel principle, due to the fact that the propagation path is much longer than the diameter of the laser source [Lutomirski and Yura 1971], [Yura 1972]. Therefore, the beam field distribution $U(\mathbf{p}, z, t, k)$ at target point \mathbf{p} is formulated as [Holmes et al 1980]

$$U(\mathbf{p}, z, t, k) = \frac{ke^{ikz}}{i(2\pi z)} \int_{s_1} d\mathbf{r} U\left(\mathbf{r}, t - \frac{z}{c}, k\right) \exp\left(\frac{ik|\mathbf{p} - \mathbf{r}|^2}{2z} + \psi_1(\mathbf{p}, \mathbf{r})\right) \quad (3-2)$$

where z is the path length, $\psi_1(\mathbf{p}, \mathbf{r})$ is a complex variable describing the laser beam phase-shift and scattering due to the turbulence when a laser beam travels from source \mathbf{r} to the target point \mathbf{p} , and s_1 is the integration domain which covers the entire laser source area.

The reflected laser field at target point \mathbf{p} is given by $U(\mathbf{p}, z, t, k) g(\mathbf{p}, z)$ where $g(\mathbf{p}, z)$ is the target reflection coefficient. Assuming that the target is a perfect diffuse target with uniform backscattering coefficient, the beams scattered from each target point are not correlated. This property can be represented by the following equation.

$$\langle g(\mathbf{p}_1, z) g^*(\mathbf{p}_2, z) \rangle = \frac{4\pi}{k^2} g^2(z) \delta(\mathbf{p}_1 - \mathbf{p}_2) \quad (3-3)$$

where $\langle \rangle$ denotes an ensemble average over the target, and $g(z)$ is the backscattering coefficient at path length z .

The backscattered laser beam propagation also obeys the Huygens-Fresnel principle. The amplitude distribution, at the receiver point \mathbf{q} , is described by

$$U(\mathbf{q}, z, t, k) = \frac{ke^{ikz}}{i(2\pi z)} \int_{s_2} d\mathbf{p} U\left(\mathbf{p}, z, t - \frac{z}{c}, k\right) g(\mathbf{p}, z) \exp\left(\frac{ik|\mathbf{q} - \mathbf{p}|^2}{2z} + \psi_2(\mathbf{q}, \mathbf{p})\right) \quad (3-4)$$

where $\psi_2(\mathbf{q}, \mathbf{p})$ denotes the reflected laser beam phase-shift and absorption due to the turbulence from the target \mathbf{p} to the receiver \mathbf{q} , and s_2 represents the integration domain of the entire reflecting medium.

Equations 3-2 and 3-4 show that the received laser field, $U(\mathbf{q}, z, t, k)$, is determined by both the laser speckle field and the turbulence-induced field ($\psi_1(\mathbf{p}, \mathbf{r})$ and $\psi_2(\mathbf{q}, \mathbf{p})$). For weak turbulence, the speckle-field signal dominates the receiving signal. Therefore, the weak turbulence signal can not be detected. In order to measure the turbulence strength, we need to remove the speckle field signal by using a high-pass optical spatial filter, as discussed in the next section.

3.2.2 Optical processing and optical spatial filtering

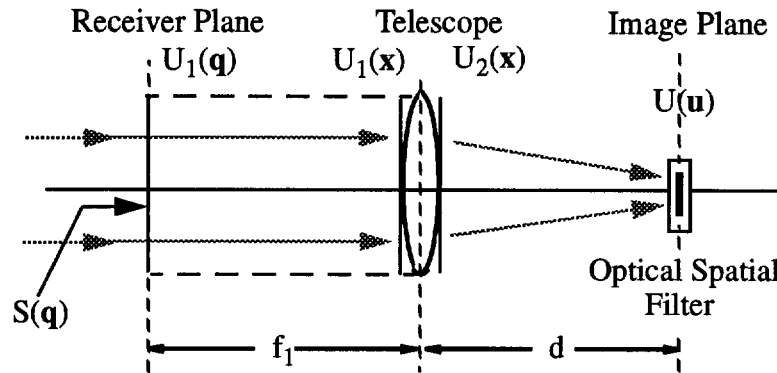


Figure 3-3: Optical Processing

When the backscattered laser signals are received by the telescope, they are first restricted by the telescope aperture. Then they are focussed by the telescope lens. The entire optical system is illustrated in figure 3-3, where $U_1(\mathbf{q})$, $U_1(\mathbf{x})$, $U_2(\mathbf{x})$, and $U(\mathbf{u})$ represent the field distribution at the telescope aperture plane, the front lens plane, the back lens plane, and the image plane respectively. In the figure, f_1 and d denote the telescope focal length and the target image distance respectively. The target image distance, d , can be evaluated by the equation $1/z + 1/d = 1/f_1$. Note that the telescope aperture plane is also the receiving plane defined in Figure 3-2. The optical spatial filtering process blocks the target-induced speckle field by placing a high pass filter at the center of the target image plane (see Figure 3-3). By eliminating the target-induced speckle field, the filtered signal becomes only a function of turbulence-induced fluctuations.

The optical processing and the optical spatial filtering involve the formulation of $U_1(\mathbf{q})$, $U_1(\mathbf{x})$, $U_2(\mathbf{x})$, and $U(\mathbf{u})$. In the receiver plane, the finite extent of the telescope aperture limits the received beam field. Hence, the field distribution is given by

$$U_1(\mathbf{q}) = U(\mathbf{q}, z, t, k) S(\mathbf{q}) \quad (3-5)$$

where $U(\mathbf{q}, z, t, k)$ is the field distribution in equation 3-4, and $S(\mathbf{q})$ is the telescope aperture function given by

$$S(\mathbf{q}) = \exp\left(-\left(\frac{\mathbf{q}}{q_0}\right)^2\right) \quad (3-6)$$

where q_0 is the telescope radius.

In the front plane of the telescope lens, the beam field distribution is the Fresnel diffraction of the laser field at the telescope aperture plane [Goodman, 1968a]. Therefore, the field distribution, $U(\mathbf{x}, z, t, k)$, at location \mathbf{x} , is given by

$$U_1(\mathbf{x}, z, t, k) = \frac{ke^{ikf_1}}{i2\pi f_1} \int d\mathbf{q} S(\mathbf{q}) U\left(\mathbf{q}, z, t - \frac{f_1}{c}, k\right) \exp\left(ik \frac{|\mathbf{x} - \mathbf{q}|^2}{2f_1}\right) \quad (3-7)$$

At the back surface of the telescope the field distribution is expressed as

$$U_2(\mathbf{x}) = U_1(\mathbf{x}, z, t, k) F(\mathbf{x}, k) \quad (3-8)$$

where the converging effect of the telescope lens, $F(\mathbf{x}, k)$, is represented by the quadratic function of a spherical wave [Goodman, 1968b] in the paraxial approximation. The telescope transfer function $F(\mathbf{x}, k)$ is illustrated as

$$F(\mathbf{x}, k) = \exp\left(-\frac{ik}{2f_1} x^2\right) \quad (3-9)$$

At the telescope image plane, the laser field distribution is the Fresnel diffraction of $U_2(\mathbf{x})$.

Hence, the field distribution $U(\mathbf{u}, t, k)$ at image location \mathbf{u} is represented by

$$U(\mathbf{u}, z, t, k) = \frac{ke^{ikd}}{i(2\pi d)} \int d\mathbf{x} F(\mathbf{x}, k) U\left(\mathbf{x}, z, t - \frac{f_1}{c}, k\right) \exp\left(ik \frac{|\mathbf{u} - \mathbf{x}|^2}{2d}\right) \quad (3-10)$$

The above discussion formulates the laser field distribution for optical processing. However, we only measured the laser intensity in this work. Equation 3-11 converts the field distribution $U(\mathbf{u}, z, t, k)$ into the measured intensity distribution $I(\mathbf{u}, z, t, k)$.

$$I(\mathbf{u}, z, t, k) = U(\mathbf{u}, z, t, k) U^*(\mathbf{u}, z, t, k) \quad (3-11)$$

Substituting equations 3-1 to 3-10 into equation 3-11, we obtain the mean intensity $\langle I(\mathbf{u}, z, t, k) \rangle$ as

$$\begin{aligned} \langle I(\mathbf{u}, z, t, k) \rangle &= \left(\frac{k^4}{16\pi^4 z^2 f_1 d} \right)^2 PRC\left(t - \frac{2z + f_1 + d}{c}\right) \int d\mathbf{x}_1 \int d\mathbf{x}_2 \\ &\bullet \exp\left(-\frac{ik}{2f_1} (x_1^2 - x_2^2)\right) \exp\left(i\frac{k}{2f_1} (|\mathbf{x}_1 - \mathbf{q}_1|^2 - |\mathbf{x}_2 - \mathbf{q}_2|^2) + i\frac{k}{2d} (|\mathbf{u} - \mathbf{x}_1|^2 - |\mathbf{u} - \mathbf{x}_2|^2)\right) \\ &\int d\mathbf{q}_1 \int d\mathbf{q}_2 \int d\mathbf{p}_1 \int d\mathbf{p}_2 \int d\mathbf{r}_1 \int d\mathbf{r}_2 \exp\left(-\left(\frac{q_1^2 + q_2^2}{q_0^2}\right)\right) \exp\left(\frac{ik}{2z} (q_1^2 - q_2^2)\right) \\ &\bullet \langle g(\mathbf{p}_1, z) g^*(\mathbf{p}_2, z) \rangle \exp\left(\frac{ik}{z} (p_1^2 - p_2^2)\right) \exp\left(-\frac{ik}{z} (\mathbf{p}_1 \cdot \mathbf{r}_1 + \mathbf{q}_1 \cdot \mathbf{p}_1 - \mathbf{p}_2 \cdot \mathbf{r}_2 - \mathbf{q}_2 \cdot \mathbf{p}_2)\right) \\ &\bullet \langle \exp\left(\Psi_1(\mathbf{p}_1, \mathbf{r}_1) + \Psi_1^*(\mathbf{p}_2, \mathbf{r}_2) + \Psi_2(\mathbf{q}_1, \mathbf{p}_1) + \Psi_2^*(\mathbf{q}_2, \mathbf{p}_2)\right) \rangle \exp\left(-\frac{r_1^2 + r_2^2}{2a_0^2}\right) \\ &\bullet \exp\left(-\frac{ik}{2} \left(\frac{1}{F} - \frac{1}{z}\right) (r_1^2 + r_2^2)\right) \end{aligned} \quad (3-12)$$

At this point, equation 3-12 can be simplified. First we consider the statistics of the turbulence-induced phase term. Assuming the transmitting path and the receiving

path are independent paths and using the property of the diffuse target (see Equation 3-3), the statistical properties of phase can be expressed by

$$\begin{aligned} & \langle \exp(\psi_1(\mathbf{p}_1, \mathbf{r}_1) + \psi_1^*(\mathbf{p}_2, \mathbf{r}_2) + \psi_2(\mathbf{q}_1, \mathbf{p}_1) + \psi_2^*(\mathbf{q}_2, \mathbf{p}_2)) \rangle = \\ & \langle \exp(\psi_1(\mathbf{p}_1, \mathbf{r}_1) + \psi_1^*(\mathbf{p}_1, \mathbf{r}_2) + \psi_2(\mathbf{q}_1, \mathbf{p}_1) + \psi_2^*(\mathbf{q}_2, \mathbf{p}_1)) \rangle = \exp\left(-\left(\frac{r}{\rho_0}\right)^{5/3} - \left(\frac{q}{\rho_0}\right)^{5/3}\right) \\ & \text{with} \quad \rho_0 = \left(0.545625k^2zC_n^2\right)^{-3/5} \end{aligned} \quad (3-13)$$

where ρ_0 is the coherence length of a spherical wave propagating in the random medium, $r = |\mathbf{r}_1 - \mathbf{r}_2|$ and $q = |\mathbf{q}_1 - \mathbf{q}_2|$ [Holmes 1980]. By substituting equations 3-3 and 3-13 into equation 3-12 and carrying out the integration over $\mathbf{x}_1, \mathbf{x}_2$ (see Appendix A), we rewrite equation 3-12 as

$$\begin{aligned} \langle I(\mathbf{u}, z, t, k) \rangle &= \frac{k^6 g^2(z)}{512\pi^6 z^4 f_1^2} PRC\left(t - \frac{2z + f_1 + d}{c}\right) \int d\mathbf{p}_1 \exp\left(-i\frac{k}{z}(\mathbf{p}_1 \cdot (\mathbf{r}_1 - \mathbf{r}_2 + \mathbf{q}_1 - \mathbf{q}_2))\right) \\ & \int d\mathbf{q}_1 \int d\mathbf{q}_2 \int d\mathbf{r}_1 \int d\mathbf{r}_2 \exp\left(-\left(\frac{r}{\rho_0}\right)^{5/3} - \left(\frac{q}{\rho_0}\right)^{5/3}\right) \exp\left(-\frac{r_1^2 + r_2^2}{2a_0^2}\right) \exp\left(-\frac{ik}{2}\left(\frac{1}{F} - \frac{1}{z}\right)(r_1^2 - r_2^2)\right) \\ & \exp\left(-\frac{q_1^2 + q_2^2}{2q_0^2}\right) \exp\left(\frac{ik}{2z}\left(1 + \frac{z}{f_1}\left(1 - \frac{d}{f_1}\right)\right)(q_1^2 - q_2^2)\right) \exp\left(-\frac{ik}{f_1}(\mathbf{q}_1 - \mathbf{q}_2) \cdot \mathbf{u}\right) \end{aligned} \quad (3-14)$$

By making the change of variable,

$$\begin{aligned} \mathbf{r} &= \mathbf{r}_1 - \mathbf{r}_2 & \mathbf{q} &= \mathbf{q}_1 - \mathbf{q}_2 \\ 2\mathbf{R} &= \mathbf{r}_1 + \mathbf{r}_2 & 2\mathbf{Q} &= \mathbf{q}_1 + \mathbf{q}_2 \end{aligned} \quad (3-15)$$

the mean intensity is represented by

$$\begin{aligned}
\langle I(\mathbf{u}, z, t, k) \rangle &= \frac{k^6 g^2(z)}{512\pi^6 z^4 f_1^2} PRC\left(t - \frac{2z + f_1 + d}{c}\right) \int d\mathbf{p}_1 \exp\left(-i\frac{k}{z}(\mathbf{p}_1 \cdot (\mathbf{r} + \mathbf{q}))\right) \\
&\int d\mathbf{q} \int d\mathbf{Q} \int d\mathbf{r} \int d\mathbf{R} \exp\left(-\left(\frac{r}{\rho_0}\right)^{5/3} - \left(\frac{q}{\rho_0}\right)^{5/3}\right) \exp\left(-\frac{R^2 + \frac{1}{4}r^2}{a_0^2}\right) \exp\left(-\frac{ik}{z}\left(1 - \frac{z}{F}\right)(\mathbf{r} \cdot \mathbf{R})\right) \\
&\exp\left(-\frac{2Q^2 + \frac{1}{2}q^2}{q_0^2}\right) \exp\left(\frac{ik}{z}\left(1 + \frac{z}{f_1}\left(1 - \frac{d}{f_1}\right)\right)(\mathbf{Q} \cdot \mathbf{q})\right) \exp\left(-\frac{ik}{f_1}\mathbf{q} \cdot \mathbf{u}\right)
\end{aligned} \tag{3-16}$$

Carrying out the integration of \mathbf{q} , \mathbf{Q} , \mathbf{r} , \mathbf{R} , and \mathbf{p}_1 (see Appendix A), we represent the mean intensity distribution at the image plane as

$$\begin{aligned}
\langle I(\mathbf{u}, z, t, k) \rangle &= \frac{k^5 g^2(z) q_0^2 a_0^2}{128\pi z^3 f_1^2} PRC\left(t - \frac{2z + f_1 + d}{c}\right) \int_0^\infty r dr \exp\left(-2\left(\frac{r}{\rho_0}\right)^{5/3}\right) \\
&\cdot \exp\left(-\frac{r^2}{4}\Delta\right) \exp\left(-\frac{ik}{f_1}ru \cos\theta_{ur}\right)
\end{aligned}$$

where,

$$\Delta = \frac{1}{a_0^2} + \frac{k^2 a_0^2}{z^2} \left(1 - \frac{z}{F}\right)^2 + \frac{2}{q_0^2} + \frac{k^2 q_0^2}{2z^2} \left(1 + \frac{z}{f_1} \left(1 - \frac{d}{f_1}\right)\right)^2 \tag{3-17}$$

Equation 3-18 describes the intensity distribution in the image plane. By integrating $\langle I(\mathbf{u}, z, t, k) \rangle$ over the image plane, we formulate the total averaged intensity $I_0(z, t, k)$ as

$$\begin{aligned}
I_0(z, t, k) &= \int_0^{2\pi} d\theta_u \int_0^u \langle I(u, z, t, k) \rangle du \\
&= \frac{k^5 g^2(z) q_0^2 a_0^2}{64z^3 f_1^2} PRC\left(t - \frac{2z + f_1 + d}{c}\right) \int_0^\infty dr r \exp\left(-2\left(\frac{r}{\rho_0}\right)^{5/3}\right) \int_0^{u_1} du u J_0\left(\frac{k}{f_1} ru\right) \exp\left(-\frac{r^2}{4}\Delta\right) \\
&= PRC\left(t - \frac{2z + f_1 + d}{c}\right) \tilde{I}_0(k, z)
\end{aligned} \tag{3-18}$$

where u_1 is the radius of the receiver fiber and

$$\tilde{I}_0(k, z) = \frac{k^5 g^2(z) q_0^2 a_0^2}{64z^3 f_1^2} \int_0^\infty dr r \exp\left(-2\left(\frac{r}{\rho_0}\right)^{5/3}\right) \int_0^{u_1} du u J_0\left(\frac{k}{f_1} ru\right) \exp\left(-\frac{r^2}{4}\Delta\right) \tag{3-19}$$

Equations 3-18 and 3-19 indicate that the total received intensity $I_0(k, t, z)$ is determined by both the turbulence-induced (ρ_0) and target-induced ($g(z)$) speckle fields. Additionally, the received intensity is dominated by the target-induced speckle field, so that the received intensity does not respond to the variation of the turbulence strength (see Section 3.3.1). As a result, $I_0(k, t, z)$ can not be used to measure turbulence strength.

In order to detect turbulence strength, we need to reduce the target-induced speckle field. This is accomplished by placing a high-pass optical spatial filter at the image plane to block the target-induced speckle field and transmit the turbulence-induced signal (see figure 3-3). The optical spatial filter is modeled by a Gaussian field transfer function in Equation 3-20 and Figure 3-4.

$$F(u) = 1 - \exp\left(-\frac{u^2}{u_0^2}\right) \tag{3-20}$$

where u_0 is the radius of the filter.

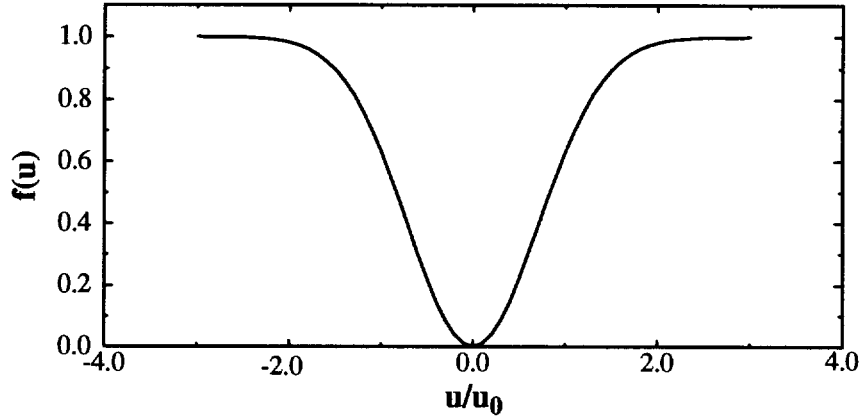


Figure 3-4: Optical spatial filter

In figure 3-4, the x-axis is the ratio of u and u_0 . The y-axis denotes the magnitude of the transfer function $f(u)$. The figure demonstrates that the filter passes high spatial frequency components and blocks the low spatial frequency components. After spatially filtering, the total received intensity $I_f(k, z, t)$ becomes

$$\begin{aligned}
 I_f(k, t, z) &= \int du \left(1 - \exp\left(-\frac{u^2}{u_0^2}\right) \right)^2 \langle I(u, k, t) \rangle \\
 &= \frac{k^5 g^2(z) q_0^2 a_0^2}{64z^3 f_1^2} PRC\left(t - \frac{2z + f_1 + d}{c}\right) \int_0^\infty dr r \exp\left(-2\left(\frac{r}{\rho_0}\right)^{5/3}\right) \exp\left(-\frac{r^2}{4}\Delta\right) \\
 &\quad \cdot \int_0^{u_0} du u \left(1 - \exp\left(-\frac{u^2}{u_0^2}\right) \right)^2 J_0\left(\frac{k}{f_1} ru\right) \\
 &= PRC\left(t - \frac{2z + f_1 + d}{c}\right) \tilde{I}_f(k, z)
 \end{aligned} \tag{3-21}$$

where

$$\begin{aligned} \tilde{I}_f(k, z) = & \frac{k^5 g^2(z) q_0^2 a_0^{2\infty}}{64 z^3 f_1^2} \int_0^\infty dr \, r \exp\left(-2\left(\frac{r}{\rho_0}\right)^{5/3}\right) \exp\left(-\frac{r^2}{4}\Delta\right) \\ & \cdot \int_0^{u_0} du \, u \left(1 - \exp\left(-\frac{u^2}{u_0^2}\right)\right)^2 J_0\left(\frac{k}{f_1} r u\right) \end{aligned} \quad (3-22)$$

Equations 3-18 and 3-21 formulate the received intensities at time t . Equation 3-21 simulates the intensity with the high-pass spatial filtering, while equation 3-18 models the intensity without the spatial filtering. Both received intensities are further decoded through the signal processing.

3.2.3 Signal processing

The signal processing consists of signal detection, signal multiplication, and signal integration. The diagram of the data processing system is shown in figure 3-5.

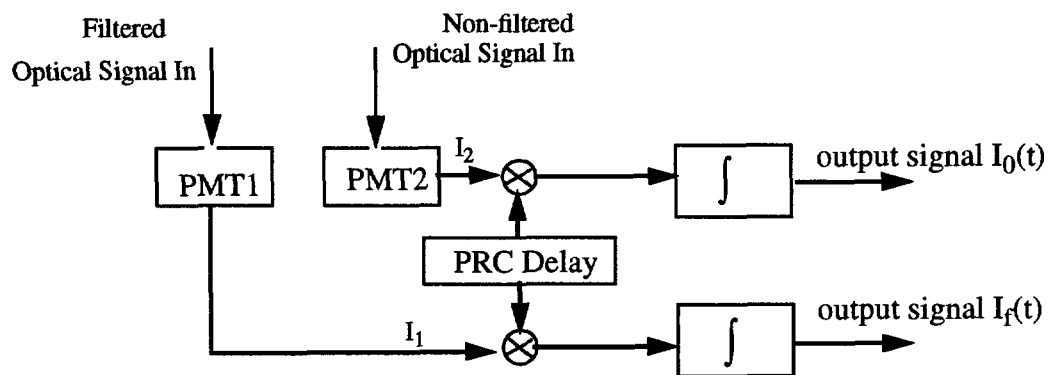


Figure 3-5: Signal Processing

The signal detection is accomplished by two PMTs (PMT1 and PMT2). They detect both the filtered optical signal and the non-filtered optical signal. Later, the two optical signals

are converted to electrical signal I_1 and I_2 .

Along the way, I_1 and I_2 are multiplied by the same PRC delay signal. Then, the multiplied signals are integrated over the PRC code period (T) to recover the range bin signal, which corresponds to the selected delay time t_d . The PRC delay signal is represented by $PRC'(t-t_d)$ in the following equation

$$PRC'(t-t_d) = 2 \times PRC(t-t_d) - 1 \quad (3-23)$$

The processes of the multiplication and integration are formulated by

$$I_{0,f}(t_0, k, z) = \int_{t_0}^{(t_0+T)} dt PRC'(t-t_d) PRC\left(t - \frac{2z+f_1+d}{c}\right) \tilde{I}_{0,f}(k, z) \quad (3-24)$$

where $I_f(t_0, k, z)$ is the received intensity with filtering and $I_0(t_0, k, z)$ is the received intensity without filtering. According to the discussions in Section 2.4.2 and equation 2-12, by assuming $2z + f_1 + d \approx 2z$, equation 3-24 yields

$$I_{0,f}(t_0, k, z) = \begin{cases} \left(1 - \left|t_d - \frac{2z}{c}\right|/T\right) \tilde{I}_{0,f}(k, z) & \left|t_d - \frac{2z}{c}\right| \leq T \\ 0 & \text{elsewhere} \end{cases} \quad (3-25)$$

where c is the speed of light and $t_d \approx 2z_0/c$. Note that z_0 is the path length of the maximum reflection position. Equation 3-25 indicates that the received intensities only respond to the intensities scattered from $z_0 - cT/2 \leq z \leq z_0 + cT/2$ range. Therefore, the processed received intensities can detect the turbulence-strength profile along the laser propagation path.

Until now, the entire theoretical analysis is based on the assumptions of a monochromatic laser source and a single target located at z . In the following equation, we release the above two assumptions to model the total received intensities in response to the reflected polychromatic laser signal from the spatially distributed targets. The total received intensities are given by

$$I_{0,f}(t_0) = \int_{\lambda_1}^{\lambda_2} P(\lambda) d\lambda \left(\int_{\left(z_0 - \frac{cT}{2}\right)}^{\left(z_0 + \frac{cT}{2}\right)} dz \left(1 - \frac{2|z - z_0|}{cT} \right) \tilde{I}_{0,f}(k, z) \right) \quad (3-26)$$

where $P(\lambda)$ is the laser spectrum, and λ_1, λ_2 refer to the lower and upper limits of the laser spectrum.

Equation 3-26 is a four-fold integration. In our experiment, we set up only one target at location z_0 along the propagation path. Accordingly, the path-reflection coefficient becomes

$$g(z) = g_0 \delta(z - z_0) \quad (3-27)$$

Also, we depict the spectrum of the polychromatic laser by the summation of Gaussian functions. Therefore, $P(\lambda)$ is given by

$$P(\lambda) = \sum_{i=1}^n \frac{1}{\sqrt{2\pi}\Delta\lambda} e^{-\frac{(\lambda - \lambda_i)^2}{2(\Delta\lambda)^2}} \quad (3-28)$$

where n is the number of Gaussian functions, λ_i is the i th center wavelength, and $\Delta\lambda$ is the half wavelength bandwidth. Here, we assume wavelength bandwidths of the Gaussian functions are the same. Substituting equations 3-27 and 3-28 into equation 3-26, the total

intensities can be reduced to

$$I_{0,f}(t_0) = \sum_{i=1}^n \int_{(\lambda_i - \Delta\lambda)}^{(\lambda_i + \Delta\lambda)} d\lambda \frac{1}{\sqrt{2\pi\Delta\lambda}} e^{-\frac{(\lambda - \lambda_i)^2}{2(\Delta\lambda)^2}} \tilde{I}_{0,f}(k, z_0) \quad (3-29)$$

Equation 3-29 demonstrates the received laser intensities are a function of the averaged turbulence variation along the laser-propagation path. The intensities are also effected by the optical-system parameters, such as the beam size a_0 , spatial filter size u_0 , wavelength λ , and target distance z_0 . The following section theoretically analyzes the effects of the above parameters on the system performance.

3.3 Numerical experiments and results

The previous section concludes that the relationship between the received laser intensities and the turbulence strength is determined by the system parameters. In order to understand the effects of these system parameters, we design the following numerical experiments. The first experiment investigates the functions of the high-pass-spatial filter. Other experiments explore the effects of the system parameters on the system performance. These parameters include the filter size, u_0 , target distance, z_0 , laser beam size, a_0 , and wavelength, λ . The understanding of these effects is essential to the experimental system design. The simulation program, `intensity.f`, is listed in Appendix C.

3.3.1 The effects of the optical spatial filter

The optical spatial filter blocks the high-spatial-frequency components of the received intensity. In this numerical experiment, we simulate the received intensities with

and without the optical spatial filter, based on equation 3-29. The function of the spatial filter can be justified by comparing the simulation results. The experimental parameters are listed in Table 3-1.

Table 3-1: The simulation parameters for intensity versus turbulence strength.

Characteristic	Symbol	Rating
Laser Center Wavelength (nm)	λ_0	690
Laser Wavelength Bandwidth (nm)	$\Delta\lambda$	0.5
Laser Beam Radius (mm)	a_0	7.0
Optical Spatial Filter Radius (μm)	u_0	170
Target Distance (m)	z_0	240
Telescope Focal Length (m)	f_1	0.91
Telescope Radius (m)	q_0	0.10

The simulation results are shown in figure 3-6. In the figure, the X-axis denotes the turbulence strength in log scale, the Y-axis represents the normalized intensities, where $I_0(t_0)$ and $I_f(t_0)$ are normalized by the maximum value of $I_0(t_0)$. The figure illustrates that the received intensity without filtering, $I_0(t_0)$, does not response to the turbulence variations in the low and medium turbulence levels. This indicates that the received intensity is dominated by the target-induced speckle field. Alternatively, the received intensity with filtering, $I_f(t_0)$, linearly responds to the turbulence variations within most of the turbulence range. This is because the optical filter obstructs the target-induced speckle field. As a result, the turbulence-induced signals control the received intensity. The difference between $I_0(t_0)$ and $I_f(t_0)$ can be further represented by the ratio $I_f(t_0)/I_0(t_0)$. By comparing $I_f(t_0)$ and $I_0(t_0)$, we conclude that (a) both the received

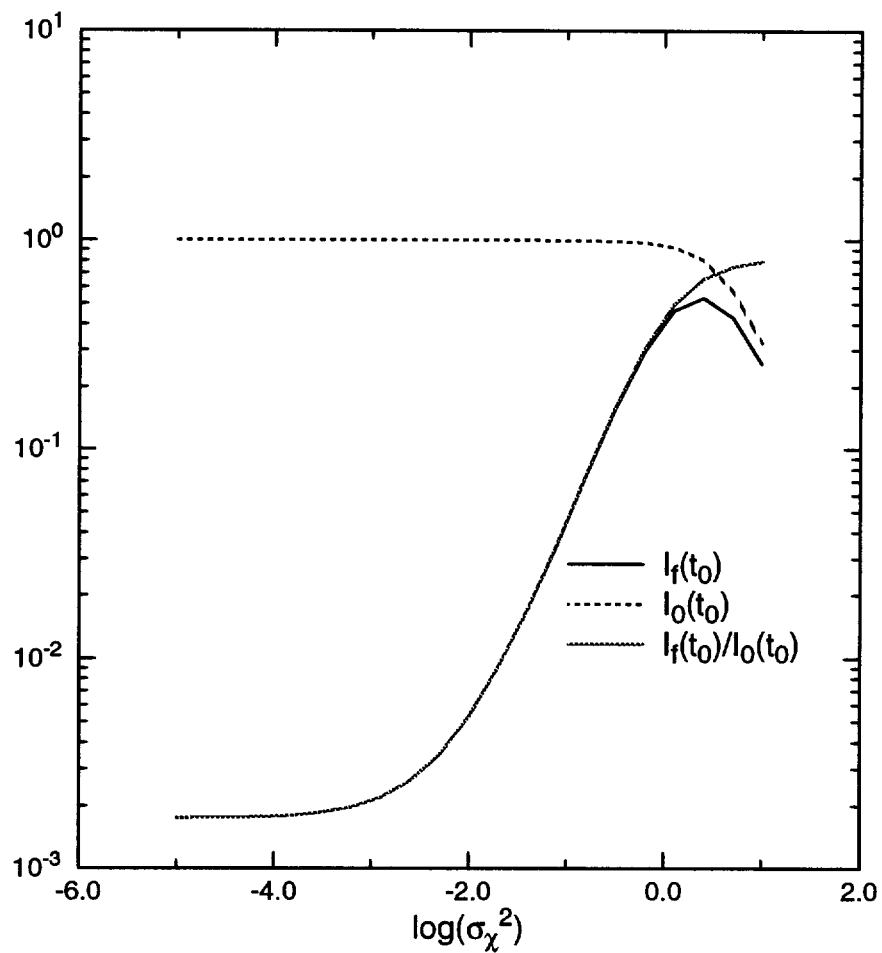


Figure 3-6: The normalized intensities versus the turbulence strength. $I_o(t_0)$ is the received intensity without the optical spatial filter, while $I_f(t_0)$ is the received intensity with the optical spatial filter (simulation results).

intensities respond to the turbulence strength variation under the simulation conditions; (b) $I_f(t_0)$ has a much wider dynamic range than that of $I_0(t_0)$; and (c) $I_f(t_0)/I_0(t_0)$ better represents the relationship between the received intensities and the turbulence variations. In summary, the optical spatial filter is essential to the turbulence measurement. We can not detect turbulence without the high-pass filter.

Note that the above simulation is not valid when $\sigma_\chi^2 > 0.3$. This is due to the fact that the above theoretical analysis fails to account for multiple scattering effects, which can not be neglected in high turbulence levels [Clifford, 1978c]. Therefore, the simulation can not represent the system performance when σ_χ^2 is greater than 0.3.

3.3.2 The effect of the filter size, u_0

The filter size, u_0 , determines the dynamic range by influencing the portion of the blocked speckle field. In the numerical experiment, we simulate the normalized receiving intensity for the different filter sizes. The simulation conditions are shown in Table 3-2.

The simulation results are illustrated in the Figure 3-7, where the x-axis represents the turbulence strength, σ_χ^2 , in log scale, and the y-axis is the normalized mean intensity in log scale, $(\log \langle I_f(t)/I_0(t) \rangle)$. In the figure, three plots correspond to three different filter sizes. Each simulation curve has two flat zones and one linear zone. The first flat zone corresponds to the extremely low turbulence level, where the turbulence-induced beam spreading and beam wander are very weak, so that the spatial filter blocks both the target-induced speckle field and turbulence-induced reflecting field. Therefore, the normalized receiving intensity keeps at a constant low level. In the linear zone, the turbulence strength is in the medium range, where the turbulence-induced beam spreading and beam wander determine the received intensity. Hence, the turbulence strength in log scale is lin-

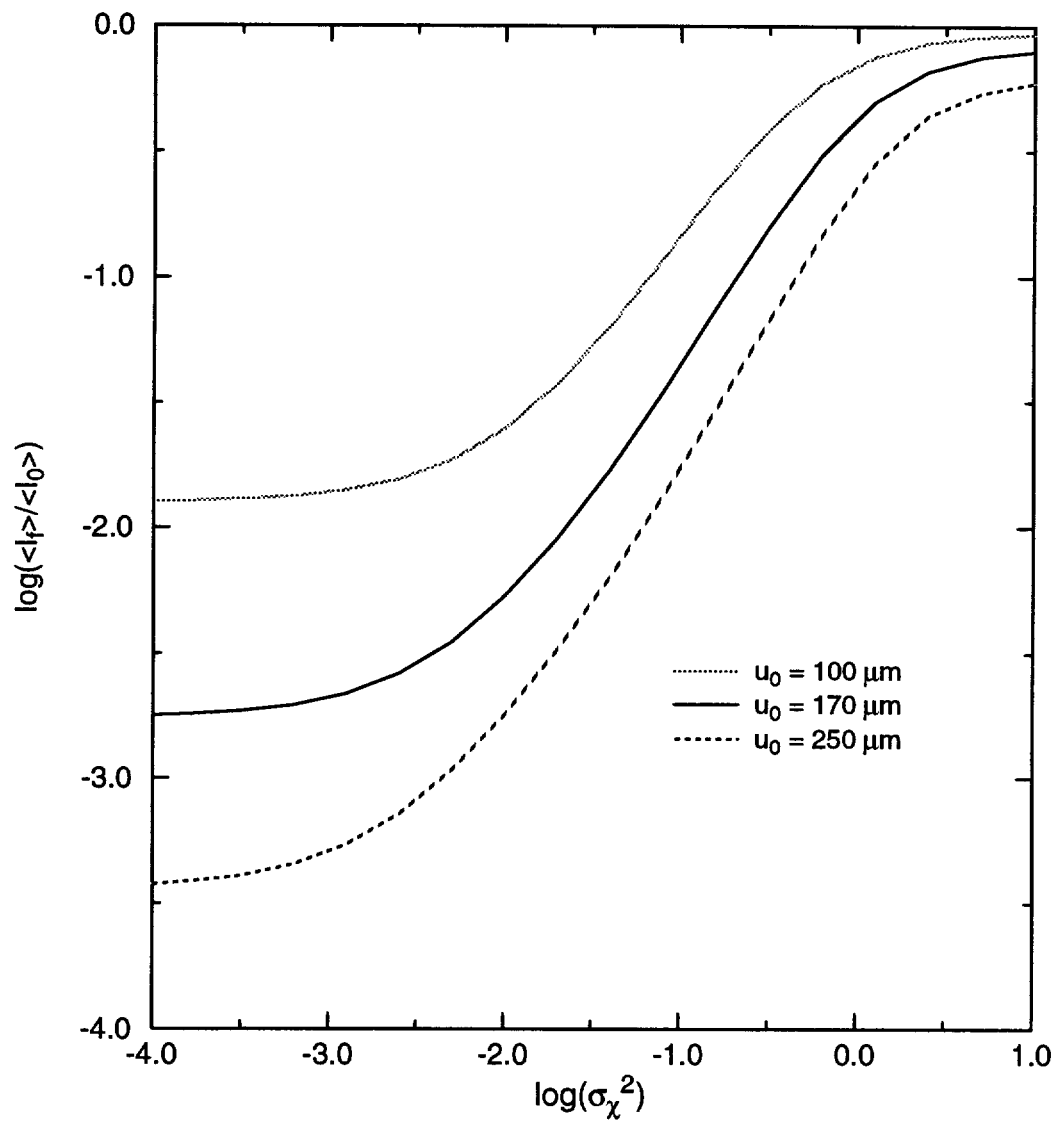


Figure 3-7: The effect of filter size on the turbulence strength measurement (simulation results)

early related to the log of the received intensity. The second flat zone corresponds to the strong turbulence range. When the turbulence strength is strong, the turbulence-induced beam spreading and beam wander exceeds the limits of the receiving fiber apertures. Therefore, both I_f and I_0 become smaller. However, the normalized receiving intensity is little changed (note that the above simulation is not valid when $\sigma_\chi^2 > 0.3$). Among the three zones, only the linear zone can be used to estimate the turbulence strength. The dynamic range determines the measurable turbulence range.

Table 3-2: Simulation conditions for the effect of the filter size.

Characteristic	Symbol	Rating
Laser Center Wavelength (nm)	λ_0	690
Laser Wavelength Bandwidth (nm)	$\Delta\lambda$	0.5
Laser Beam Radius (mm)	a_0	7.0
Target Distance (m)	z_0	240
Telescope Focal Length (m)	f_1	0.91
Telescope Radius (m)	q_0	0.10

Figure 3-7 also illustrates the effects of the optical filter sizes. On the one hand, large filter size increases the detecting dynamic range, as larger filter size blocks more target-induced field. On the other hand, a larger filter size decreases the received intensity, which usually results in low SNR. Therefore, the filter size selection is a trade-off between the dynamic range and the SNR. In our system, we prefer to detect the dynamic range between $\sigma_\chi^2 = 10^{-2}$ and $\sigma_\chi^2 = 10^{-1}$, and the normalized received intensity greater than 10^{-3} . Thus, we expect that the filter size is around 150 μm .

3.3.3 The effect of the target distance, z_0

The target distance determines the size of the target-induced speckle field. In this numerical experiment, we model the received intensities corresponding to the different target locations. The simulation conditions are described in Table 3-3 and the simulation results are shown in figure 3-8.

Table 3-3: Simulation conditions for the effect of the target distance.

Characteristic	Symbol	Rating
Laser Center Wavelength (nm)	λ_0	690
Laser Wavelength Bandwidth (nm)	$\Delta\lambda$	0.5
Laser Beam Radius (mm)	a_0	7.0
Optical Spatial Filter Radius (μm)	u_0	170
Telescope Focal Length (m)	f_1	0.91
Telescope Radius (m)	q_0	0.10

The simulation results clearly demonstrate that the detected dynamic range increases as the target distance increase. This is because the far-field target has a small image size at the image plane of the telescope. When the image size becomes small, the same filter blocks more target-induced speckle field. Consequently, the received intensity is more controlled by the turbulence signal. Hence, the system with long target distance has a wider detecting dynamic range. However, since the received intensity is inversely proportional to the square of the distance to the target, the received intensity decreases when the target distance increases. Therefore, the target distance has a limit, beyond

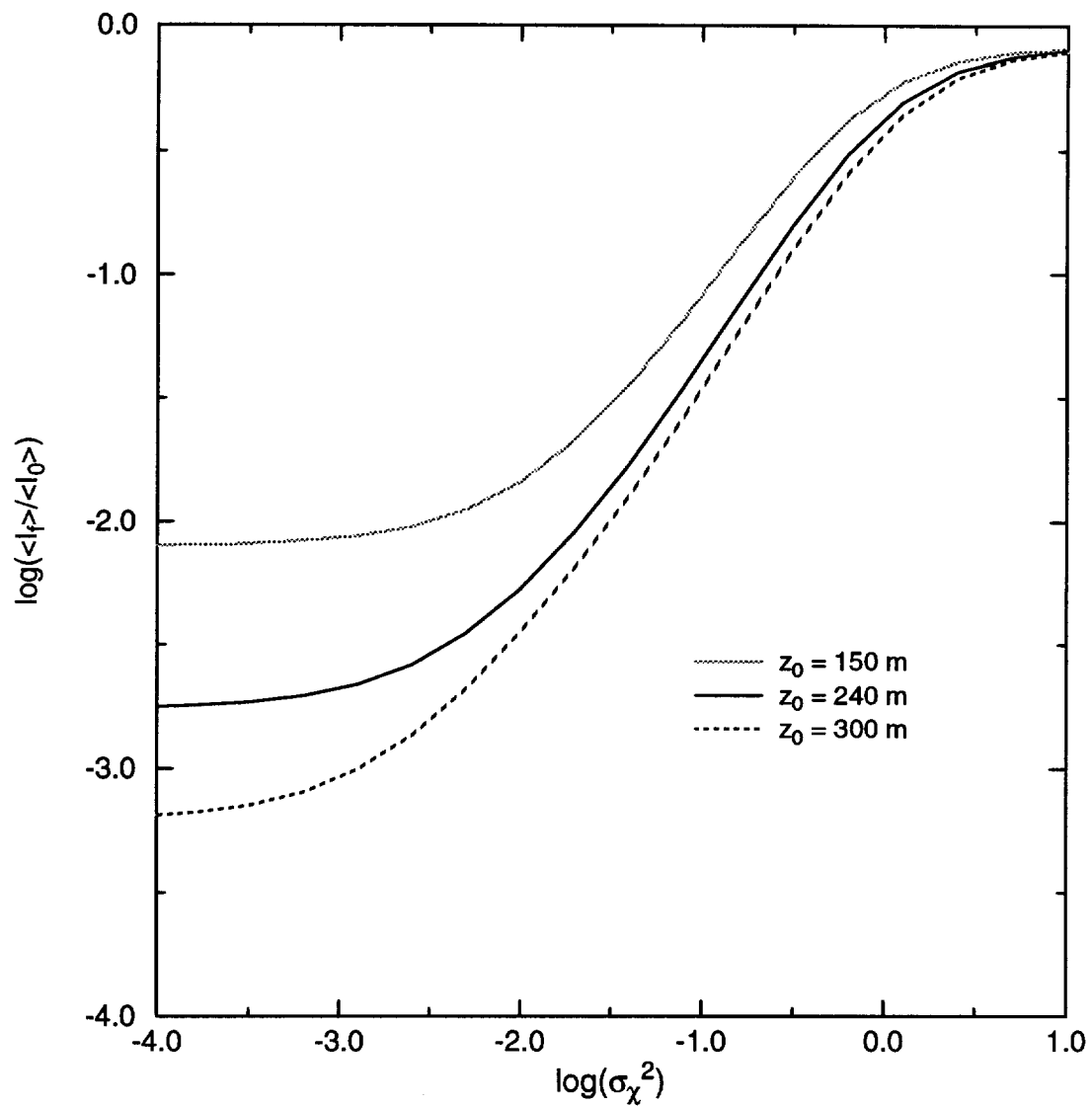


Figure 3-8: The effect of the target distance on the turbulence strength measurement (simulation results)

which the received signal is too weak to be detected. Obviously, the trade-off between the dynamic range and received intensity determines the target distance.

3.3.4 The effect of the laser beam size a_0

The laser beam size determines the detected dynamic range by changing the target-speckle field size. This effect has been simulated according to the following conditions (Table 3-4):

Table 3-4: Simulation conditions for the effect of laser beam size.

Characteristic	Symbol	Rating
Laser Center Wavelength (nm)	λ_0	690
Laser Wavelength Bandwidth (nm)	$\Delta\lambda$	0.5
Optical Spatial Filter Radius (μm)	u_0	170
Target Distance (m)	z_0	240
Telescope Focal Length (m)	f_1	0.91
Telescope Radius (m)	q_0	0.10

The simulation result (see figure 3-9) shows that a large laser beam size reduces the dynamic range. This is due to the fact that large beam size causes large target-induced spot size at the image plane of the telescope. The large spot size makes the unblocked target-induced signal stronger than that of the small spot size. As a result, the received signal is more dominated by the target-induced speckle field. Therefore, the detected dynamic range of the larger beam size is narrower than the dynamic range of the smaller beam size.

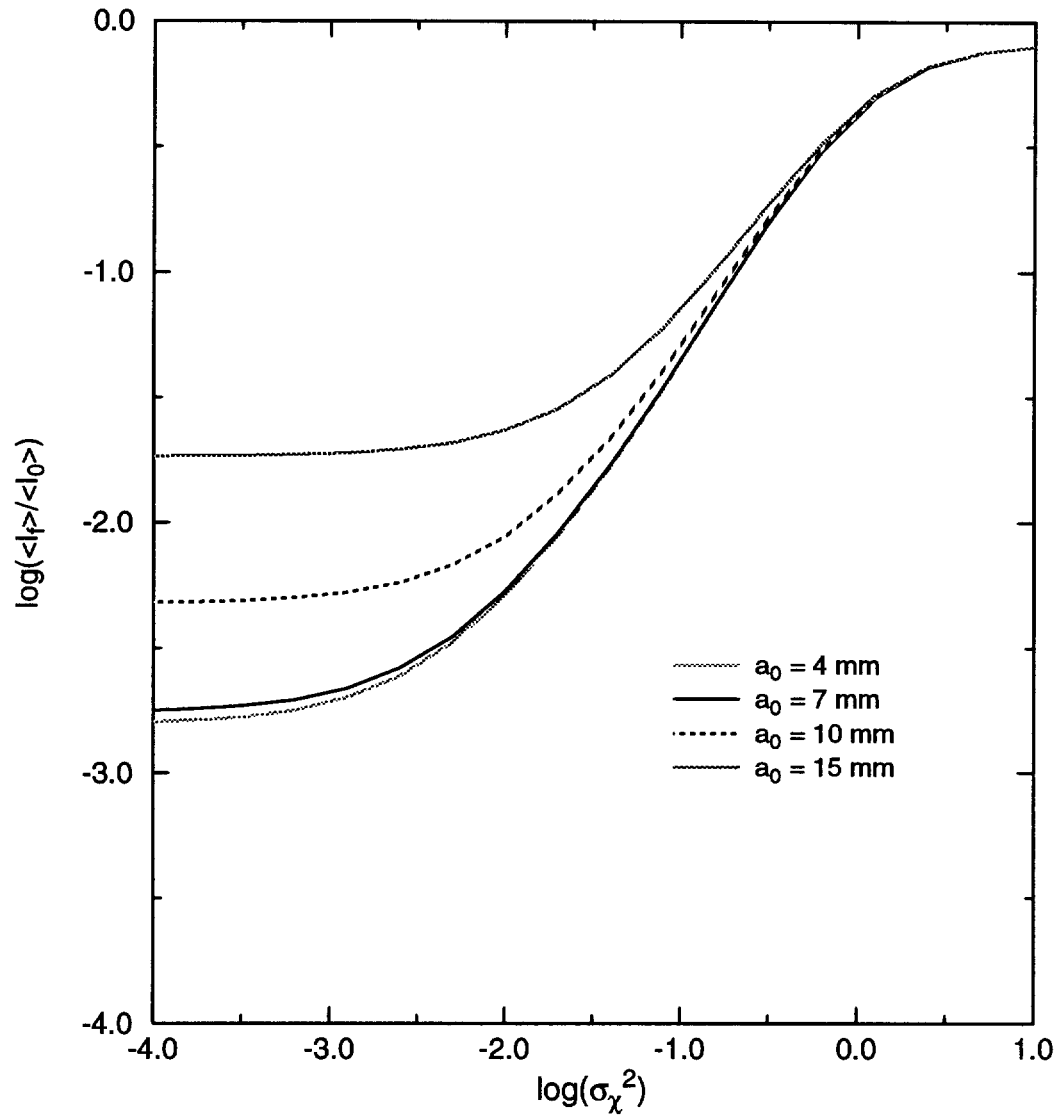


Figure 3-9: The effect of the laser beam size on the turbulence strength measurement (simulation results)

Obviously, in order to increase the detected dynamic range of the large beam size condition, we have to increase the optical filter size.

3.3.5 The effect of the wavelength, λ

The experimental system uses a polychromatic diode laser. In this simulation, we chose three wavelength (680 nm, 690 nm, 700 nm) to represent this polychromatic diode laser to analyze the system performance under the polychromatic condition. Using the conditions in Table 3-5, the results are shown in figure 3-10.

Table 3-5: Simulation conditions for effect of the laser wavelength.

Characteristic	Symbol	Rating
Laser Beam Radius (mm)	a_0	7.0
Laser Wavelength Bandwidth (nm)	$\Delta\lambda$	0.5
Optical Spatial Filter Radius (μm)	u_0	170
Target Distance (m)	z_0	240
Telescope Focal Length (m)	f_1	0.91
Telescope Radius (m)	q_0	0.10

The simulation results illustrate that the wavelength does not change the relationship between the received intensity and the turbulence strength for the simulated system. Under the same turbulence level, when the laser wavelength changes within 680 nm~700 nm, the normalized intensities are very close to each other. Therefore, we can utilize the polychromatic laser source and use one of the turbulence-intensity curves to estimate the turbulence strength in the experiment.

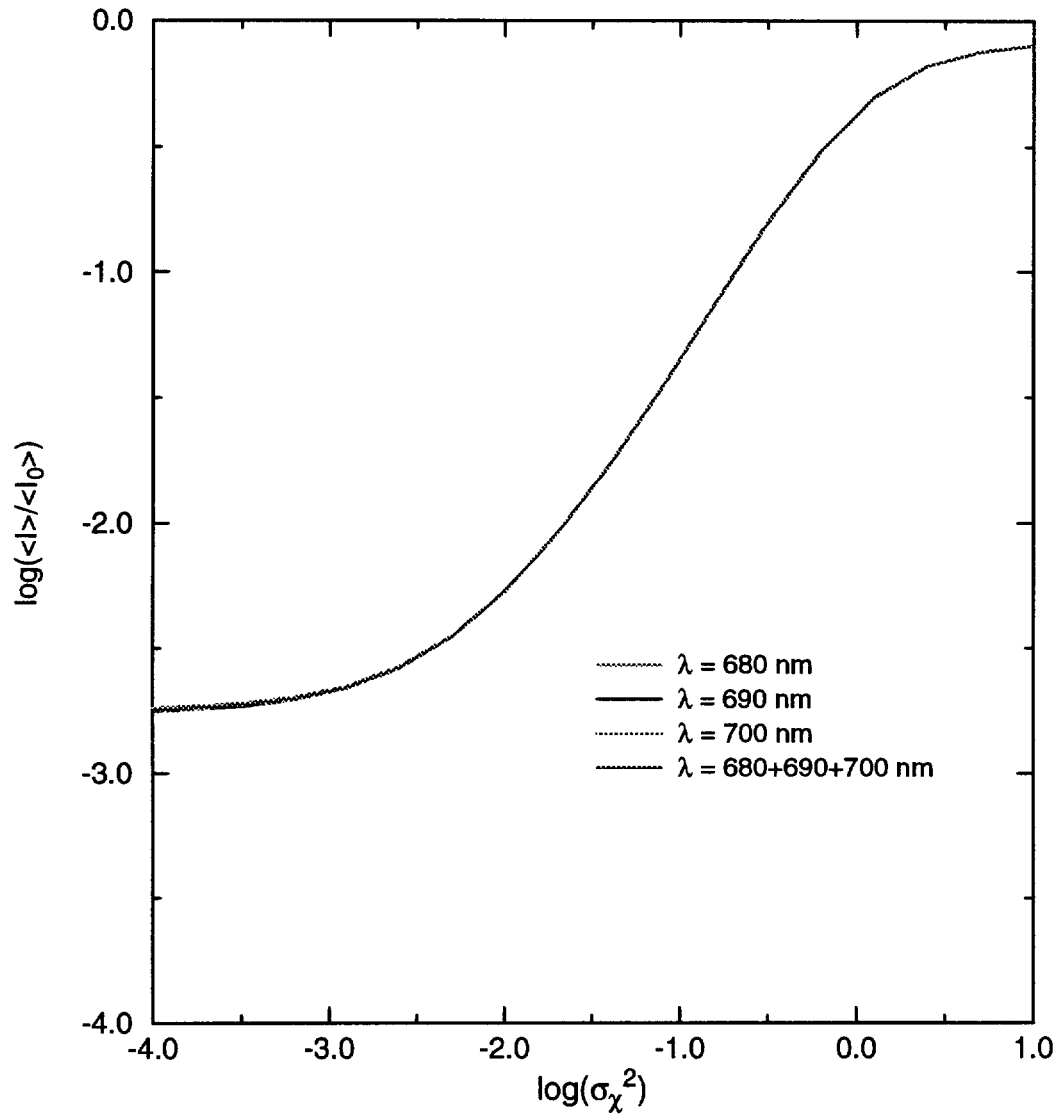


Figure 3-10: The effect of the laser wavelength on the turbulence strength measurement. (simulation results).

CHAPTER 4

Experimental System

4.1 Introduction

The experimental system consists of the following four subsystems: the transmitting subsystem, the receiving subsystem, the data processing subsystem, and the calibrating subsystem (see Figure 4-1). The transmitting subsystem generates a modulated laser beam and transmits the beam into the atmosphere. The receiving subsystem collects the backscattered optical signal from the target, optically filters the received signal and transforms the optical signal into an electrical signal. Then the data processing subsystem decodes the electrical signal to recover the range bin information, which is later sampled by the A/D board and processed by the developed computer program so as to obtain the corresponding normalized receiving beam intensity. In addition to the above subsystems, the calibrating subsystem measures the path-averaged atmospheric turbulence strength(σ_{χ}^2) and combine with the normalized beam intensity to validate the theoretical prediction. By combining the above four subsystems, the experimental system can work on turbulence detection and range finding.

4.2 Transmitting subsystem

The transmitting subsystem comprises a laser source and a laser controller, a PRC sequence generator, and a fiber-optic transmitter as shown in Figure 4-2.

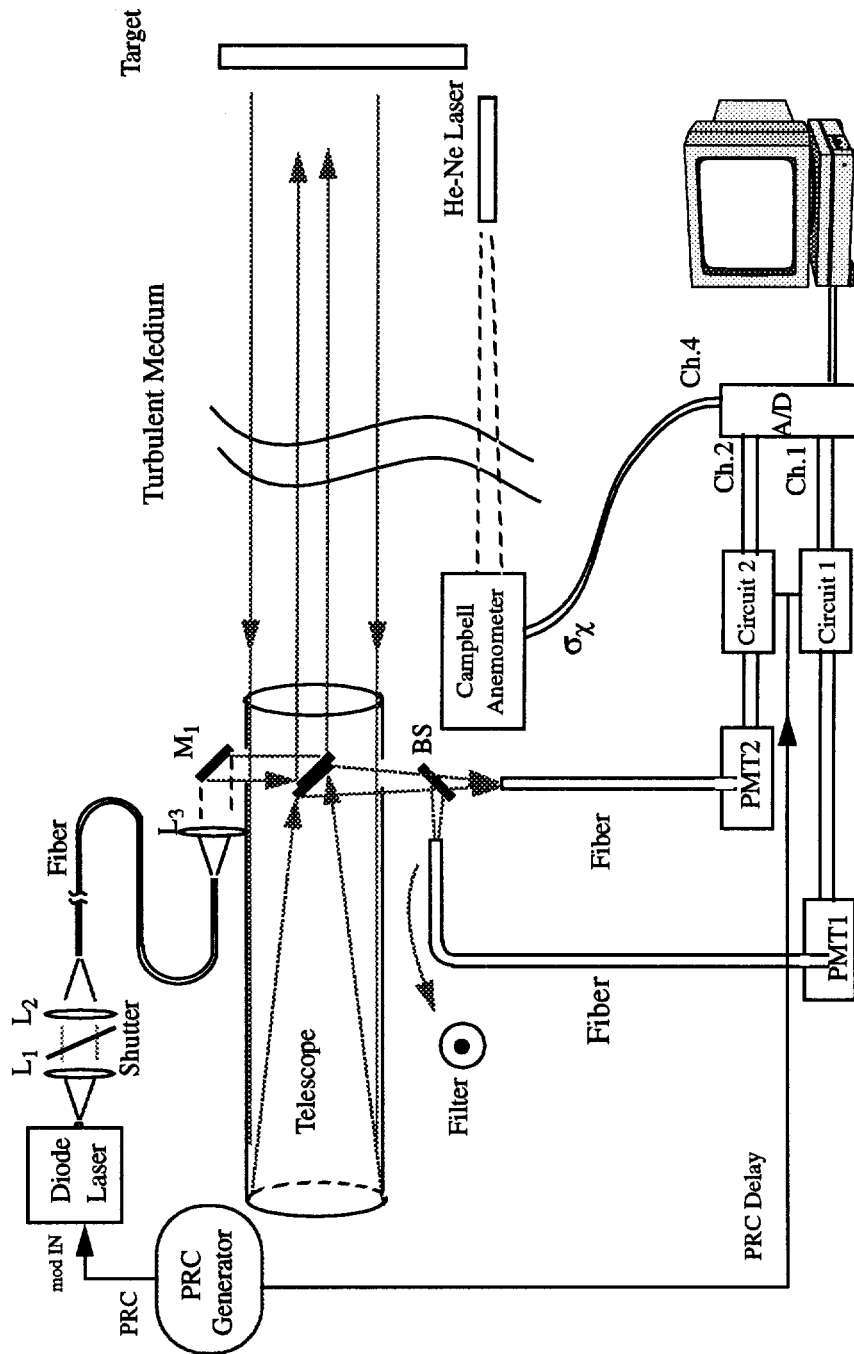


Figure 4-1: The experimental system diagram.

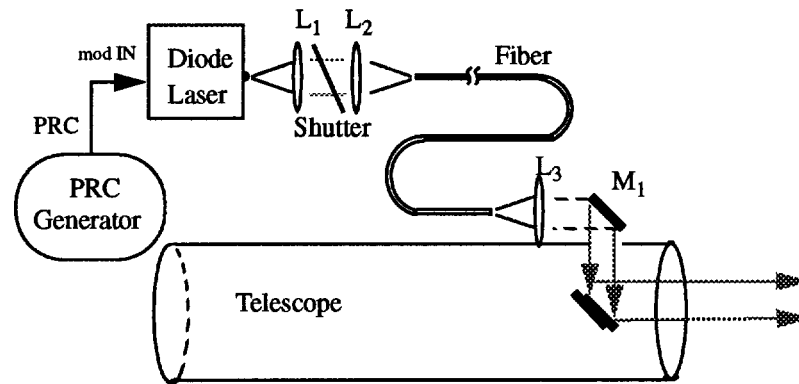


Figure 4-2: The transmitting subsystem.

4.2.1 Laser source and laser controller

The selection of the laser source depends on many factors, such as the modulation bandwidth, fiber coupling efficiency, transmission power, temperature stability and operation feasibility. In our research, high transmitting power is the top priority. This is because the reflecting coefficient of the target is very weak. Hence, we need a high power laser in order to obtain at least threshold SNR at the receiver. In addition to the high power request, the thermal stabilities of laser power and laser frequency are also very critical, due to the fact that the developed method is quite sensitive to the power and frequency of the laser source. Finally, the laser source must be able to response to the 1MHz PRC modulating signal and have a low laser-fiber coupling loss. Depending on the above considerations, we selected the diode laser as the laser source of our system.

Specifically, the laser we used is an index guided laser diode, model TOLD9150(s). Its characteristics are shown in Table 4-1.

Table 4-1: TOLD9150 specifications.

CHARACTERISTIC	SYMBOL	RATING	UNIT
Maximum Output Power	P_o	30	mW
Lasing Wavelength	λ_p	690	nm
Threshold Current	I_{th}	50	mA
Beam divergence	$\phi_{//}$	8.5	deg.
	ϕ_{\perp}	18	deg.
Package		9	mm

From Table 4-1, the maximum output power of TOLD9150(s) is 30 mW, which is among the highest diode lasers commercially available. Also, the parallel and perpendicular divergence angles are the 8.5 degrees and 18 degrees respectively, which are the smallest we have found. In addition, TOLD9150 is compact and lightweight so that it can readily be kept in a temperature-stable environment to avoid threshold current fluctuations and frequency/wavelength fluctuations. Consequently it has high reliability. Moreover, it responds to the high frequency modulation so that it can be directly modulated by the 1MHz PRC. Finally, TOLD9150 emits visible light (690 nm), which makes it easy to align the optical system. In summery, TOLD9150 meets our experiment requirement.

The TOLD9150 diode laser is controlled by a Melles Griot 06DLD103 diode laser controller. The 06DLD103 consists of a precision low noise current source for the diode laser and a precision thermoelectric cooler controller (TCC). The TCC provides a stable thermal environment to achieve a constant output laser power and frequency. We measured the TOLD9150 transmitting wavelength versus temperature. The results in Table 4-2 illustrate that the wavelength only changes about 1.0 nm while the output power variates

from 10 mW to 30 mW, if the temperature is kept stable by the TCC. Therefore, the laser source is stable enough for the developed method.

Table 4-2: TOLD9150 peak wavelength versus temperature

Power (mW)	Laser Peak Wavelength (nm)				
	T=15 °C	T=20 °C	T=25 °C	T=30 °C	T=35 °C
10	687.7 or 687.8	687.9 or 688.0	688.8	689.0	690.4 or 690.3
20	687.7 or 687.8	688.0 or 687.9	689.4 or 688.8	690.0	690.3 or 691.1
30	687.7 or 687.8	688.9	690.0	690.5	691.4 or 691.7

4.2.2 PRC Generators

The PRC generators used in our experiment are a 511-PRC generator and a modified Wavetek Noise Generator. They both generate 1 MHz PRC, 1 MHz delay PRC, and synchronized control signals with different code periods. Their PRC pulse width is 1 MHz in order to reach a 300 m detecting range resolution.

4.2.3 511 PRC generator

The 511 PRC generator provides: a) a 1 MHz PRC signal with $511 (2^9 - 1)$ code length; b) a 1MHz PRC delay signal with 0.2 μ s delay time resolution; c) five synchronized control signals for PRC integrating and A/D sampling.

The schematic diagram demonstrates the four functional blocks as shown in Fig. 1 of Appendix B. The first block is the PRC pulse clock generator. It contains one internal 10 MHz oscillator and two divider chips, so that it can generate the 1 MHz signal for the PRC clock and the delay PRC clock. At the same time, it also provides a 5 MHz PRC delay time clock. The second part is the PRC generator, which utilizes the shift register and the Exclusive-OR gates to implement the PRC sequence based on its primitive polynomial ($h(x) = x^9 + x^4 + 1$) [MacWilliams and Sloane, 1976]. Its output modulates the 9150 diode laser to produce the PRC coded outgoing laser beam. The third block is the PRC delay unit, which shifts the 511 PRC sequence by a $0.2 \mu s$ shift resolution. The PRC delay time is determined by the detecting path length. Suppose we want to measure the turbulence profile within 200 m, the maximum PRC delay time is $2 \times 200 / 3 \times 10^8 = 1.3 \mu s$. Therefore, we can sweep the PRC delay time as 0, 0.2, 0.4, . . . , $1.4 \mu s$ to obtain the detected profile along the path. In our system, the selection of the PRC delay time shift is achieved by a 386 PC. The output of the PRC delay signal are the inputs of the post-processing circuit (see Fig. 1 of Appendix B). The fourth part is the synchronized control signal generator. It produces the two-integrator control signals (Reset A, Reset B, Hold A, Hold B) and an A/D board sampling control signal (A/D trigger) as shown in the schematic. The output of the synchronized control signal are also the inputs of the post-processing analog circuit (see Fig. 1 in Appendix B). It is worth while to point out that all of the above output signals are synchronized periodic signals with a period of $511 \mu s$.

The 511 code length is not long enough to obtain the required SNR when detecting a weak signal. In our experiment, 511 PRC is only used to detect the signal backscattered from the high reflection diffuse target. In order to further improve the SNR for weak signals, we need the long-code-length PRC sequence.

4.2.4 The Modified Wavetek PRC generator

The Modified Wavetek PRC generator includes a Wavetek Noise Generator and its auxiliary circuit. The Wavetek Noise Generator generates a pulse width adjustable PRC with code lengths of 1023 ($2^{10} - 1$), 32,767 ($2^{15} - 1$), and 1,048,575 ($2^{20} - 1$). Similar to the 511 PRC case, the PRC pulse frequency in the Wavetek Noise Generator is 1 MHz.

The Wavetek Noise Generator has a PRC sequence, PRC synchronizing pulse, and clock outputs. Unfortunately, they are not the standard TTL signals. Therefore, we developed an auxiliary circuit to both convert those signals to TTL and produce the delay PRC, and the synchronized control signals. The schematic diagram of the auxiliary circuit is illustrated in Fig. 2 of Appendix B. Unlike the 511 PRC generator, when the PRC delay time is less than $1\mu s$, the auxiliary circuit utilizes a mono-stable multi-vibrating chip (one-shot) to generate the delay time. When the PRC delay time is greater than $1\mu s$, it uses the computer-generated-signal to produce the delay time. For instance, $3.4\mu s$ delay time can be separated into 2 parts, $3.0\mu s$ and $0.4\mu s$. The $3.0\mu s$ delay is produced by computer and the $0.4\mu s$ delay is generated by the one-shot chip.

Compared with the 511 PRC generator, the Modified Wavetek PRC Generator provides a much longer signal integration time for weak signals than the 511 PRC does. Quantitatively, the three generated PRC periods (i.e. integrating time) by the Modified Wavetek PRC Generator are about 1.0 ms, 32.8 ms and 1.0 s respectively. They are 2, 64, and 2048 times longer than the code period of the 511 PRC. Obviously, the use of Wavetek PRC Generator will increase the SNR ratio. In our research, the long code PRC is used to detect weak signals reflected from low reflection targets, like the screen target. The experiment results confirmed that the long code PRC is successful for weak signal detection (See Chapter 5 for details).

4.2.5 Fiber-optical transmitter system

The fiber-optic transmitting system includes two laser-fiber coupling lenses (L_1 and L_2), a transmitting fiber, a beam expanding lens (L_3) and two reflecting mirrors (see Fig. 4-2). The laser-fiber coupling lenses consist of a collimating lens (L_1) and a focal lens (L_2). The collimating lens transfers the diverging light from the laser diode into a collimation beam. Then the focal lens converges the beam into the fiber. In the beam expanding-reflecting part, a beam-expanding lens collimates the fiber output beam and two reflecting mirrors redirect the beam from the center of the telescope into the air.

The features of the fiber and the lenses are selected to obtain the lowest laser-fiber coupling loss. The fiber we use is a multi-mode fiber. This is because (a) the multimode fibers have low laser-fiber coupling loss; (b) they have enough information carrying capability for this low BL product applications ($B = 1$ MHz/bit and $L = 20$ m); c) even though the multimode fibers can cause mode interference distortion, it will not affect the total receiving light intensity. Therefore, the multi-mode fiber is the appropriate choice for our application.

The selection of the multimode fiber size is a trade-off between the laser-fiber coupling efficiency and the laser beam size at the far field target. Generally, a larger fiber core size reduces the coupling loss. On the other hand, larger fiber core size will lead to the bigger laser spot size on the target. Consequently, it generates a larger laser speckle size on the receiver, which will decrease the system's dynamic range. Therefore, we must optimally select the fiber core size to compromise the loss of the detection's dynamic range due to the increasing of coupling efficiency. According to the above considerations, we chose the Newport F-MSD multimode fiber, which has a $50\ \mu\text{m}$ core size, 0.2 NA, and 20 m transmitting length.

The diameter and the focal length of both coupling lenses and transmitting lenses are chosen based on the selection of the laser diode and the fiber. For the coupling lenses, their diameter and focal length should be chosen according to the divergence angle of the laser diode and the NA of the multi-mode fiber. For the transmitting lens, its diameter is determined by the transmitting beam size and its focal length is decided by the NA of the fiber. In our system we choose: (a) in the laser-fiber coupling system, the collimation lens has 12.7 mm diameter and 19.0 mm focal length. The focal lens has 12.7 mm diameter and 38.1 mm focal length. (b) in the beam expanding and reflecting system, the collimation lens has 25.4 mm diameter and 50.8 mm focal length. The two reflecting mirrors have 25.4 mm diameters. The above fiber-optical configuration has about 50% coupling loss and the detection dynamic range meets the experiment's requirement.

The advantages of this fiber-optic system are its stability and reliability, as discussed in Chapter 2. In our experiment, the laser-fiber coupling system is mounted on the optical bench in the lab, while the beam-expanding system is mounted on the telescope. This design provides the feasibility of moving the telescope to the outdoor desired position and keeps the sensitive laser-fiber coupling system in the thermal and mechanically stable indoor environment.

4.2.6 Shutter

A shutter is used to control the switch of the transmitting laser so that the system is able to record the laser signal and the background signal alternatively. The shutter we used is a black screen attached to an aluminum bar, which can rotate in the plane perpendicular to the optical path. In order to block the transmission laser beam when background signals are recorded, it is located between the collimated lens and the focal lens in the

laser-fiber coupling system (see Figure 4-2). The switch of the shutter is controlled by a 386 PC. The shutter driver circuit is shown in the Fig. 3 in Appendix B. Obviously, the computer controlled shutter design automates the entire system operation.

4.3 Receiving subsystem

The receiver subsystem consists of a telescope, a fiber-optic receiver, an optical spatial filter, and two photodetectors. Their sequential functions are: (a) collecting the backscattering signals from the far-field targets; (b) separating the received laser beam into two channels; (c) applying the optical spatial filter on one channel; and (d) converting the two optical signals into two electrical signals. The above four functions determine the performance of the signal detecting subsystem.

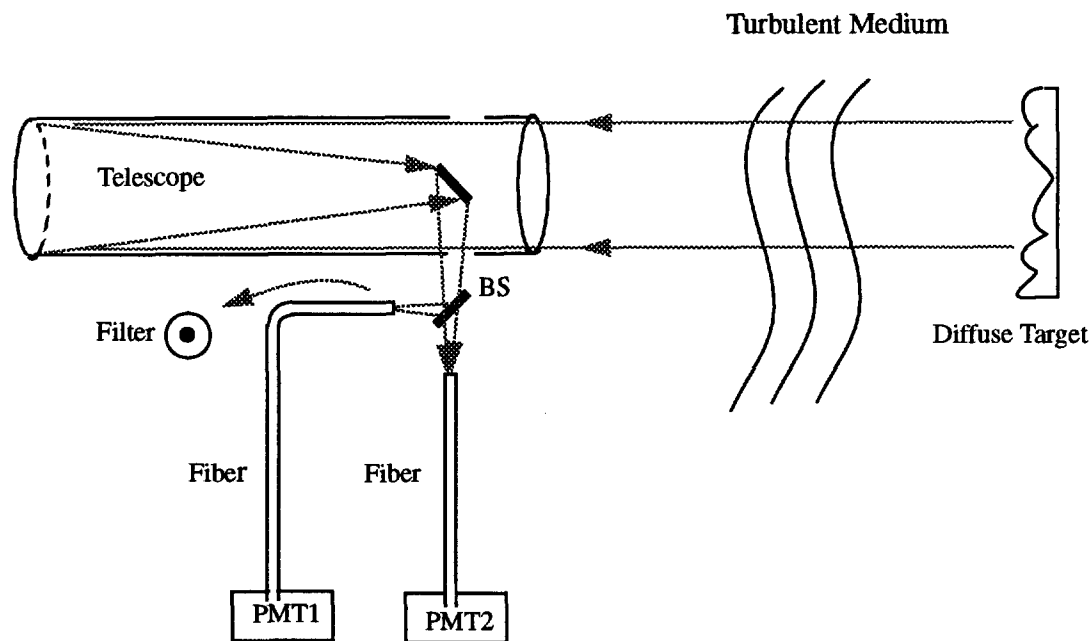


Figure 4-3: The receiving subsystem

4.3.1 Telescope

The target backscattering light is collected by a telescope. In addition to its light collection function, the telescope also supports both the fiber-optic transmitter and the fiber-optic receiver, which are mounted on the two sides of the telescope tube. There are two major benefits of attaching the transmitter and receiver on the telescope. First, the receiver is coaxial with the transmitter. Therefore, as long as the optical system is aligned, we can easily measure the turbulence at different directions by rotating the telescope. Second, this design enhances the system's environment perturbation immunity. With our design, both the receiver and the transmitter can move together, when a small perturbation happens, such as ground shaking due to cars moving. As a result, the optical system alignment is very reliable. Otherwise, a small perturbation of the transmitter or receiver may totally destroy the system alignment. In reality, as the laser transmission path length is much longer than the focal length of the telescope, the system's stability is very essential to success of the far-field-weak-signal detection.

The telescope we used is an ODYSSEY 8 model Newtonian type telescope. Its mirror diameter is 8 inch and the focal length is 36 inch. The turning mirror in the telescope blocks 7.1% of the receiving area.

4.3.2 Fiber-optic receiver

The fiber-optic receiver, attached on one side of the telescope tube, consists of a beam splitter and two receiving fibers (see Figure 4-3). The beam splitter splits the received laser beam into a reflection channel and a transmission channel. In the reflection channel, the beam is optically filtered by a high-pass spatial filter, while in the transmission channel, the laser beam is not changed. Consequently, we can normalize the filtered

signal by the unfiltered signal. As the high-pass spatial filter blocks most of the received beam in the reflection channel, we select a high reflecting beam splitter so that the filtered signal can reach the detector's threshold. In our system, we use a neutral-density-filter as the beam splitter. At 690 nm wavelength, its reflection coefficient is 60%, and transmission coefficient is 10%. Its absorption loss is about 30%.

The reflected and transmitted laser signals are focused into two receiving fibers, which are the same type of multi-mode fibers. One of the fibers has an optical spatial filter on its center. The diameters of the two fibers are 1 mm, based on the laser beam spot size at the target more than 240 meters away. The NA of the two fibers are 0.39. In the experiment, both fiber positions are adjusted three dimensionally by the micrometers to minimize the receiving laser-fiber coupling loss. The fiber output signals are fed into the two photodetectors for further processing.

4.3.3 Field-of-View (FOV)

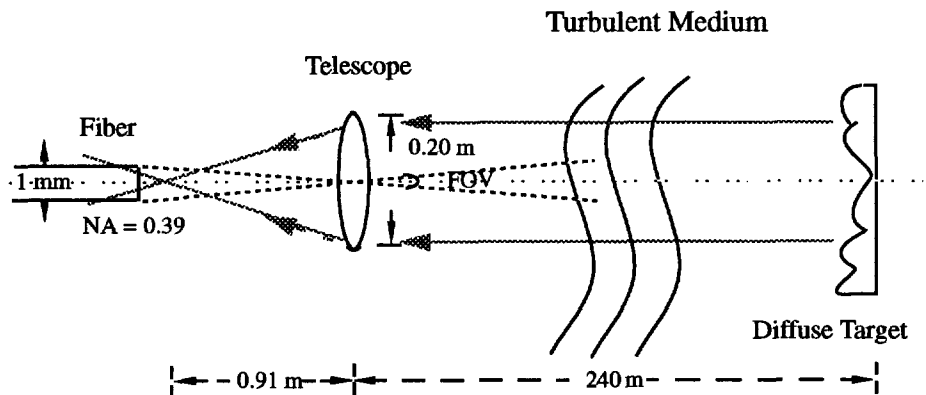


Figure 4-4: Field of view of the system

A Field-of-View of a system limits the system's receiving angle. In our case, it is determined by the size of the receiver fiber and the telescope focal length, which are specified in Figure 4-4. According to this configuration, the Field-of-View of this system is given by

$$FOV = 1.0 \times 10^{-3} / 0.91 = 1.1 \times 10^{-3} \text{ rad}$$

The value of the FOV should be less than the NAs of the receiving fibers, so that the receiving fibers do not confine the system's receiving angle. In our design, the FOV is much less than the NA of the fiber ($0.39 \times 2 = 0.78$), therefore, the performance of the receiving system is not degraded by using the 1 mm fibers.

4.3.4 Optical spatial filter

An optical spatial filter is a transparency with certain spatial amplitude or phase distribution. It can enhance or suppress certain spatial frequencies of an optical signal. The idea of the spatial filtering is based on the fact that a lens forms the Fourier transform of its front focal plane field distributions at its back focal plane (the Fourier plane). The field distribution at the back focal plane represents the optical-signal's spatial frequency distribution. Therefore, we can change the image property by inserting an optical spatial filter in its Fourier plane.

In our research, the purpose of utilizing an optical spatial filter is to block the target-induced speckle field and to pass the turbulence-induced backscattered field. The target-induced speckle field is confined to the center of the optical axis, which corresponds to low spatial frequencies. On the other hand, due to the beam spread and beam wander, the

turbulence-induced backscattering field extends to the off-axis area, which relates to high spatial frequencies. Therefore, we chose a high-pass spatial filter to accomplish our goal.

Our high-pass spatial filter can be represented by the Gaussian type transfer function (see Equation 4-1 and Figure 3-4)

$$F(q) = 1 - \exp\left(-\frac{q^2}{q_0^2}\right) \quad (4-1)$$

where $q_0 = d_0/2$ is the effective filter size and d_0 is the diameter of the center spot. According to the transfer function and the simulation in Section 3.3.2, we chose the filter diameter as $340 \mu m$ to get the expected detecting dynamic range, when the target is about 240 meters away and the laser wavelength is 690 nm.

Notice that in this specific case, we could put the optical spatial filter at the target's image plane, instead of the telescope focal plane. The first reason is that the image plane is very close to the focal plane. When the object distance ($s = 240$ m) is much larger than the focal length of the telescope ($f = 0.91$ m), the distance (Δ) between the focal plane and image plane is given by

$$\Delta = \frac{f^2}{s-f} = 3.4 \text{ mm} \quad (4-2)$$

A 3.4 mm distance is so small that we can consider the image plane as the focal plane. The other reason is that the image plane is easier to identify than the focal plane. The final reason is based on the simulations in Chapter 3, which confirm that we can get the desired dynamic range, when we put the spatial filter at the image plane.

4.3.5 Photodetectors and Wavelength Filters

Based on the discussion in Section 2.5.3.3, we chose the photomultiplier tubes (PMTs) as the photodetectors. In our experimental system, the two PMTs are both model R446 manufactured by Hamamatsu. Their characteristics are shown in Table 4-3.

Table 4-3: The characteristics of R446 NOTE: ENI refers to the amount of input light in Watts to produce a SNR of unity in the output of a PMT

Characteristics	Specifications
Spectral Range (nm)	185 ~ 870
Peak Wavelength (nm)	330
Max. Anode Current (mA)	.1
Max. Anode to Cathode Voltage (V)	1250
Cathode Sensitivity (mA/W)	40
Anode Sensitivity (A/W)	2.0×10^5
Current Gain	5×10^6
Anode Dark Current (nA)	2
ENI (W/\sqrt{Hz})	1.3×10^{-15}

R446 is a side-on type PMT with nine dynode stages. Its photocathode spectral response ranges from $185nm \leq \lambda \leq 870nm$ with the response peak at 330 nm. For the 690 nm wavelength, R446 has an approximate radiant sensitivity value of 15 mA/W. Also, R446 has lower Equivalent Noise power referred to the Input (ENI= 1.3×10^{-15} (W/\sqrt{Hz})) than other types of PMTs. Therefore, R446 is better for detecting weak signals.

The current gain of the PMT is determined by the voltage distribution ratio of the dynodes and the supply voltage. We build a voltage divider circuit to control the PMT's current gain (see Fig. 4 in Appendix B). Based on this circuit configuration, the dynode stages can produce a current gain of 5×10^6 for a 1000-volt supply. Another function of the circuit is to convert the PMT anode output into a voltage signal by using a transimpedance amplifier. The transimpedance amplifier is implemented by a $10 \text{ k}\Omega$ resistor across a MA322 op-amp. The maximum anode saturation current is about 0.1 mA, and the maximum voltage output is 1V ($0.1 \text{ mA} \times 10 \text{ k}\Omega = 1 \text{ V}$). It is worth pointing out that a small capacitor across the MA322 limits the amplifier bandwidth below 2 Mhz, so that the circuit can eliminate the high frequency noise.

As PMT has wide wavelength response range, the background signals are also going to be amplified with the laser signal. Therefore, we use an optical wavelength filter to eliminate the unwanted background noise. The two optical wavelength filters used in our case have a central transmission wavelength of 690 nm and a half peak bandwidth of 8.8 nm. As a result, the 690 nm laser signals can transmit into the PMTs and most of the background noises are filtered out. Obviously, the optical wavelength filters raise the system SNR. This is essential to the success of daytime experiments.

Each PMT, electronic circuit, and wavelength band-pass filter is built into one Aluminum box, which has a 1.5 mm diameter hole for the 1 mm receiving fiber and one MVT connector for the high voltage supply. The output voltage signals are connected with the data processing subsystem for signal processing.

4.4 Data processing subsystem

The data processing subsystem can be categorized into the hardware and the software. The hardware contains an analog circuit, a A/D board, and a 386 computer. The software includes the data sampling codes and the data processing codes. The combination of the hardware and software makes the whole data processing very efficient.

4.4.1 Analog circuit

The analog circuit can be divided into three stages: an amplifier stage, a multiplier stage and an integrator stage (see Fig. 5 in Appendix B). It amplifies, decodes and integrates the electrical signal from the receiving subsystem in order to enhance the laser signals and suppress the background noise.

The amplifier stage provides full scale input signals for the next multiplier stage. It utilizes three cascade op-amps to reach a total gain of 300. Additionally, the amplifier stage also employs an AC coupling capacitor to block the sunlight background and PMT dark currents (see Figure 5 in Appendix B). The AC coupling approach efficiently removes the noise, because the majority of the sunlight background noise and PMT dark current are low frequency components. After being amplified and AC coupled, the processed signal enters the multiplier stage. The multiplier stage accomplishes the $PRC'(t) \times PRC(t)$ operation. It uses an AD734 multiplier to multiply the PRC coded signal and the delayed PRC' signal. The delayed PRC' signal is derived from the delay TTL PRC signal by an AC coupling capacitor. Its voltage ranges from -2.5 V to +2.5 V. After the multiplication, the output signals are transferred to the integration stage. The integration stage integrate the selected range-bin $PRC'(t) \times PRC(t)$ signal over the PRC period T to

eliminate both the low frequency noise and the other range-bin signals. It uses an ACF2101 integrator to accomplish the following integrating function:

$$V_{out} = \frac{I_i t}{C_{INT}} \quad (4-3)$$

In the above equation, V_{out} is the integrator output, I_i is the input current, and C_{INT} is the integration capacitance. In order to obtain the full scale V_{out} , three C_{INT} values are selected for the different PRC periods. Their values are 100 pf, 1000 pf and 0.01 μ f respectively. The integration stage also uses an inverter to flip and buffer the V_{out} signal. This is because the next section requires 0 V to 10 V input range and the V_{out} provides 0.5 V to -10.0 V output. Therefore, we need an inverter to reverse V_{out} .

The output signal of the analog circuit was further sampled by a computer controlled A/D board.

4.4.2 A/D board

The A/D board comprises a CIO-SSH16 A/D board (SSH16) and a CIO-AD16 I/O board (AD16). The SSH16 board accomplishes the simultaneous sampling function, while the AD16 board implements the automatic detection control function.

SSH16 is an external A/D periphery. It is able to sample and hold up to 16 channels so that the AD16 can sample the data in 16 channels simultaneously. In our system, we use 4 of the 16 channels. The first and second channels are the optical spatial filtered channel and unfiltered channel respectively. The third channel is an optional channel, which connects with the calibration subsystem for recording the wind speed. The fourth channel also connects with the calibration subsystem for sampling the turbulence strength

(σ_χ) . Therefore, the SSH16 can simultaneously sample and hold the receiving optical intensity and the turbulence information.

The AD16 board connects with both the SSH16 board and the 386 PC. It samples the SSH16 hold signals, converts them to 12 bit digital signals and saves the digital signals into PC memory arrays. When the signal full scale is 10 volts, the sampling resolution is 2.44 mV/bit, which is appropriate for this application. The AD16 sampling frequency are 511 ns, 1.02 ms, 32.77 ms, and 1.05 s corresponding to the 2^9-1 , $2^{10}-1$, $2^{15}-1$, and $2^{20}-1$ 1 MHz PRC respectively. Other than data sampling, the AD16 board also controls the PRC delay time and the laser shutter switch through a digital I/O connector. Therefore, the AD16 assists the automatic data collection.

The combination of SSH16 and AD16 realizes the simultaneous and automatic data collection, which makes the whole experimental system more reliable and efficient.

4.4.3 Computer software processing

The data processing software includes the data sampling codes and data processing codes. Practically, the data sampling codes control the whole data collection procedure, which are range finding, channel calibration, and data recording. Their codes, named as `prctds3.for`, `calib.for`, and `records4.for`, are listed in Appendix C. After the data collection, the data files are transferred to the EEAP Unix system. The data processing program, named as `p4.c` in Appendix C, calculates the normalized receiving laser intensity and the corresponding turbulence strength. The developed software successfully supports the signal collecting and the data processing.

4.5 Calibrating subsystem

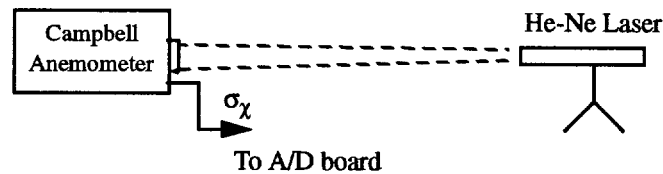


Figure 4-5: The calibrating subsystem

The calibrating subsystem consists of a CA-9 Space Averaging Anemometer and a He-Ne laser, as shown in Fig. 4-5. It provides the path averaging turbulence strength for calibrating the developed experiment system. The CA-9 anemometer measures the strength of the turbulence fluctuations, σ_χ , in the line-of-sight propagation. Inside the CA-9 anemometer, the σ_χ -card detects the turbulence strength by log-amplifying and averaging the received optical field. The relation between the σ_χ and C_n^2 is given by

$$C_n^2 = 1.24 \times 10^{-12} \left(\frac{500}{z} \right)^{11/6} \sigma_\chi^2 \quad (4-4)$$

where z is the propagation path length in meters.

The He-Ne laser provides the light source for the CA-9 unit. Its output power is about 5 mW and its wavelength is 632.8 nm. In the experiment, the He-Ne laser locates close to the target and the anemometer is mounted close to the receiver. By this configuration, the path averaged turbulence strength measured by the CA-9 anemometer represents the field turbulence strength. The combination of the measured turbulence strength and the received laser intensity are used to validate the developed single-ended turbulence measurement method.

CHAPTER 5

Experimental Results

5.1 Introduction

By using the experimental system described in Chapter 4, we conducted experiments to measure the range resolving capability and the turbulence strength. These experiments were performed at the OGI laser remote sensing lab and in the nearby fields. The range resolution experiments (Section 5.2) are done in both high SNR (Section 5.2.1) and low SNR conditions (Section 5.2.2). Similarly, the turbulence measurement was also performed in both high SNR (Section 5.3.1) and low SNR (Section 5.3.2) situations. The results of both range resolution and turbulence measurements are illustrated and discussed in this chapter.

5.2 Range resolution

The range resolution experiments detected the laser beam scattering profile along its propagation path by decoding the received PRC-modulated laser signals. It can locate strong scattering sources, such as a hard target, screen targets, or aerosols. Based on the detected target locations, we can select the PRC delay time t_d to be used for the turbulence strength measurements. The range resolution experimental system is similar to the turbulence measurement experimental system. There are only two major differences. First of all, since range resolution does not require turbulence information, its experimental set-up does not include the calibrating system (Section 4.5). Secondly, because range resolution

does not need to separate the target induced scattering field and turbulence-induced scattering field, the experimental system does not need the optical spatial filter.

In our research, we utilized range resolution to locate different reflecting targets. Among them, the high-reflection target is a hard target covered with Scotch light (~ 90% reflection coefficient). The medium reflecting target is a sand-blasted aluminum plate (~ 10% reflection coefficient). The low-reflecting target is a screen target, which can both reflect (~0.1% reflection) and transmit a laser beam. It is important to point out that only one Scotch light target or one aluminum plate can be used in a single-hard-target experiment, while more than one screen targets can be applied in one experiment to simulate a distributed-target situation.

5.2.1 Single-hard-target range resolution

The single-hard-target range finding is useful to verify the range resolving capability of the developed experimental system. This is because in high SNR situations, it is easy to detect system defects. The experiment uses a Scotch light target or a sand-blasted aluminum plate to examine the system performance by comparing the measured and calculated delay time corresponding to the range of hard target. In the experiment, the distance between the hard target and receiver is about 240 meters. The PRC code period is 511 μ s and its pulse width is 1 μ s. According to the PRC pulse width and the target distance, the PRC delay time corresponding to the target should be the round-trip propagation distance divided by the speed of light

$$t_d = 2 \times 240 \text{ (m)} / 3 \times 10^8 \text{ (m/s)} = 1.6 \text{ (\mu s)} \quad (5.1)$$

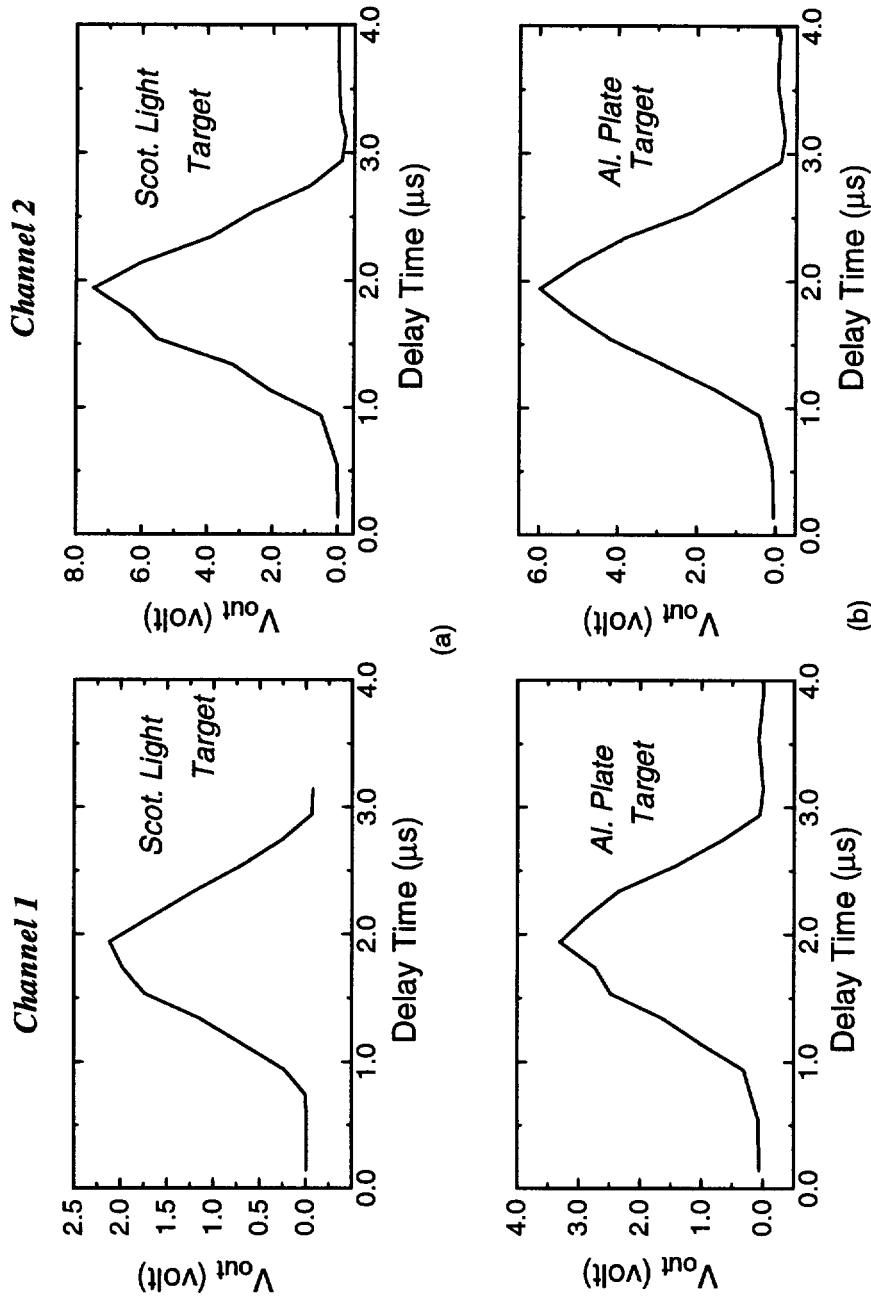


Figure 5-1: The single-hard-target range resolution result, laser intensity in channel 1 and channel 2 (11/23/93) (a) Scotch light hard target, (b) Sand-blasted aluminium hard target

Based on the above calculation, we swept the PRC delay time from 0 to 4.0 μs with a 0.2 μs time step during the experiment. After subtracting the background signal, the measured laser intensity due to the PRC delay time variation is shown in Figure 5-1. In the figure, the X-axis represents the PRC delay time with 0.2 μs time resolution. The Y-axis denotes the received signal after removing the signal due to background light. This figure shows that the received laser intensity curves are triangles with a $\pm 1 \mu\text{s}$ base time, which is consistent with that predicted from the theory (see Section 2.4.2). Also, the figures display that the PRC delay time corresponding to the target location is 1.9 μs for both the Scotch light and aluminum targets. It is slightly different from the evaluated 1.6 μs according to Equation 5-1. The 0.3 μs difference is due to the delay offset in the system. Therefore, the measured PRC delay (1.9 μs) is the summation of both propagation delay (1.6 μs) and the system delay offset (0.3 μs). Obviously, when using the measured delay time to calculate the target location, we must use the propagation delay time. Moreover, the received laser intensities vary from channel to channel, due to the fact that the gain of each channel is different. Over all, the experiment confirms that the developed experiment system is able to successfully fulfill the range resolving task under conditions of high reflection (Scotch light hard target) and medium reflection (sand-blasted aluminum target).

5.2.2 Multiple-screen-targets range resolution

In the previous experiment, we demonstrated that the developed system could successfully locate a target under high SNR conditions. This experiment tested the system performance under low SNR situations. In this experiment, we put two window screen targets along the laser propagation path. The two screens were located at about 110 meters and 450 meters from the receiver. The distance between them was chosen to be

greater than the range finding resolution (300 m). In order to detect the low SNR signal, we used a long code length PRC ($2^{15}-1$), which had a 32-ms code period, to both suppress the background signal and enhance the laser signal. In addition, we conducted the experiment at night in order to eliminate the sunlight-related background noise. Based on the above experiment conditions, we estimated the required PRC delay time of the two screens to be about 1.1 μs and 3.3 μs respectively.

Figures 5-2 and 5-3 present two range finding results conducted on Feb. 2, 1995. Both plots show the three high reflecting areas along the propagation path. The first peak, corresponding to the 1.0- μs delay time, is the reflecting signal from the first screen target; the second peak, corresponding to 3.3- μs delay time, is from the second screen target; the third peak is around 5.3 μs to 5.5 μs . The last peak matches the distance from 750 meters to 780 meters in the laser propagation path, where several new houses were located. Apparently, the third peak results from the reflections from these houses.

The received laser intensity also confirms the relationship between the peak intensity and the corresponding targets. Because the two screen targets have the same reflection coefficients, the range finding intensities are inversely proportional to the square of the distance between the target and the receiver. Theoretically, the ratio of the second peak intensity over the first peak intensity is about $(100/450)^2 = 5\%$. The ratios evaluated from Figures 5-2 and 5-3 are about 4.4% ~ 5%, which validate the peak-target corresponding relationship. For the house reflecting signal, we can not estimate the peak-peak ratio, because we don't know the house-reflecting coefficient. Actually, the experiment shows that the peak intensity reflected from the house is about the same level as that of the second screen target. Therefore, the houses must have a higher coefficient of reflection. In summary, both the peak locations and their relative intensities prove that the developed experimental system is capable of range finding under low SNR conditions.

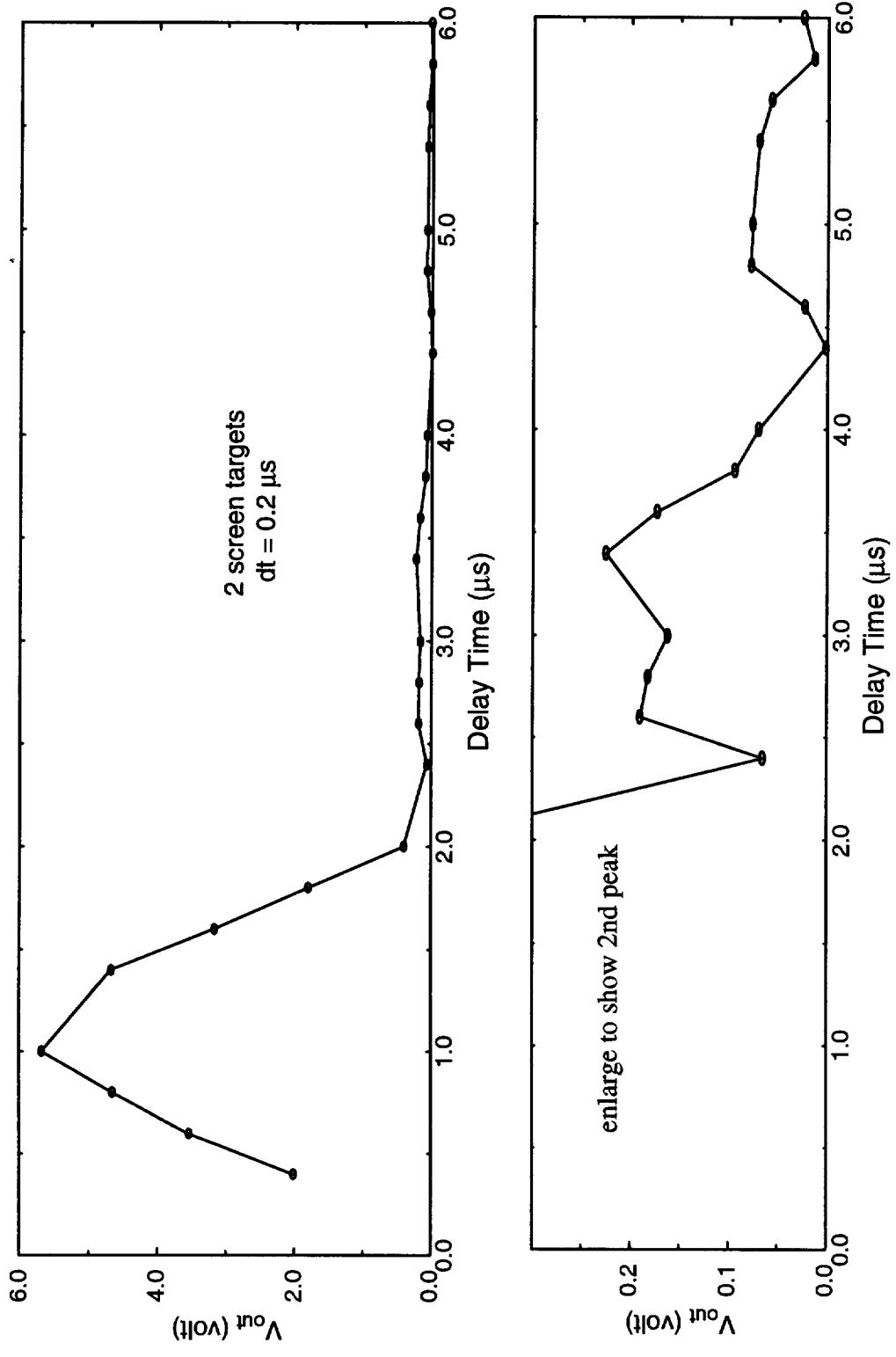


Figure 5-2: Experiment results for screen target range resolving (2/2/95) data set 1

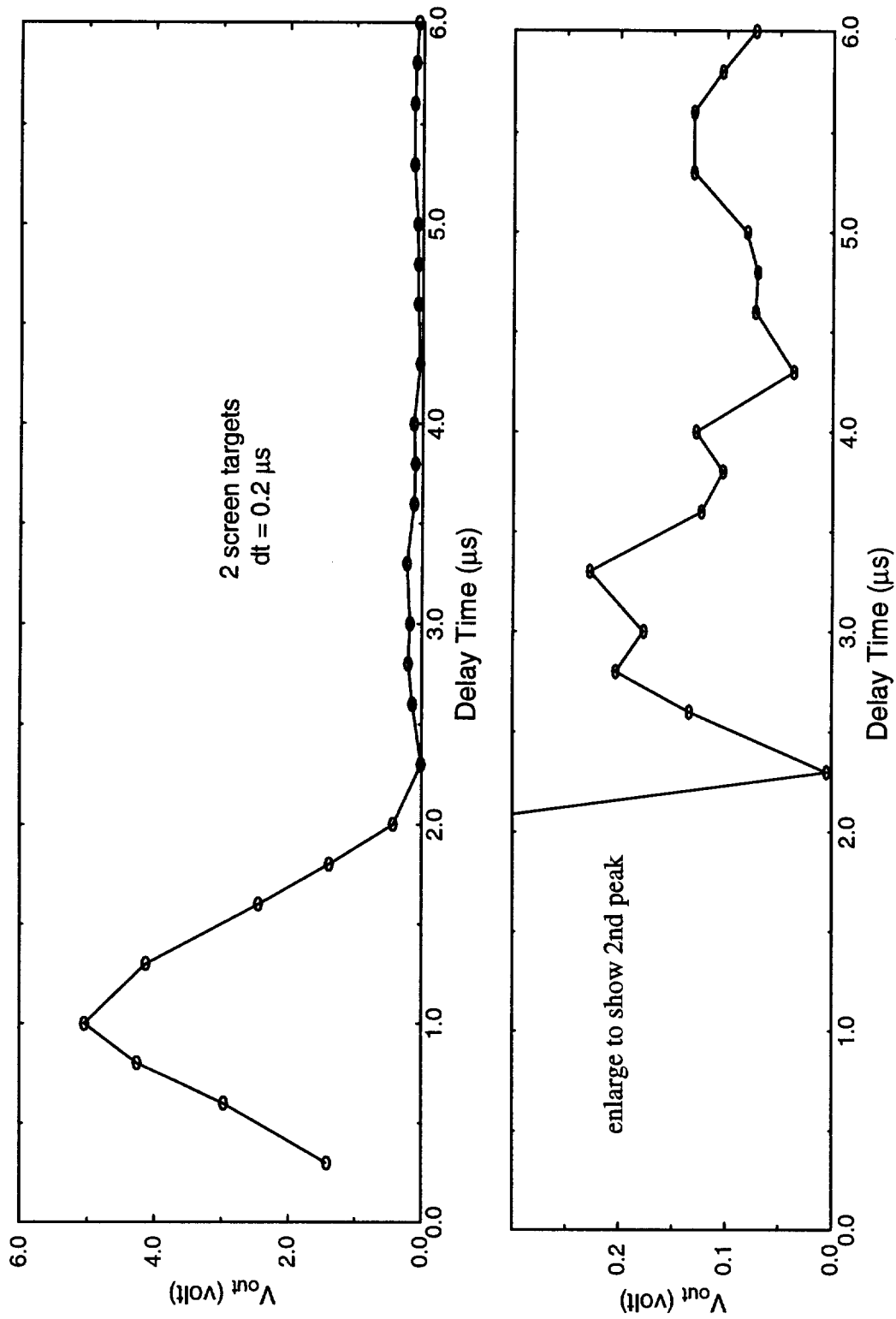


Figure 5-3: Experiment results for screen target range resolving (2/2/95) data set 2

5.3 Turbulence Strength Measurements

The second application of the experimental system is to measure the turbulence strength. Unlike range finding, turbulence measurements require (a) the optical filter to block the target speckle field, (b) the two data-recording-channels to normalize the filtered laser intensity, and (c) the calibration system to verify the theoretical estimation of turbulence strength. The entire experimental system is described in Chapter 4, which is used to measure turbulence strength in both higher SNR and lower SNR situations. For high SNR cases, we use the Scotch light hard target, while for the low SNR case, we utilize the screen target. The experimental results are discussed in Section 5.3.1 and Section 5.3.2.

5.3.1 Turbulence measurement in cases of high SNR

The experimental system to measure turbulence strength was first tested under high SNR conditions. In this experiment, we used a Scotch light as the hard target, which was located about 240 m from the receiver. Also, the calibration system was set up to monitor the path-averaged turbulence strength by placing the He-Ne laser near the target and the CA-9 unit close to the receiver. In addition, the PRC code length was $2^{10}-1$ and its total code period was about 1 ms.

The entire experimental procedures can be divided into three steps. The first step is to align the optical system, which is critical in getting reliable results. The second step is to calibrate both channels, which accounts for the two channel gain-difference. The final step is to record data, which is fully controlled by a 386PC. The recorded data signals are the filtered intensity, I_f , unfiltered intensity, I_0 , and the log amplitude standard

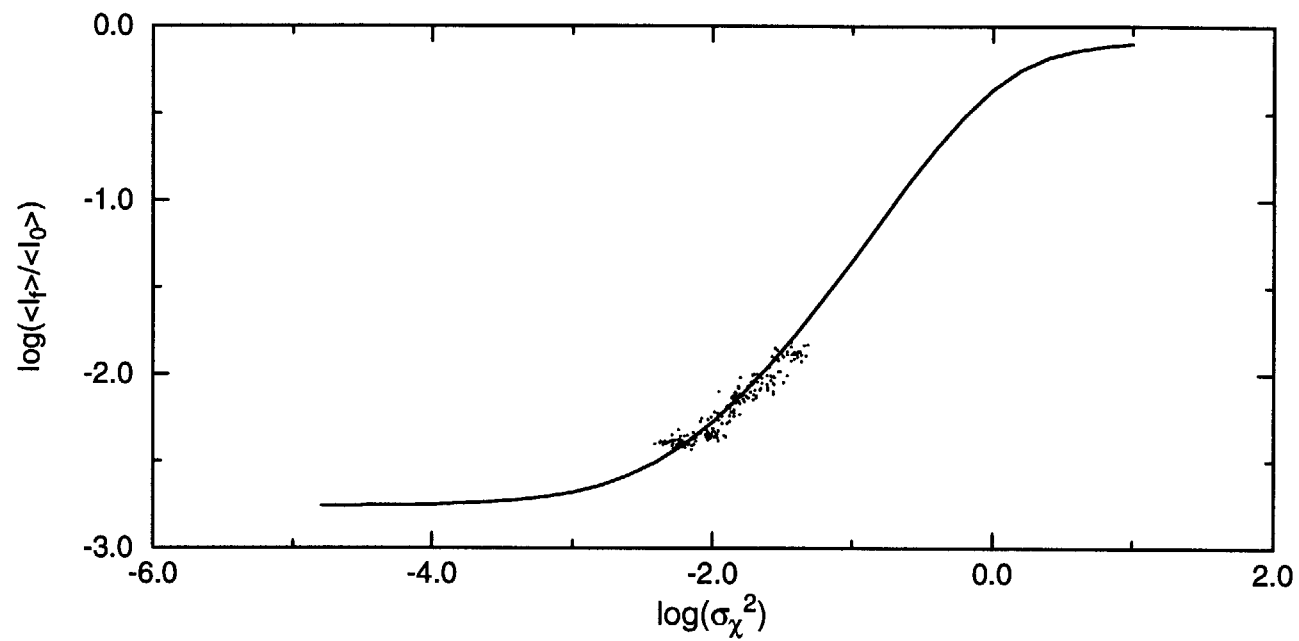


Figure 5-4: Turbulence measurement under high SNR situations. Solid line is the theoretical curve, dos are the experimental results (9/7/94)

deviation, σ_χ (see section 4.5). The relation between the σ_χ and C_n^2 is given by Equation (4-4). The details of the data-recording procedure are described in Appendix D.

The recorded data for the high SNR experiment is plotted in Figure 5-4. In this figure, the X-axis is the log-scale of path-average of (σ_χ^2) measured by the CA-9 unit. The Y-axis represents $(\log(I_f/I_0))$. The solid-line denotes the theoretical estimation for the experiment condition, based on the analysis in Chapter 3, while the dots represent the measured data. Each dot is the average of 400 data points and each data points is the integrated laser intensity over 1 ms period. During this experiment, $\log(\sigma_\chi^2)$ changes from -2 to -1, corresponding to medium turbulence strengths. The recorded data is very close to the theoretical estimation, demonstrating that the system can be used to measure σ_χ^2 which is proportional to the strength of turbulence C_n^2 .

5.3.2 Turbulence measurements in the cases of low SNR

Our final goal is to accomplish low SNR turbulence measurements. Therefore, this experiment uses the screen target to simulate low SNR conditions. Also, we use a longer code-length PRC ($2^{15}-1$), which is 32 times longer than the PRC code used in the high SNR case. Note that the periods of low SNR PRC and the high SNR PRC are 32 ms and 1 ms, respectively. Moreover, the experiment is done during a sunny day in the summer of 1995, when the background noise is much stronger than the screen-target backscattering signal. All other experimental conditions are similar to those of the high SNR situation. Following the same experimental procedures described in the previous section, we measure the atmospheric turbulence strength (see Figure 5-5).

This figure shows that the system is capable of estimating turbulence strength under low SNR situations. The measured signal intensity agrees with the theoretical cal-

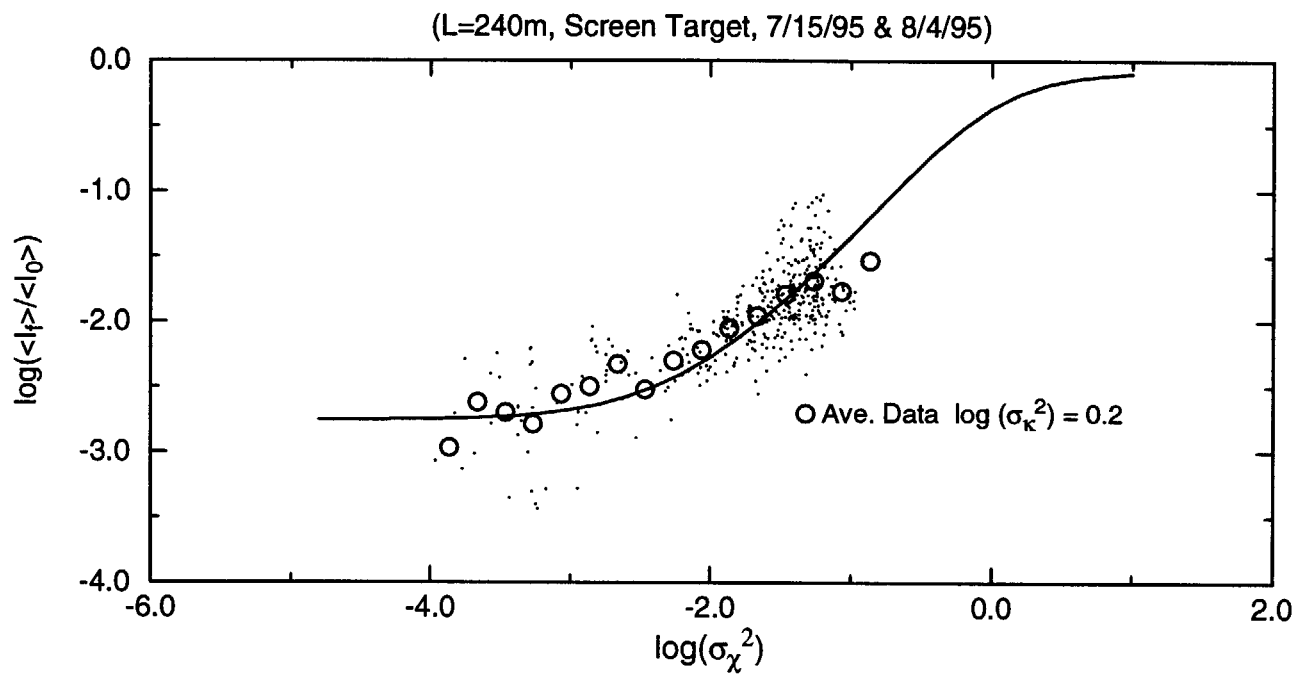


Figure 5-5: Turbulence measurement under low SNR situations. Solid line is the theoretical curve, dos are the experimental results.

ulation. This is shown by the measured dot-data which varies according to the calculated solid line. Also, the average signal intensity over the step $\Delta\left(\log\left(\sigma_x^2\right)\right)=0.2$, denoted by the circle, averages some of the noise and improves the fit between the measured intensity and the theoretical estimation. Therefore, we can estimate the turbulence strength by measuring the target-reflected-laser-signal using the optical spatial filtering system.

Notice that the data fluctuations due to weak turbulence is stronger than the data fluctuation of the strong turbulence. The reason is that both spot dancing and beam spread are weaker under low turbulence than under high turbulence. In fact, the optical spatial filter blocks most of the received laser signal under low turbulence. As a result, when the turbulence level is low, the received signal is dominated by the background noise.

Clearly, the noise reduction is the limiting factor in improving the system performance. The noise sources include the sunlight background, the PMT dark current, and the circuit noise. In the system design, many approaches have been made to suppress these noises. First, we applied a ± 8.8 nm wavelength filter to minimize sunlight-related noise. Secondly, we cover the receiving fiber with a black jacket to block the background light. Finally, we improved the circuit layout and shielded the 1 MHz PRC source to reduce the pick-up noise of the circuits. By applying these noise reduction techniques, it is possible to measure turbulence strength under low SNR conditions.

5.4 Target speckle image reduction

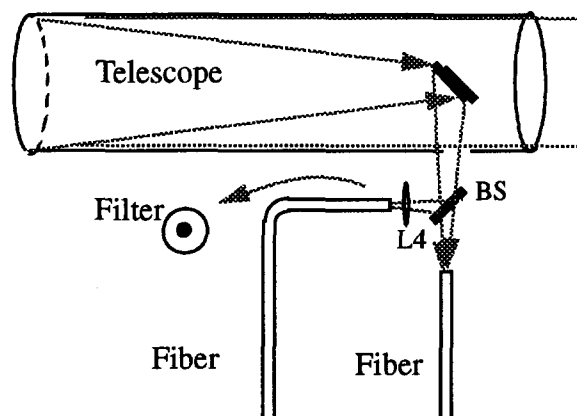


Figure 5-6: Modified receiver system. The de-magnification lens L_4 is inserted between telescope and the receiving fiber

Although we assume the laser beam is a perfect collimated beam in the theoretical analysis, it is impossible to accomplish it in reality. Practically, the laser source is a diverging beam, which makes the laser spot size at the target larger than the theoretical size. Consequently, the spot size at the telescope's image plane is larger than the theoretical prediction. As a result, the designed optical spatial filter can not efficiently block the target speckle field. In order to reduce the spot size in the image plane, we placed another lens (L_4) between the telescope lens and the receiver fiber to de-magnify the image spot size (see Fig. 5-6). After the spot size de-magnification, we were able to achieve the desired turbulence detecting dynamic range. The lens we used is a symmetric convex lens with 5 mm diameter and 10 mm focal length. The image-spot-size-reduction increases the dynamic range of measurements and allows turbulence measurements under both low and high SNR situations possible.

CHAPTER 6

Summary and Conclusion

In this research, we have developed the theory needed to characterize and construct a single-ended atmospheric-turbulence-remote-sensing system. Based on the theory, we designed and developed an electro-optic system. In the experimental system, a PRC-modulated laser beam is transmitted into the atmosphere. The beam is backscattered by a low reflecting target. The received signals are optically filtered and electronically demodulated to estimate the turbulence profile along the laser propagation path. In addition, we carried out experiments to verify the theory and tested the experimental system using both high and low reflecting targets. Both the theoretical analysis and the experimental results lead to the following conclusions.

(1) In the single-ended detection system, the received intensities consist of both the target-induced speckle field and the turbulence-induced field. When turbulence strength is in the weak and medium levels, the received intensities are dominated by the target-induced speckle field. Therefore, the measured intensities alone can not estimate the turbulence strength.

(2) A high-pass optical-spatial-filter, at the image plane of the telescope, can be used to block the target-induced speckle field. Optically filtered, the normalized received intensity (in log scale) is linearly related to the path averaged turbulence strength (in log scale). The linear dynamic range strongly depends on the optical spatial filter size. A large filter size results in a wide dynamic range. By applying the high-pass filter, we are able to measure the turbulence profile along the laser propagation path.

(3) In addition to the filter size, the detected dynamic-range is also determined by the transmitted laser beam size and the transmission path length. A small laser beam size and a long path length lead to a wide dynamic range. When these parameters and optical filter size are properly selected, we can estimate the turbulence strength from the received laser intensity.

(4) The proposed PRC modulation method can accomplish the turbulence spatial variation measurement and enhance the detected SNR. The PRC pulse-width determines the range resolution. A short PRC pulse-width decreases the range bin size. Meanwhile, the PRC code-length affects the system SNR. A long code-length PRC raises the ratio of the signal over background noise.

(5) A polychromatic laser source, such as a laser diode or a LED, can be used in this application. The theoretical analysis suggests that the received intensity is little affected by the polychromatic condition ($680 \text{ nm} < \lambda < 700 \text{ nm}$). Therefore, this polychromatic source does not degrade the measurement accuracy.

(6) The developed experimental system is an effective and reliable turbulence detection system. In the system, the coaxial fiber-optic transmitter and receiver provide a stable experimental apparatus. Additionally, the computer coordinates the electro-optic subsystems to support high speed real-time turbulence measurements. Practically, this design makes it possible to build a compact turbulence detector.

REFERENCES

1. G. P. Agrawal, Fiber-Optic Communication Systems, John Wiley & Sons, Inc., 1992, pp. 34-35.
2. D. N. Asimakopoulis, R. S. Cole, S. J. Caughey, and B. A. Crease, "A Quantitative Comparison Between Acoustic Sounder Returns and the Direct Measurement of Atmospheric Temperature Fluctuations", Boundary Layer Meteorol., Vol. 10, 1976, pp. 137.
3. D. Atlas, K. R. Hardy, K. M. Glover, I. Katz, and T. G. Konrad, "Tropopause Detected by Radar", Science, Vol. 153, 1966, pp. 1110.
4. M. Azouit, J. Vernin, R. Barletti, G. Ceppatelli, A. Righini, and N. Speroni, "Remote Sensing of Atmospheric Turbulence By Means of a Fast Optical Method: a Comparison With Simultaneous, in-situ Measurements", J. Appl. Meteorol., Vol. 19, 1980, pp. 834-838.
5. B. Balsley and V. L. Peterson, "Doppler-radar Measurements of Clear Air Turbulence at 1290 MHz", J. Appl. Meteorol., Vol. 20, 1981, pp. 266.
6. R. R. Beland, "Propagation Through Atmospheric Optical Turbulence", in The Infrared and Electro-Optic Handbook, F. G. Smith, ed., Society of Photo-Optical Instrumentation Engineers, Bellingham, Wash., Vol. 2, Chap. 2, 1993, pp. 1157-1232.
7. D. W. Beran, W. H. Hooke, and S. F. Clifford, "Acoustic Echo-sounding techniques and their application to gravity-wave, turbulence, and stability studies", Boundary Layer Meteorol., Vol. 4, 1973, pp. 133.
8. E. H. Brown and F. F. Hall, Jr., "Advances in Atmospheric Acoustics", Rev. Geophys. Space Phys., Vol. 16, 1978, pp. 47.
9. J. L. Bufton, P. O. Minott, M. W. Fitzmaurice, and P. J. Titterton, "Measurements of Turbulence Profile in the Troposphere", J. Opt. Soc. Am., Vol. 62, 1972, pp. 1068.
10. R. V. Chadwick and K. P. Moran, "Long-term Measurements of C_n^2 in the Boundary Layer," Radio Sci., Vol. 15, 1980, pp. 355.
11. L. A. Chernov, Wave Propagation in a Random Medium, McGraw-Hill, New York, 1960.
12. T. Chiba, "Spot Dancing of the Laser Beam Propagated Through the Turbulent

- Atmosphere”, Appl. Opt., Vol. 10, November 1971, pp. 2456.
13. S. F. Clifford, “The Classical Theory of Wave Propagation in a Turbulent Medium”, in Laser Beam Propagation in the Atmosphere, Springer-Verlag, J. W. Strohben, ed., New York, Ch. 2, 1978a, pp. 21-23.
 14. S. F. Clifford, “The Classical Theory of Wave Propagation in a Turbulent Medium”, in Laser Beam Propagation in the Atmosphere, Springer-Verlag, J. W. Strohben, ed., New York, Ch. 2, 1978b, pp. 39-41.
 15. S. F. Clifford, “The Classical Theory of Wave Propagation in a Turbulent Medium”, in Laser Beam Propagation in the Atmosphere, Springer-Verlag, J. W. Strohben, ed., New York, Ch. 2, 1978c, pp. 37.
 16. S. F. Clifford and J. H. Churnside, “Refractive Turbulence Profiling Using Synthetic Aperture Spatial Filtering of Scintillation,” Appl. Opt., Vol. 26, 1987, pp. 1295-1303.
 17. D. Draper, J. F. Holmes, J. Hunt, and J. Peacock, “Simple Two-Laser Optical Heterodyne System with Large Transmitter-Local Oscillator Isolation”, Appl. Opt., Vol. 19, Oct. 1989, pp. 4048-4050.
 18. J. R. Dunphy, Propagation of Laser Radiation through Atmospheric Turbulence, Ph.D thesis, Dept. of EEAP, OGI, 1974, pp. 52.
 19. D. L. Fried, “Remote Probing of the Optical Strength of Atmospheric Turbulence and of Wind Velocity,” Proc. IEEE, Vol. 57, 1969, pp. 415.
 20. M. Fukushima, Kin-ichiro Akita, and H. Tanaka, “Night-time Profiles of Temperature Fluctuations Deduced from Two-year Solar Observation,” J. Meteorol. Soc. Jpn. Vol. 53, 1975, pp. 487.
 21. K. S. Gage and B. B. Balsley, “Doppler Radar Probing of the Clear Atmosphere,” Bull. Am. Meteorol. Soc., Vol.59, 1978, pp.1074.
 22. G. W. Gilman, H. B. Coxhead, and F. H. Willis, “Reflection of Sound Signals in the Troposphere,” J. Acoust. Soc. Am., Vol. 18, 1946, pp. 274.
 23. R. E. Good, B. J. Watkins, A. F. Quesada, J. H. Brown, and G. B. Loriot, “Radar and Optical Measurements of C_n^2 ,” Appl. Opt., Vol. 21, No. 18, 1982, pp. 3373-3376.
 24. J. W. Goodman, Introduction to Fourier Optics, McGraw-Hill, Inc., 1968a, pp. 59.
 25. J. W. Goodman, Introduction to Fourier Optics, McGraw-Hill, Inc., 1968b, pp. 80.

26. E. E. Gossard, R. B. Chadwick, T. R. Detman, and J. Gaynor, "Capability of surface-based Clear-air Doppler Radar for Monitoring Meteorological Structure of Elevated Layers", J. Climate Appl. Meteorol. Vol. 23, 1984, pp. 474.
27. E. E. Gossard, J. E. Gaynor, R. J. Zamora, and W. D. Neff, "Fine Structure of Elevated Stable Layers Observed by Sounder and in situ Tower Sensors", J. Atmos. Sci., Vol. 42, 1985, pp. 2156.
28. V. S. R. Gudimetla, J. F. Holmes, M. E. Fossey, and P. A. Pincus, "Covariance of the Received Intensity of a Partially Coherent Laser Speckle Pattern in the Turbulent Atmosphere", Appl. Opt., Vol. 30, No. 9, March 1992, pp. 1286-1293.
29. K. R. Hardy and I. Katz, "Probing the Clear Atmosphere with High Power, High Resolution Radars", Proc. IEEE, Vol. 57, 1969, pp. 468-480.
30. J. F. Holmes, "Enhancement of Backscattered Intensity for a Bistatic LIDAR Operating in Atmospheric Turbulence", Appl. Opt., Vol. 30, No. 18, June 1991, pp. 2643-2646.
31. J. F. Holmes, F. Amzajerjian, and J. M. Hunt, "Improved Optical Local-Oscillator Isolation Using Multiple Acousto-Optic Modulator and Frequency Diversity", Opt. Lett., Vol. 12, No. 8, Aug. 1987, pp. 637-639.
32. J. F. Holmes, M. H. Lee, and J. R. Kerr, "Effect on the Log-Amplitude Covariance Function on the Statistics of Speckle Propagation Through the Turbulence Atmosphere", J. Opt. Soc. Am., Vol. 70, April 1980, pp. 355-360.
33. J. F. Holmes and B. J. Rask, "Optimum, Optical Local Oscillator Levels for Coherent Detection Using Photodiodes", Appl. Opt., Vol. 34, No. 6, February 1995, pp. 927-933.
34. R. A. Kropfli, I. Katz, T. G. Konrad, and E. B. Dobson, "Simultaneous Radar Reflectivity Measurements and Refractive Index Spectra in the Clear Atmosphere", Radio Sci., Vol. 3, 1968, pp. 991.
35. J. A. Lane, "Radar Echoes from Tropospheric Layers by Incoherent Backscatter", Electron. Lett. Vol.3, 1967, pp. 173
36. R. S. Lawrence, G. R. Ochs, and S. F. Clifford, "Measurements of Atmospheric Turbulence Relevant to Optical Propagation", J. Opt. Soc. Am., Vol. 60, 1970, pp. 826-830.
37. M. H. Lee, J. F. Holmes, and J. R. Kerr, "Statistics of Speckle Propagation Through

- the Turbulent Atmosphere”, J. Opt. Soc. Am., Vol. 66, November 1976, pp. 1164-1169.
38. R. W. Lee, “Remote Probing Using Spatially Filtered Apertures”, J. Opt. Soc. Am., Vol. 64, No. 10, Oct. 1974, pp. 1295-1303.
 39. C. G. Little, “Acoustic Methods for the Remote Probing of the Lower Atmosphere”, Proc. of IEEE, Vol. 57, No. 4, April 1969, pp. 571-578.
 40. R. F. Lutomirski and H. T. Yura, “Propagation of a Finite Optical Beam in an Inhomogeneous Medium”, Appl. Opt., Vol. 10, No. 7, 1971, pp. 1652-1658.
 41. R. F. Lutomirski and H. T. Yura, “Wave Structure Function and Mutual Coherence Function of an Optical Wave in a Turbulent Atmosphere”, J. Opt. Soc. Am., Vol. 61, 1971, pp. 482-487.
 42. F. J. MacWilliams and N. J. A. Sloane, “Pseudo-Random Sequences and Arrays”, Proceedings of The IEEE, Vol. 64, No. 12, December 1976, pp. 1715-1729.
 43. Donald E. Martens, Implementing a Pseudo-Random Modulation Code to an Existing Optical Signal Processing System, MS thesis, Dept. of EEAP, OGI, Sept. 1991.
 44. L. G. McAllister, “Acoustic Sounding of the Lower Troposphere”, J. Atmos. Terr. Phys. Vol 30, 1968, pp. 1439.
 45. L. G. McAllister, J. R. Pollard, A. R. Mahoney, P. J. R. Shaw, “Acoustic Sounding--A New Approach to the Study of Atmospheric Structure”, Proc. of IEEE, Vol. 57, No. 4, April 1969, pp. 579-587.
 46. A. H. Mikesell, A. A. Hoag, and J. S. Hall, “The Scintillation of Starlight”, J. Opt. Soc. Am., Vol. 41, No. 10, 1951, pp. 689-695.
 47. C. Nagasawa, M. Abo, H. Yamamoto, and O. Uchino, “Random Modulation cw Lidar Using New Random Sequence”, Appl. Opt., Vol. 29, No. 10, April 1990, pp. 1466-1470.
 48. G. R. Ochs, “Measurements of 0.63 μm Laser-Beam Scintillation in Strong Atmospheric Turbulence”, ESSA Tech. Report, ERL 154-WPL, Vol. 10, 1970.
 49. G. R. Ochs, Ting-i Wang, R. S. Lawrence, and S. F. Clifford, “Refractive Turbulence Profiles Measured by One-Dimensional Spatial Filtering of Scintillation”, Appl. Opt., Vol. 15, 1976, pp. 2504.

50. A. Peskoff, "Theory of Remote Sensing of Clear-Air Turbulence Profiles", J. Opt. Soc. Am., Vol. 58, 1968, pp. 1032.
51. W. M. Protheroe, "The Motion and Structure of Stellar Shadow-band Patterns", Q. J. R. Meteorol. Soc., Vol. 90, 1964, pp. 27.
52. A. Rocca, F. Roddier, and J. Vernin, "Detection of Atmospheric Turbulent Layers by Spatiotemporal and Spatioangular Correlation Measurements of Stellar-Light Scintillation", J. Opt. Soc. Am., Vol. 64, 1974, pp. 1000.
53. D. E. Quinn, "Optical Fibers", in Fiber Optical Handbook for Engineers and Scientists, Ed. by F.C. Allard, McGraw-Hill, Inc., 1990, pp. 1.18.
54. Liang-chi Shen, "Remote Probing of Atmosphere and Wind Velocity by Millimeter Waves", IEEE Trans. Antennas Propag., AP-18, 1970, pp. 493.
55. J. W. Strohbehn, "Remote Sensing of Clear-Air Turbulence", J. Opt. Soc. Am. Vol. 60, 1970, pp. 948.
56. L. Sun, The Effect of Optical Spatial Filtering on the Statistics of Laser Radiation Propagating through the Turbulent Atmosphere, Ph.D Dissertation. Dept. of EEAP, Oregon Graduate Institute of Science and Technology, 1988.
57. H. R. D. Sunak, "Fiber-Optic Systems Design", in Fiber Optical Handbook for Engineers and Scientists, Ed. by F.C. Allard, McGraw-Hill, Inc., 1990, pp. 9.19.
58. V. I. Tatarskii, Wave Propagation in a Turbulent Medium, McGraw-Hill Book company, Inc., 1961a, pp. 58.
59. V. I. Tatarskii, Wave Propagation in a Random Medium, McGraw-Hill, New York, 1961b.
60. V. I. Tatarskii, Wave Propagation in a Random Medium, McGraw-Hill, New York, 1961c, pp. 57-58.
61. A. A. Townsend, "The Interpretation of Stellar Shadow-bands as a Consequence of Turbulence Mixing", Q. J. R. Meteorol. Soc., Vol. 91, 1965, pp. 1.
62. T. E. VanZandt, J. L. Green, K. S. Gage, and W. L. Clark, "Vertical Profiles of Refractivity Turbulence Structure Constant: Comparison of Observations by the Sunset Radar with a new Theoretical Model", Radio Sci., Vol. 13, 1978, pp. 819.
63. J. Vernin and F. Roddier, "Experimental Determination of Two-Dimensional

- Spatiotemporal Power Spectra of Stellar Light Scintillation. Evidence for a Multi-layer Structure of Air Turbulence in the Upper Troposphere”, J. Opt. Soc. Am., Vol. 63, 1973, pp. 270.
64. S. Vogt, P. Thomas, “SODAR - A Useful Remote Sounder to Measure Wind and Turbulence”, J. Wind Eng. Ind. Aerodyn. Vol. 54/55, 1995, pp. 163-172.
 65. D. L. Walters, “Measurements of Optical Turbulence with Higher-order Structure Functions”, Applied Optics, Vol. 34, No. 9, March 1995, pp. 1591-1597.
 66. Ting-i Wang, S. F. Clifford, and G. R. Ochs, “Wind and Refractive-Turbulent Sensing Using Crossed Laser Beam”, Appl. Opt., Vol. 13, 1974, pp. 2602.
 67. H. Weichel, Laser Beam Propagation in the Atmosphere, SPIE, 1990a, pp. 54.
 68. H. Weichel, Laser Beam Propagation in the Atmosphere, SPIE, 1990b, pp. 61.
 69. H. T. Yura, “Mutual Coherence Function of a Finite Cross Section Optical Beam Propagating in a Turbulent Medium”, Appl. Opt., Vol. 11, No. 6, 1972, pp. 1399-1406.
 70. H. T. Yura, “Atmospheric Turbulence Induced Laser Beam Spread”, Appl. Opt., Vol. 10, December 1971, pp. 2771.

Appendix A

A.1 Intensity distribution

In Chapt3, the mean intensity distribution in Equation 3-12 is given by

$$\begin{aligned}
 \langle I(\mathbf{u}, z, t, k) \rangle &= \left(\frac{k^4}{16\pi^4 z^2 f_1 d} \right)^2 PRC\left(t - \frac{2z + f_1 + d}{c}\right) \int d\mathbf{x}_1 \int d\mathbf{x}_2 \\
 &\bullet \exp\left(-\frac{ik}{2f_1}(x_1^2 - x_2^2)\right) \exp\left(i\frac{k}{2f_1}(|\mathbf{x}_1 - \mathbf{q}_1|^2 - |\mathbf{x}_2 - \mathbf{q}_2|^2) + i\frac{k}{2d}(|\mathbf{u} - \mathbf{x}_1|^2 - |\mathbf{u} - \mathbf{x}_2|^2)\right) \\
 &\int dq_1 \int dq_2 \int dp_1 \int dp_2 \int dr_1 \int dr_2 \exp\left(-\left(\frac{q_1^2 + q_2^2}{q_0^2}\right)\right) \exp\left(\frac{ik}{2z}(q_1^2 - q_2^2)\right) \\
 &\bullet \langle g(\mathbf{p}_1, z) g^*(\mathbf{p}_2, z) \rangle \exp\left(\frac{ik}{z}(p_1^2 - p_2^2)\right) \exp\left(-\frac{ik}{z}(\mathbf{p}_1 \cdot \mathbf{r}_1 + \mathbf{q}_1 \cdot \mathbf{p}_1 - \mathbf{p}_2 \cdot \mathbf{r}_2 - \mathbf{q}_2 \cdot \mathbf{p}_2)\right) \\
 &\bullet \langle \exp\left(\Psi_1(\mathbf{p}_1, \mathbf{r}_1) + \Psi_1^*(\mathbf{p}_2, \mathbf{r}_2) + \Psi_2(\mathbf{q}_1, \mathbf{p}_1) + \Psi_2^*(\mathbf{q}_2, \mathbf{p}_2)\right) \rangle \exp\left(-\frac{r_1^2 + r_2^2}{2a_0^2}\right) \\
 &\bullet \exp\left(-\frac{ik}{2}\left(\frac{1}{F} - \frac{1}{z}\right)(r_1^2 + r_2^2)\right)
 \end{aligned}$$

(A-1)

For simplifying Equation 1, we need to calculate the integration over \mathbf{x}_1 , which is denoted by I_{x_1} , as following

$$\begin{aligned}
Ix_1 &= \int_0^{q_0} dx_1 \exp\left(-\frac{ik}{2f_1}(x_1^2 - x_1^2) - \frac{ik}{f_1}x_1q_1 + \frac{ik}{2f_1}q_1^2 + \frac{ik}{2d}(u_1^2 - 2(u \cdot x_1) + x_1^2)\right) \\
&= \int_0^{q_0} dx_1 \exp\left(\frac{ik}{2d}\left|x_1 - \frac{d}{f_1}q_1 - u\right|^2\right) \exp\left(\frac{ik}{2f_1}\left(\left(1 - \frac{d}{f_1}\right)q_1^2 - (2q_1 \cdot u)\right)\right)
\end{aligned}$$

(A-2)

In the above equation

$$\int_0^{q_0} dx_1 \exp\left(\frac{ik}{2d}\left|x_1 - \frac{d}{f_1}q_1 - u\right|^2\right) = \left(\sqrt{\frac{2d}{k}}\right)^2 \int_0^{\sqrt{\frac{k}{2d}}q_0} d\left(\sqrt{\frac{k}{2d}}x_1\right) \exp\left(i\left(\sqrt{\frac{k}{2d}}\left|x_1 - \frac{d}{f_1}q_1 - u\right|\right)^2\right)$$

(A-3)

Applying $\sqrt{\frac{k}{2d}}q_0 \rightarrow \infty$ and $\int_0^{\infty} \exp(ix^2) dx = \frac{2}{\sqrt{2\pi}}(1+i)$, yield

$$Ix_1 = \frac{\pi d}{2k}(1+i) \exp\left(\frac{ik}{2f_1}\left(\left(1 - \frac{d}{f_1}\right)q_1^2 - 2q_1 \cdot u\right)\right)$$

(A-4)

Obviously, the integration over x_2 gives the similar results. Substituting these results and Equations 3-3 and 3-13 into Equation 1, the intensity distribution at the image plane is rewritten as

$$\begin{aligned}
\langle I(\mathbf{u}, z, t, k) \rangle &= \frac{k^6 g^2(z)}{512\pi^6 z f_1^2} PRC\left(t - \frac{2z + f_1 + d}{c}\right) \int d\mathbf{p}_1 \exp\left(-i\frac{k}{z}(\mathbf{p}_1 \cdot (\mathbf{r}_1 - \mathbf{r}_2 + \mathbf{q}_1 - \mathbf{q}_2))\right) \\
&\int d\mathbf{q}_1 \int d\mathbf{q}_2 \int d\mathbf{r}_1 \int d\mathbf{r}_2 \exp\left(-\left(\frac{r}{\rho_0}\right)^{5/3} - \left(\frac{q}{\rho_0}\right)^{5/3}\right) \exp\left(-\frac{r_1^2 + r_2^2}{2a_0^2}\right) \exp\left(-\frac{ik}{2}\left(\frac{1}{F} - \frac{1}{z}\right)(r_1^2 - r_2^2)\right) \\
&\exp\left(-\frac{q_1^2 + q_2^2}{2q_0^2}\right) \exp\left(\frac{ik}{2z}\left(1 + \frac{z}{f_1}\left(1 - \frac{d}{f_1}\right)\right)(q_1^2 - q_2^2)\right) \exp\left(-\frac{ik}{f_1}(\mathbf{q}_1 - \mathbf{q}_2) \cdot \mathbf{u}\right)
\end{aligned} \tag{A-5}$$

By making the change of variable,

$$\begin{aligned}
\mathbf{r} &= \mathbf{r}_1 - \mathbf{r}_2 & \mathbf{q} &= \mathbf{q}_1 - \mathbf{q}_2 \\
2\mathbf{R} &= \mathbf{r}_1 + \mathbf{r}_2 & 2\mathbf{Q} &= \mathbf{q}_1 + \mathbf{q}_2
\end{aligned} \tag{A-6}$$

the mean intensity can be represented by

$$\begin{aligned}
\langle I(\mathbf{u}, z, t, k) \rangle &= \frac{k^6 T_0^2}{512\pi^6 z f_1^2} PRC\left(t - \frac{2z + f_1 + d}{c}\right) \int d\mathbf{p}_1 \exp\left(-i\frac{k}{z}(\mathbf{p}_1 \cdot (\mathbf{r} + \mathbf{q}))\right) \\
&\int d\mathbf{q} \int d\mathbf{Q} \int d\mathbf{r} \int d\mathbf{R} \exp\left(-\left(\frac{r}{\rho_0}\right)^{5/3} - \left(\frac{q}{\rho_0}\right)^{5/3}\right) \exp\left(-\frac{R^2 + \frac{1}{4}r^2}{a_0^2}\right) \exp\left(-\frac{ik}{z}\left(1 - \frac{z}{F}\right)(\mathbf{r} \cdot \mathbf{R})\right) \\
&\exp\left(-\frac{2Q^2 + \frac{1}{2}q^2}{q_0^2}\right) \exp\left(\frac{ik}{z}\left(1 + \frac{z}{f_1}\left(1 - \frac{d}{f_1}\right)\right)(\mathbf{Q} \cdot \mathbf{q})\right) \exp\left(-\frac{ik}{f_1}\mathbf{q} \cdot \mathbf{u}\right)
\end{aligned} \tag{A-7}$$

In Equation 6, the integral over variable \mathbf{Q} gives the following result

$$\begin{aligned}
& \int d\mathbf{Q} \exp\left(-\frac{2Q^2}{q_0^2}\right) \exp\left(\frac{ik}{z}\left(1 + \frac{z}{f_1}\left(1 - \frac{d}{f_1}\right)\right)(\mathbf{Q} \cdot \mathbf{q})\right) \\
&= \int_0^\infty Q dQ \int_0^{2\pi} d\phi \exp\left(-\frac{2Q^2}{q_0^2}\right) \exp\left(\frac{ik}{z}\left(1 + \frac{z}{f_1}\left(1 - \frac{d}{f_1}\right)\right)Qq \cos\phi\right) \\
&= 2\pi \int_0^\infty Q dQ \exp\left(-\frac{2Q^2}{q_0^2}\right) J_0\left(\frac{k}{z}\left(1 + \frac{z}{f_1}\left(1 - \frac{d}{f_1}\right)\right)Qq\right) \\
&= \frac{\pi q_0^2}{2} \exp\left(-\frac{k^2 q^2 q_0^2}{8z^2}\left(1 + \frac{z}{f_1}\left(1 - \frac{d}{f_1}\right)\right)^2\right)
\end{aligned} \tag{A-8}$$

And the integral over variable \mathbf{R} yields

$$\begin{aligned}
& \int d\mathbf{R} \exp\left(-\frac{R^2}{a_0^2}\right) \exp\left(\frac{ik}{z}\left(1 - \frac{z}{F}\right)(\mathbf{r} \cdot \mathbf{R})\right) \\
&= \int_0^\infty R \exp\left(-\frac{R^2}{a_0^2}\right) dR \int_0^{2\pi} d\phi \exp\left(\frac{ik}{z}\left(1 - \frac{z}{F}\right)rR \cos\phi\right) \\
&= 2\pi \int_0^\infty R \exp\left(-\frac{R^2}{a_0^2}\right) J_0\left(\frac{k}{z}\left(1 - \frac{z}{F}\right)rR\right) dR \\
&= \pi a_0^2 \exp\left(-\frac{k^2 a_0^2 r^2}{4z^2}\left(1 - \frac{z}{F}\right)^2\right)
\end{aligned} \tag{A-9}$$

Substituting Equations 8 and 9 into Equation 7, the mean intensity distribution is given by

$$\begin{aligned}
\langle I(u, z, t, k) \rangle &= \frac{k^6 T_0^2 q_0^2 a_0^2}{32^2 \pi^4 z^4 f_1^2} \cdot PRC\left(t - \frac{2z + f_1 + d}{c}\right) \int d\mathbf{p}_1 \exp\left(-\frac{ik}{z} p_1 r \cos\theta_{rp_1}\right) \\
&\cdot \exp\left(-\frac{ik}{z} q p_1 \cos\theta_{qp_1}\right) \int_0^\infty r dr \int_0^{2\pi} d\theta_{rp_1} \int_0^\infty q dq \int_0^{2\pi} d\theta_{qp_1} \exp\left(-\left(\frac{r}{\rho_0}\right)^{5/3} - \left(\frac{q}{\rho_0}\right)^{5/3}\right) \\
&\cdot \exp\left(-\frac{r^2}{4a_0^2}\right) \exp\left(-\frac{k^2 a_0^2 r^2}{4z^2} \left(1 - \frac{z}{F}\right)^2\right) \exp\left(-\frac{q^2}{2q_0^2}\right) \exp\left(-\frac{k^2 q^2 q_0^2}{8z^2} \left(1 + \frac{z}{f_1} \left(1 - \frac{d}{f_1}\right)\right)^2\right) \\
&\cdot \exp\left(-\frac{ik}{f_1} q u \cos\theta_{uq}\right)
\end{aligned} \tag{A-10}$$

According to the property of Bessel function represented in Equation 11,

$$\int_0^\infty J_\gamma(\alpha P) J_\gamma(\alpha' \rho) \rho d\rho = \frac{1}{\alpha} \delta(\alpha - \alpha') \tag{A-11}$$

the integral over p_1 , in Equation 10, yields

$$\begin{aligned}
&\int d\mathbf{p}_1 \int_0^{2\pi} d\theta_{rp_1} \exp\left(-\frac{ik}{z} p_1 r \cos\theta_{rp_1}\right) \int_0^{2\pi} d\theta_{qp_1} \exp\left(-\frac{ik}{z} p_1 q \cos\theta_{qp_1}\right) \\
&= 4\pi^2 \int d\mathbf{p}_1 J_0\left(\frac{k}{z} p_1 r\right) J_0\left(\frac{k}{z} p_1 q\right) = 4\pi^2 \int_0^\infty p_1 dp_1 J_0\left(\frac{k}{z} p_1 r\right) J_0\left(\frac{k}{z} p_1 q\right) \int_0^{2\pi} d\theta_p \\
&= \frac{8\pi^3 z}{kr} \delta(r - q)
\end{aligned} \tag{A-12}$$

Substitute Equation 12 back into Equation 10, the expression of the mean intensity distribution in the image plane can be further reduced to

$$\langle I(\mathbf{u}, z, t, k) \rangle = \frac{k^5 T^2 q_0^2 a_0^2}{128 \pi z^3 f_1^2} \text{PRC} \left(t - \frac{2z + f_1 + d}{c} \right) \int_0^\infty r dr \exp \left(-2 \left(\frac{r}{\rho_0} \right)^{5/3} \right) \\ \cdot \exp \left(-\frac{r^2}{4} \Delta \right) \exp \left(-\frac{ik}{f_1} r u \cos \theta_{ur} \right)$$

where,

$$\Delta = \frac{1}{a_0^2} + \frac{k^2 a_0^2}{z^2} \left(1 - \frac{z}{F} \right)^2 + \frac{2}{q_0^2} + \frac{k^2 q_0^2}{2z^2} \left(1 + \frac{z}{f_1} \left(1 - \frac{d}{f_1} \right) \right)^2 \quad (\text{A-13})$$

Appendix B

B.1 The schematic diagrams of electric circuits

B.1.1 Schematic of the 511 PRC generator

B.1.2 Schematic of the auxiliary circuit of Wavetek PRC generator

B.1.3 Schematic of the shutter control circuit

B.1.4 Schematic of the PMT circuit

B.1.5 Schematic of the analog circuit

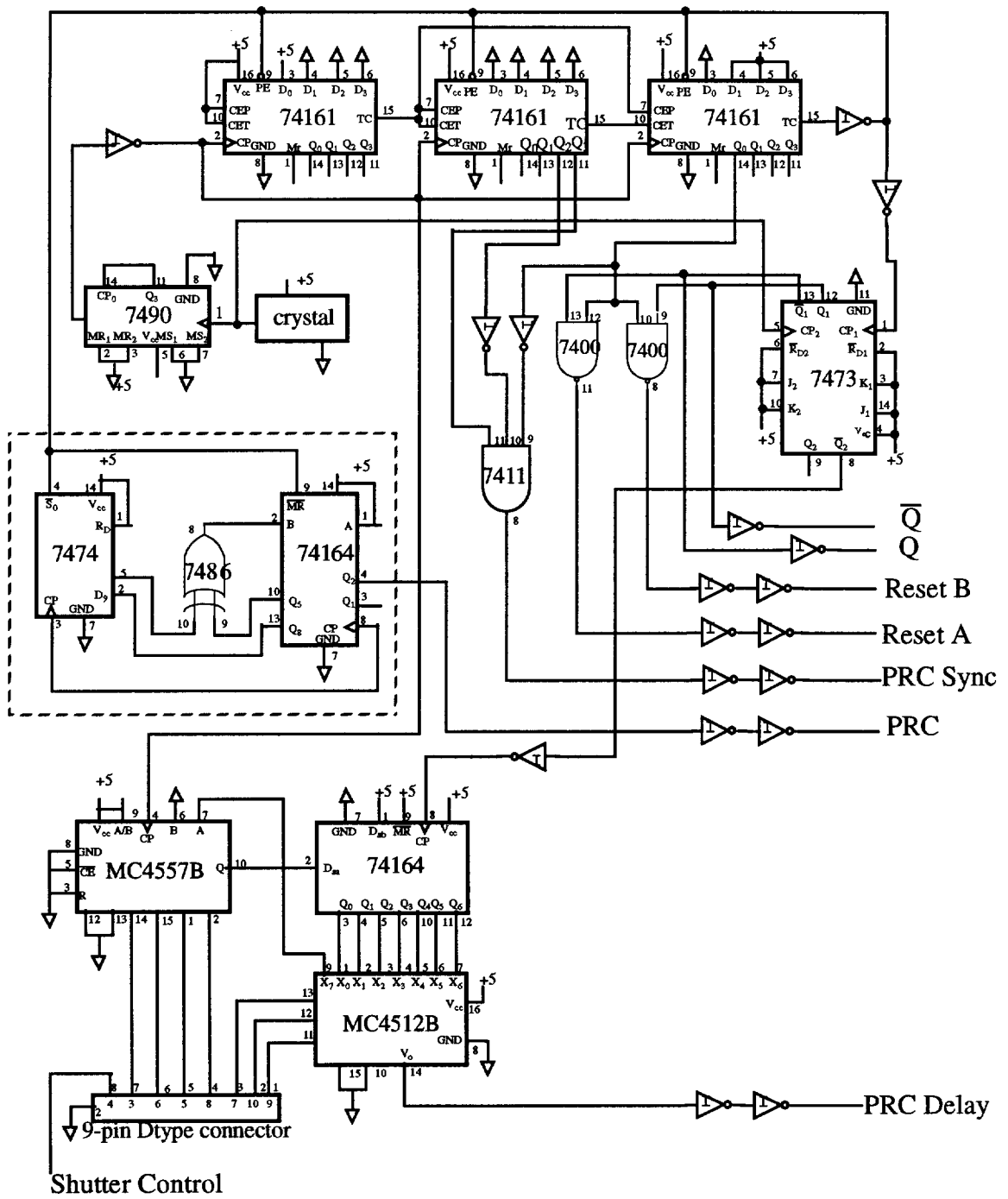


Figure B-1: The schematic of the 511 PRC generator

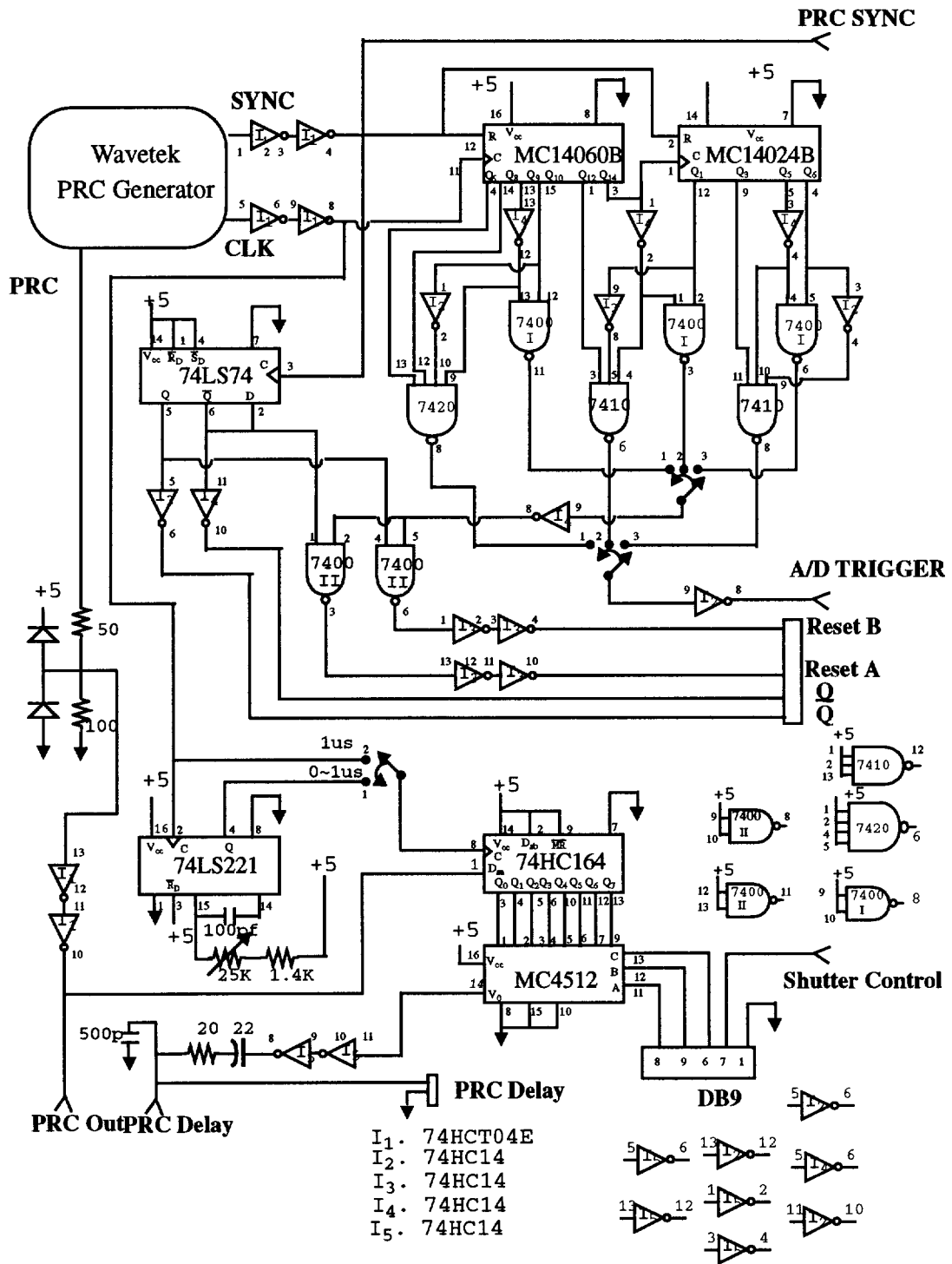


Figure B-2: The schematic of the auxiliary circuit of Wavetek PRC generator

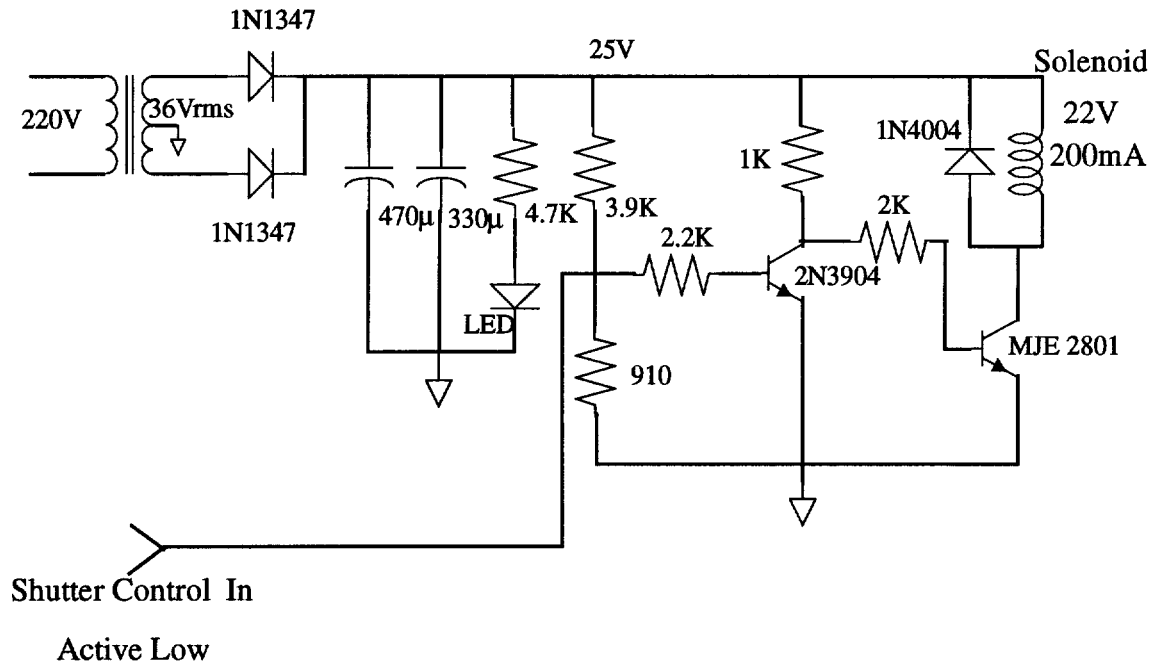
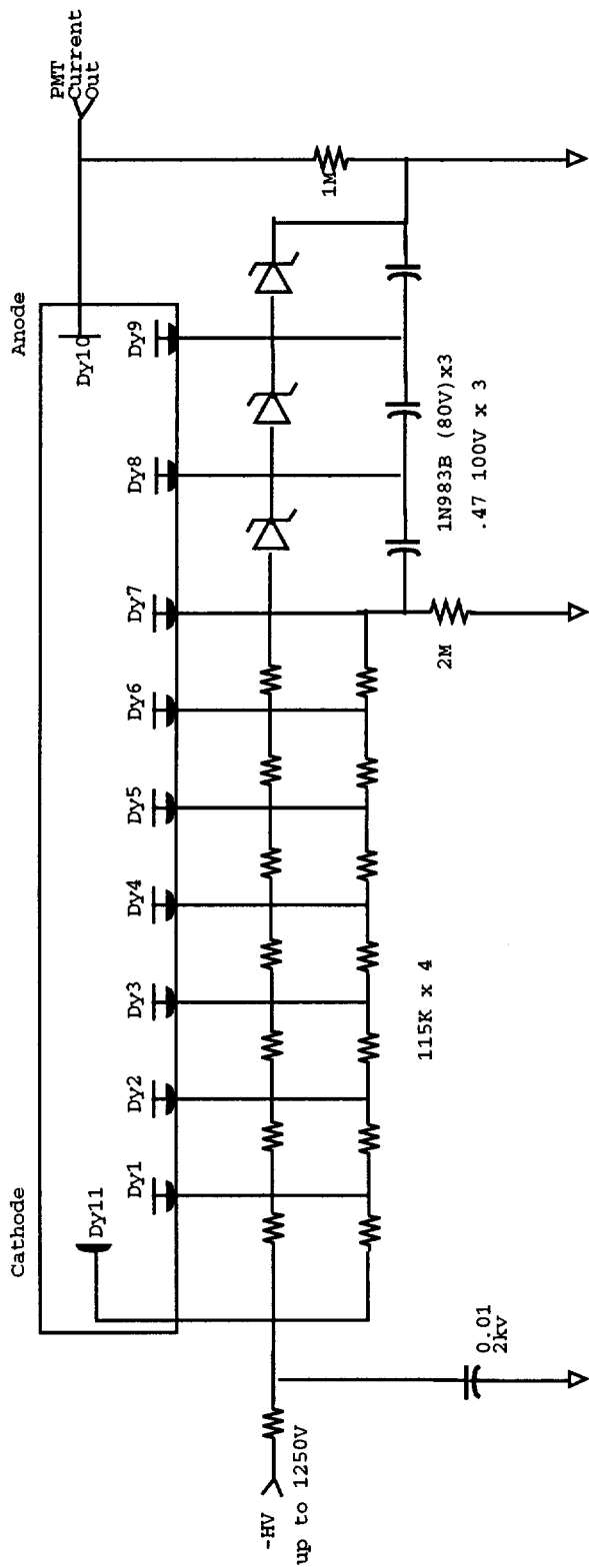


Figure B-3: The schematic of the shutter control circuit

R 446 (II)



Note: All the resistances are 1%
 Anode Current maximum value 0.1mA, bias current 2.0mA
 new bias current is 20 X anode current

Figure B-4: The schematic of the Photomultiplier Tube circuit

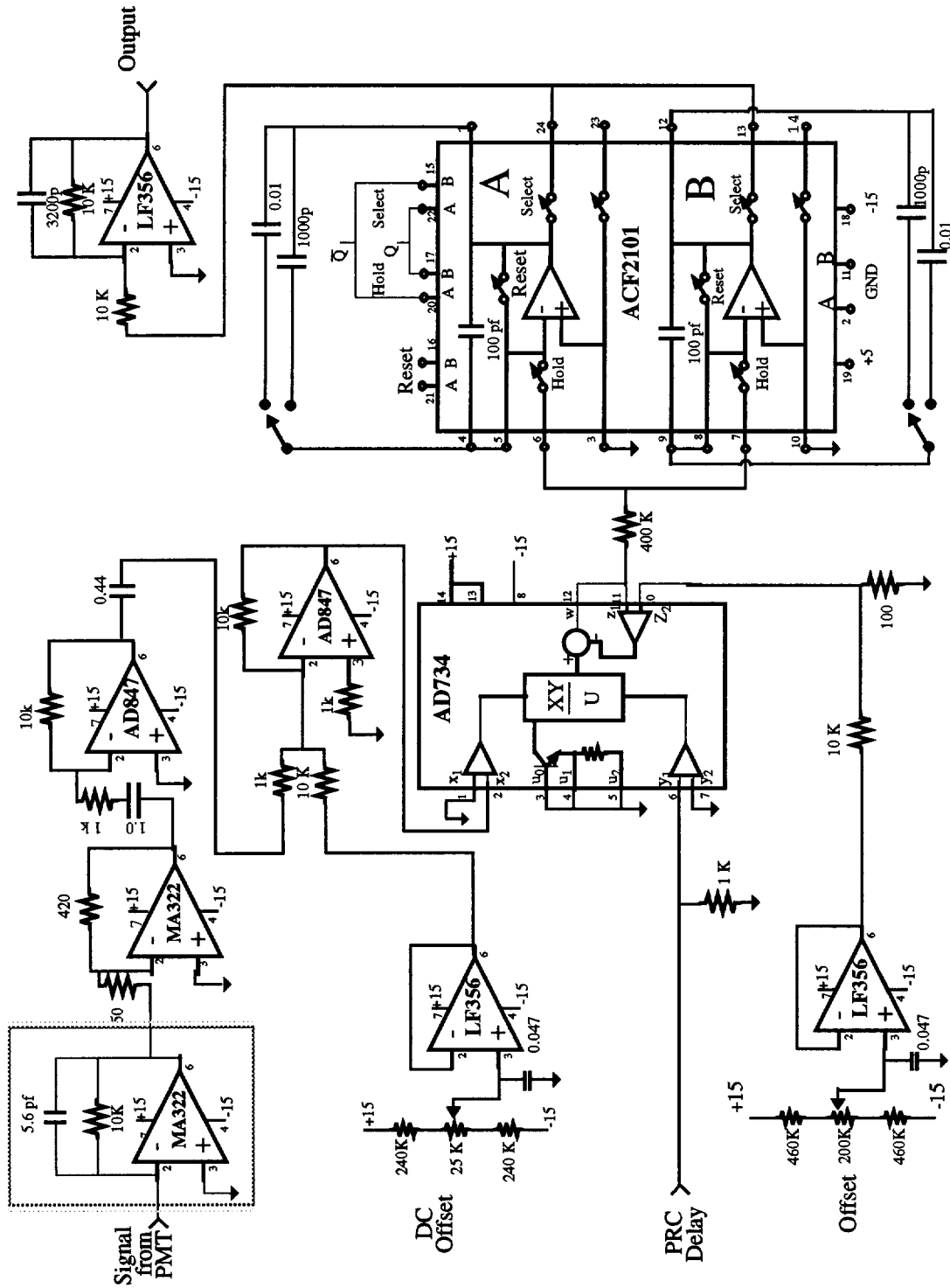


Figure B-5: The schematic of the analog circuit

Appendix C

C.1 Programs

C.1.1 The program for range finding (prctds3.for)

C.1.1.1 Main Program

```

C      PRCTDS3.FOR by Chunyan Zhou
C      To get prc mutiply prc dalay signal
C      Automatically Delay and Shutter Control
C      **For Wavetek**
C      begin 2/11/94, finished 9/18/94
C      compile with "fl prctds3.for hi ad se set pl ta dasg.lib se.lib graphics.lib"

C      Development version, runs a/d

      implicit integer(A-Z)

      real*4 bgmen(3), bgvar(3), tpdS
      character*1 YorN, Dumy
      character*16 ifile
      character*70 itext(20)
      integer*2 icmd, itrig

      integer*4 inum, isize, iseg, ibdata
      integer*2 ibig[allocatable, huge](:)
      integer*2 idata(5048)
      integer iterm, imean, ihva1, ihva2, ichan, iii, ibg
      real itime, period, initper, ilpwr
      real idelayh
      real itdelay(100), mean1(100), mean2(100), itdelay1
      integer*2 port, outdat

      write(*, '(////////)')
      print *, ' *****'
      print *, ' *      PRCTDS3.FOR Last Modified:Feb.11,1994      *'
      print *, ' * *'
      print *, ' *      This program for testing the PRC mutiply      *'
      print *, ' *      by PRC Delay signal, the result is in      *'
      print *, ' *      a file.      *'
      print *, ' *      FOR WAVETEK ONLY      *'
      print *, ' * *'
      print *, ' *      NOTE: Parentheses enclose default responceS      *'
      print *, ' *****'
      write(*, '(////////)')
      print *, ' Press <RETURN> to Continue.'
      read(*,1003) Dumy

10      inum=0

C*****
C      Allocate 64k element array in order to be sure
C      that some portion will be stored at the start of a new
C      page in physical memory and that at least 32k elements
C      will be in that page.

      isize = 64*1024

```

```

allocate (ibig(isize), stat = ierr)
if (ierr .ne. 0) then
    print *, 'bad ibig allocate status: ', ierr
    goto 980
endif

200 write(*, '(////)')
print *, '-----'
print *, '                MAIN MENU                '
print *, '-----'
print *, '                1. record data                '
print *, '                2. view data                  '
print *, '                3. plot correlated data       '
print *, '                4. plot data                  '
print *, '                5. exit                        '
print *, '-----'
print *, '

write(*, '(////)')
print 1001, 'Enter the number ', 'of your choice (1) --> '
read(*, 1010, err=200) icmd

if (icmd.eq.0) icmd=1
if(icmd .eq. 1) goto 300
if(icmd .eq. 2) goto 400
if(icmd .eq. 3) goto 600
if(icmd .eq. 4) goto 700
if(icmd .eq. 5) goto 900
goto 200

C -----***** Default Parameters *****-----
300 continue
C      item = 1      ! type of PRC source

C      determine and print physical address of ibig.
C      The values "index" and "iseg" are returned by caddr.
C      index is array index to element that is located at
C      the start of a physical memory page.
C      iseg is the segment for that page.

C      call caddr(ibig(1), index, iseg)
C      write(*, '(1x,i6,2x,z8,a)')index, iseg, 'index and seg'

C      initialize a/d board

50  call adinit(ierr)
    if (ierr .ne. 0) then
        print *, 'bad init a/d board status: ', ierr
        goto 980
    endif

1001 format(1x,2a,\)
1002 format(/1x, a)
1003 format(a1)
1004 format(1x, a)
1005 format(1x, a, \)
1006 format(1x,a,i6,a)
1007 format(1x,a,i1,a)
1008 format(1x,2a,f7.3,a)
1010 format(i5)

C      initialize I/O register
    port=787
    outdat=139
    call outbyt(port, outdat)

C -----***** Main Loop For Creating Entire Files *****-----
C      read parameter file
40  open (9, file='prctds3.par', err=40, status='old')
49  open (10, file='temp', err=49, status='unknown')

C      laser power
41  print *
    read(9, *, err=41) ilpwr

```

```

print 1008, 'The transmitted laser power ', '(in Milliwatts) (' , ilpwr , ')'

c      No. of channels, 2 channel data
42     read(9, *, err=42) ichan
       print 1007, 'No. of Channels (' , ichan, ')'

c      No. of data is recorded, including 2 channels
43     read(9, *, err=43) ibdata
       print 1006, 'No. of data in each set (' , ibdata, ')'

c      No. of data is recorded, including 2 channels
44     read(9, *, err=44) ibg
       print 1006, 'No. of bg data in each set (' , ibg, ')'

print *
print *, 'The High Voltage to the No1. PMT may be ', 'set from -300V to -1110V.'
238    read(9, *, err=238) ihva1
       write(*, 1120) "High Voltage (PMT1): ", -ihva1, "V"

240    print *
       print *, 'The High Voltage to the No2. PMT may be ', 'set from -500V to -1110V.'
       read(9, *, err=240) ihva2
       write(*, 1120) "High Voltage (PMT2): ", -ihva2, "V"
1120   format (1x, a, i5, a\ )

70     write(*, '//1x, a') "The sampling trigger type: "
       read(9, *, err=70) itrigr
       write(*, '(1x, 2a, i2, a\ )') "1. Internal  2. External", " [1 or 2] (*, itrigr, )"

71     write(*, '//1x, a') "The PRC type: "
       read(9, *, err=70) iterm

72     if (itrigr.eq.1) then
75         call periset(initper, ierr)
           if (ierr .ne. 0) then
               print *, 'bad a/d period set status: ', ierr
               goto 75
           endif
       else
c       set the trigger source and its period
       call trigset(initper, iterm)
       endif

       itime=initper*1.0e6
       print *
       print 1015, 'Sampling Period =', itime, ' micro-sec;      ', 'Sampling Frequency =', 1.0/initper, '
Hertz '
1015   format (1x, a, f12.3, a, a, f10.3, a)

       tpds = itime * 1.0e-3      ! time per data set (seconds)

       print 1002, 'The sampling rate will be:'
       print 1030, 1/tpds      !data sets per second
1030   format(2x, 'or', 16x, f8.2, ' data sets/second')

       print 1035, tpds, tpds/60
1035   format(2x, 'or', 16x, f8.2, ' seconds/data set  (' , f5.3, ' minutes/data set)')

c      set the Maximum delay time want to record
150    read(9, *, err=150) idelayh
       print 1037, 'The MAX. delay times to record is '
       print 1040, '[in microsec] (' , idelayh, ') '
1037   format (/1x, a\ )
1040   format (1x, a, f7.3, a)

       close(9)

c      ----***** Open Data File *****----
2010   print *
       print 1005, 'Enter the Data File Name --> '
       read(*, '(a16)') ifile

       open (20, file=ifile, err=2030, status='old')
2020   write(*, 1005) "The File Exist, Overwrite It? [Y/N] "
       read(*, 1003) YorN

```

```

if ((YorN .eq. 'Y').or.(YorN .eq. 'y')) goto 2040
if ((YorN .ne. 'N').and.(YorN .ne. 'n')) then
  print *, char(7)
  write(*, '(1x, a/)') "It sould be Y or N! "
  goto 2020
end if

goto 2010

2030 open (20, file=ifile, err=2010, status='new')
c write(*, '(1x,a,a16)') "ifile= ", ifile

C -----***** Read Comments Into As Part Of Header *****-----
2040 print 1002, 'Enter text for comment block in file header.'
print 1002, ' But no more than 20 lines'
print *, ' (Terminate with a blank line!)'
print *, '-----'
print *

do 2050 n=1, 20
  read(*, '(a)') itext(n)
  if (itext(n).eq.' ') goto 350
  write(20, '(1x, a)') itext(n)
2050 continue

C -----***** Finished Reading Comments *****-----

350 print *
print *, 'Do you need to change the parameters', ' or reenter the text?'
print 1005, ' [Y/N] -->'
read(*, 1003) YorN
if ((YorN .eq. 'Y').or.(YorN .eq. 'y')) goto 40
if ((YorN .ne. 'N').and.(YorN .ne. 'n')) then
  print 1005, char(7)
  goto 350
endif

print 1002, ' Adjust fiber position for MAXIMUM signal.'
print *, ' THEN press <RETURN> to began recording the data.'
read(*, 1003) Dmy

C Executive call to get current time
call getdat(iyr, imon, iday)
call gettim(ihr, imin, isec, i100th)

C *****
C Write Header Block For Data File

write(20, '(1x,i4.2,1h-,i2.2,1h-,i2.2,5x,i2.2,1h:,i2.2)') iyr, imon, iday, ihr, imin
write(20, '(1x, a, f10.3, a)') "laser power = ", ilpwr, " mW"
write(20, '(1x, a, f15.3, a)') "sampling period = ", itime, " (us)"
write(20, '(1x,a,15,a)') "No. of data/set/channel= (", ibdata/2, ")"
write(20, '(1x,a,15,a)') "No. of bg data/set/channel= (", ibg/2, ")"
write(20, '(1x,a,12)') "prc type = ", iterm
write(20, '(1x, a, f6.3, a)') "max. of delay time = (", idelayh, " ) us"
write(20, '(1x, a, 15, a)') "high voltage of PMT1 = (", -ihva1, " ) Volts"
write(20, '(1x, a, 15, a)') "high voltage of PMT2 = (", -ihva2, " ) Volts"

write(20, '(1x, a/)') "***** End of Commends *****"
write(20, '(1x, a, a/)') "Hr. Min Sec Delay(us) ",
* " BG1(v) V1(v) BG2(v) V2(v)"

C -----***** Begin Recording Data *****-----
ibadds = 0 ! number of bad data sets
imean = 0 ! number of data
itdelay1 = 0 ! set zero delay
port = 784 ! A I/O digit register

C set channel 0 and record data
n=ichan-1
call chanset(0, n, ierr)

C Choosing the Delay Time
6000 print *

```

```

        outdat=8
        call outbyt(port, outdat)
        print '/(1x,a,f6.3,a)', 'The last ADJUSTABLE DELAY TIME is', itdelay1, ' microsec'
        print 1075, 'Changing the Resistance to get', ' ADJUSTABLE DELAY TIME  you prefer !'
6015    print 1075, 'Please enter the Adjustable Delay Time', ' (0-1 us) or Enter 2.0 to EXIT --> '
        read(*, '(f6.3)', err=6015) itdelay1
1075    format(/1x,2a\ )
        if (itdelay1 .gt. 1.0) then
6020    print *, ' The Adjustable Delay Time should be less than 1'
        print '(2a\)', ' Enter <RETURN> to continue, or -1 to finish', ' this data set --> '
        read(*, '(i2)') l
        if ( l .eq. 0) goto 6015
        if ( l .eq. -1) goto 810
        goto 6020
        endif

        write(*, '/(1x, a, f6.3, a)') *The adjustable delay time is *, itdelay1, " microsec"
        write(*,1005) *Do you want to chang it ? [Y/N] --> *
        read(*,1003) YorN
        if ((YorN .ne. 'N').and.(YorN .ne. 'n')) then
            goto 6015
        endif

1065    print 1065, 'Time', 'Data Sets', 'Bad Blocks'
        format (/16x,a,20x,a,6x,a)
        print *, ' -----', '-----'
        print *, ' minutes   seconds   tics(1/100)   Data No.', ' Total'
        print *

c      recording data

        do 5910 i=1, 9
            imean = imean+1
            itdelay(imean) = (i-1)+itdelay1

C      if delay time larger than max delay, next data set.
        if (itdelay(imean) .gt. idelayh) then
            imean = imean-1
            goto 6000 ! next data set
        endif

        outdat = i-1
        call outbyt(port, outdat)
        print '/(a,f9.5, a)', ' The delay time is', itdelay(imean), ' us'

C      delay loop
        do 1400 iii=1, 1000000
1400    continue

C      record the background signal
580    call dstats(ibg,ibig(index),iseg, bgmen,bgvar,0,itrig, ierr)
        if (ierr. ne. 0) then
            print *, ' error in sampling the data, try again'
            goto 580
        endif

C      Executive call to get current time
        call gettim(ihr1, imin1, isec1, i100th1)

C      Recording the data
        outdat=i+7
        call outbyt(port, outdat)
        call takead(ibig(index), ibdata, idata, iseg,1,itrig,ierr)
            inum = ibdata ! useful when seedat

C      delay loop
        do 1405 iii=1, 1000000
1405    continue

        mean1(imean) = 0.0
        mean2(imean) = 0.0

        do 1062 k=1, inum, 2

c      For unipolar data
            j=k+1

```

```

write(10, *) idata(k), idata(j)
mean1(imean) = mean1(imean) + idata(k)
mean2(imean) = mean2(imean) + idata(j)
1062 continue

mean1(imean) = (2.0*mean1(imean)/inum-bgmen(1))*0.002426
mean2(imean) = (2.0*mean2(imean)/inum-bgmen(2))*0.002426

write(20, '(1x, 3(i2,2x), 2x,f6.3, 4x, 4f10.3)')
* ihrl, imin1, isec1, itdelay(imean), bgmen(1)*0.002426,
* mean1(imean), bgmen(2)*0.002426, mean2(imean)

if (ierr .ne. 0) ibadds = ibadds + 1! count bad data sets

1070 print 1070, imin1, isec1, i100th1, imean, ibadds
format (3(8x,i2),9x,i6,9x,i6)

C -----***** End Block Loop For This Data Set *****-----
5910 continue

C -----***** End Data Set Loop For This File *****-----

810 print *, 'Finished recording data file.'

820 print *, 'Would you like to record another file of data?'
print 1005, ' [Y/N] --> '
read(*,1003)YorN
if ((YorN .eq. 'Y').or.(YorN .eq. 'y')) then
goto 40
elseif ((YorN .ne. 'N').and.(YorN .ne. 'n')) then
print 1005, char(7)
goto 820! ask again
endif
print *

close(20)
close(10)
period = initper ! set period save
call clearwindow
goto 200

*****

400 call seedat(ibig(index), inum, idata(1) )
goto 200

600 call setgr
call corplot(itdelay(1), mean1(1), imean)
read(*,*) ! save screen until key pressed
call clearwindow
call corplot(itdelay(1), mean2(1), imean)
read(*,*) ! save screen until key pressed
call clearwindow
call closeSEgraphics
goto 200

700 call setgr
call plot(idata(5), period)
read(*,*) ! save screen until key pressed
call clearwindow
call closeSEgraphics
goto 200

*****

900 deallocate (ibig, stat = ierr)
if (ierr .ne. 0) then
print *, 'bad deallocate status: ',ierr
goto 980
endif

c print *, 'deallocated ibig'

*****
980 write(*, '(1x,a,\)') 'Are you sure to quit? [Y/N] --> '

```

```

        read(*,1003) YorN
        if ((YorN .ne. 'Y').and.(YorN .ne. 'y')) then
            goto 10
        endif
990    call closeSEgraphics
        end

*****
*          corplot subroutine
*****

c      Graph is plotted using setools subroutines.

        subroutine corplot(xdata, ydata, inum)

        REAL xdata(0:100), ydata(0:100), tdata(0:100)
        INTEGER inum, i
        real xtics
        character*25 ctitle
        character*7 cfactor

        do 10 i=1, inum
            tdata(i)=xdata(i)
10        continue

        *      transfer jdata array to real array for plotting
        *      also create x data array
        *      convert a/d counts to volts 5V/2047 counts = 2.44 mV / count

        xtics = 0.2
        call setplot(xtics, tdata(inum-1), 0.0, 10.0)

c      calculate time/division

        write(cfactor, '(f6.1)') xtics
        ctitle = cfactor // 'microsec/div'

        call titlexaxis(ctitle, 0)

        ipoints = inum          ! points to plot
        CALL SortDataX(tdata, ydata, ipoints, 1)
        CALL LinePlotData(tdata, ydata, ipoints, 10, 0)

        return

        end

```

C.1.1.2 prctds3.par

```

33.0    laser power
2       Channel No.
200    No. of data in each data set, for 2 channels
400    No. of data in each background data set, for 2 channels
650    high voltage for PMT1
800    high voltage for PMT2
2       trig type 2. e 1. i
3       type of PRC, 1:9 2:10 3:15 4:20 5:other
3.0    maximum delay in us

```

C.1.2 The program of calibrating two channels (calib.for)

C.1.2.1 main program

```

C      CALIB.FOR by Chunyan Zhou
C      To get the calibration factor for two channels
C      begin 4/24/94, finished 4/24/94

      implicit integer(A-Z)

      real*4 bgmen(3), bgvar(3), tpsd
      character*1 YorN, Dumy
      character*16 ifile
      integer*2 icmd, itrigr

      integer*4 inum, isize, iseg, ibdata
      integer*2 ibig[allocatable, huge](:)
      integer*2 idata(5000)
      integer iterm, imean
      real itime, initper, ical
      real idelayh
      real mean(3)
      integer*2 port, outdat, icode, mm
      integer iii, ihva1, ihva2

      write(*, '(/////)' )
      print *, ' *****'
      print *, ' * CALIB.FOR   Last Modified: May. 10, 1994   *'
      print *, ' *'
      print *, ' *   This program for getting calibration factor *'
      print *, ' *   in two channel data processing   *'
      print *, ' *   NOTE: Parentheses enclose default responses *'
      print *, ' *****'
      write(*, '(/////)' )
      print *, ' Press <RETURN> to Continue.'
      read(*,1003) Dumy

10     inum=0

      *****
      C      Allocate 64k element array in order to be sure
      C      that some portion will be stored at the start of a new
      C      page in physical memory and that at least 32k elements
      C      will be in that page.

      isize = 64*1024

      allocate (ibig(isize), stat = ierr)
      if (ierr .ne. 0) then
         print *, 'bad ibig allocate status: ',ierr
         goto 980
      endif

200    write(*, '(/////)' )
      print *, ' -----'
      print *, ' |                               |'
      print *, ' |           MAIN MENU           |'
      print *, ' |-----|'
      print *, ' |           1. record data       |'
      print *, ' |           2. exit              |'
      print *, ' |-----|'
      print *, ' -----'
      print *

      write(*, '(/////)' )
      print 1001, 'Enter the number ', 'of your choice (1) --> '
      read(*, 1010, err=200) icmd

      if (icmd.eq.0) icmd=1
      if(icmd .eq. 1) goto 300

```

```

        if(icmd .eq. 2) goto 900
        goto 200

C -----***** Default Parameters *****-----
300      ibdata= 400          ! # of data per data set
        iterm = 3          ! type of external trigger source

C      determine and print physical address of ibig.
C      The values "index" and "iseg" are returned by caddr.
C      index is array index to element that is located at
C      the start of a physical memory page.
C      iseg is the segment for that page.

        call caddr(ibig(1), index, iseg)
c      write(*, '(1x,i6,2x,z8,a)')index, iseg, 'index and seg'

C      initialize a/d board

50      call adinit(ierr)
        if (ierr .ne. 0) then
            print *, 'bad init a/d board status: ',ierr
            goto 980
        endif

1001     format(1x,2a,\)
1002     format(/1x, a)
1003     format(a1)
1004     format(1x, a)
1005     format(1x, a, \)
1006     format(1x,2a,i5,a,\)
1010     format(i5)

C      initialize I/O register
        port=787
        outdat=139
        call outbyt(port, outdat)

C -----***** Main Loop For Creating Entire Files *****-----

c      read parameter file
40      open (9, file='calib.par', err=2030, status='old')

c      chose the delay time
        print *
65      read (9, *, err=65) idelayh
68      read (9,*,err=68) icode
        write(*, '(a, f7.3, a, i3, a)') " The delay time is ",
*      idelayh," (us). The corresponding code is (",icode,")"

        print *
        print *, 'The High Voltage to the No1. PMT may be ', 'set from -300V to -1110V.'
238     read(9,*,err=238) ihva1
        write(*,1120) "High Voltage (PMT1): ", -ihva1, "V"

240     print *
        print *, 'The High Voltage to the No2. PMT may be ', 'set from -500V to -1110V.'
        read(9,*,err=240) ihva2
        write(*,1120) "High Voltage (PMT2): ", -ihva2, "V"
1120    format (1x,a,i5,a\)

70      write(*,'(//1x,a)') "The sampling trigger type: "
        read(9,*, err=70) itrig
        write(*,'(1x, 2a, i2, a)') "1. Internal  2. External", " [1 or 2] (", itrig, ")"

        close(9)
72      if (itrig.eq.1) then
75      call periset(initper, ierr)
        if (ierr .ne. 0) then
            print *, 'bad a/d period set status: ',ierr
            goto 75
        endif

        else
c      set the trigger source and its period
        call trigset(initper, iterm)

```

```

endif

    itime=initper*1.0e6
    print 1015, 'Sampling Period =',itime,' micro-sec;      ',
*   'Sampling Frequency =',1.0/initper,' Hertz'
1015 format (1x,a,f12.3,a,a,f10.3,a)

    tpd = itime * 1.0e-3      ! time per data set (seconds)

    print 1002,'The sampling rate will be:'
    print 1030, 1/tpds      !data sets per second
1030 format(2x,'or',16x,f8.2,' data sets/second')

    print 1035, tpd, tpd/60
1035 format(2x,'or',16x, f8.2, ' seconds/data set (' ,f5.3, ' minutes/data set)')

350   print *
    print *, 'Do you need to change the parameters ?'
    print 1005, ' [Y/N] -->'
    read(*,1003) YorN
    if ((YorN .eq. 'Y').or.(YorN .eq. 'y')) goto 40
    if ((YorN .ne. 'N').and.(YorN .ne. 'n')) then
        print 1005, char(7)
        goto 350
    endif

C     -----***** Open Data File *****-----
2010   print *
    print 1005,'Enter the Data File Name --> '
    read(*, '(a16)') ifile

2020   open (10, file=ifile, err=2030, status='old')
    write(*,1005) *The File Exist, Overwrite It? [Y/N] *
    read(*,1003) YorN
    if ((YorN .eq. 'Y').or.(YorN .eq. 'y')) goto 2040
    if ((YorN .ne. 'N').and.(YorN .ne. 'n')) then
        print *, char(7)          ! ring beeper
        write(*, '(1x, a/)') *It should be Y or N! *
        goto 2020
    end if

    goto 2010

2030   open (10, file=ifile, err=2010, status='new')
c     write(*, '(1x,a,a16)') *ifile= ", ifile

C     Executive call to get current time
2040   call getdat(iyr, imon, iday)
    call gettim(ihr, imin, isec, i100th)

C     *****
C     Write Header Block For Data File

    write(10, '(/1x,i4.2,1h-,i2.2,1h-,i2.2,5x,i2.2,1h:,i2.2)') iyr, imon, iday, ihr, imin
    write(10, '(1x, a, f6.3, a)') "Delay time = (", idelayh, ") us"
    write(10, '(1x, a, i5, a)') "high voltage of PMT1 = (", ihva1, ") Volts"
    write(10, '(1x, a, i5, a)') "high voltage of PMT2 = (", ihva2, ") Volts"

1020   format(1x, a, f10.2, 8x, a, e10.4)

C     -----***** Begin Recording Data *****-----
    port=784          ! A I/O digit register

    do 6000 imean = 1, 2

        if (imean.eq.1) then
            print 1002, 'Recording Signal from Channel 1 (filter chan.)'
            print 1002, 'Put fiber into PMT1, wait for 10 sec.'
            print *, 'Press <RETURN> to began recording the data.'
            read(*,1003) Dummy
            endif

            if (imean.eq.2) then
                print *, 'Recording Signal from Channel 2 '
                print *, 'Put fiber into PMT2, wait for 10 sec.'
                print *, 'Press <RETURN> to began recording the data.'

```

```

        read(*,1003) Dmy
        endif

C      Choosing the Delay Time and record the background
1060    call outbyt(port, icode)
        call chanset(0, 1, ierr)

C      delay loop
1450    do 1450 iii=1, 1000000
        continue

C      record the background signal
580    call dstats(400,ibig(index),iseg, bgmen,bgvar,0,itrig,ierr)
        if (ierr.ne. 0) then
            print *, ' error in sampling the data, try again'
            goto 580
        endif

C      Recording the data
        mm=icode+8
        call outbyt(port, mm)

        n=imean-1
        call chanset(0, n, ierr)

C      delay loop
1400    do 1400 iii=1, 1000000
        continue

        inum = (n+1)*ibdata
        call takead(ibig(index), inum, idata,iseg,1,itrig,ierr)

        mean(imean) = 0.0

        do 1062                i=1, ibdata
c      For unipolar data
        k=(n+1)*i
        mean(imean) = mean(imean) + 1.0*idata(k)
1062    continue

C      for testing
c      bgmen(imean)=0.0

        mean(imean) = mean(imean)/(1.0*ibdata)-bgmen(imean)
c      In volts unit, for unipolar data
        mean(imean) = mean(imean)*2.44e-3!V
        write(*,1064) " mean(*,imean,")= ",mean(imean)," V"

1063    print *,'Do you want to record data again ?'
        print 1005,' [Y/N] -->'
        read(*,1003) YorN
        if ((YorN .eq. 'Y').or.(YorN .eq. 'y')) goto 1060
        if ((YorN .ne. 'N').and.(YorN .ne. 'n')) goto 1063
6000    continue

        ical= 6.0*mean(1)/mean(2)
        write(10, '(2f10.3)') mean(1), mean(2)
        write(10, '(a, f10.3)') "ical= ", ical
1064    format(a, i3, a, f10.5, a)
C      -----***** End Data Set Loop For This File *****-----

        print *,'Finished recording data file.'
        print 1005, char(7)

820    print *, 'Would you like to record another file of data?'
        print 1005, ' [Y/N] --> '
        read(*,1003)YorN
        if ((YorN .eq. 'Y').or.(YorN .eq. 'y')) then
            goto 350
        elseif ((YorN .ne. 'N').and.(YorN .ne. 'n')) then
            print 1005, char(7)
            goto 820                ! ask again
        endif
        print *

        close(10)

```

```

goto 200

c *****
900 deallocate (ibig, stat = ierr)
    if (ierr .ne. 0) then
        print *, 'bad deallocate status: ', ierr
        goto 980
    endif

c print * , 'deallocated ibig'

c *****
980 write(*, '(1x,a,\)') "Are you sure to quit? [Y/N] --> "
    read(*,1003) YorN
    if ((YorN .ne. 'Y').and.(YorN .ne. 'y')) then
        goto 10
    endif

end

```

C.1.2.2 calib.par

```

2.00 delay time
1 delay code
600 high voltage for PMT1
750 high voltage for PMT2
2 trig type 2. e 1. i

```

C.1.3 The program of recording two channel data (records4.for)

C.1.3.1 main program

```

C RECORDS4.FOR by Chunyan Zhou
C based on RECORD.FOR
C to run on a record data program in CIO-AD16
C begin 03/03/95, finished 03/16/95
C compile with "fl prctds3.for hi ad se set pl ta fft dasg.lib se.lib graphics.lib"

C With Automatical Delay and Shutter Chose
C ** recording background in each data sets **
C A file consists of a header block followed by a group of
C data sets.
C Each data set is 2048 bytes long and contains 1000 data
C values

C Incorporate file containing parameter and common declarations

implicit integer(A-Z)

real*4 bgmen(3), bgvar(3), tpd8
character*1 YorN, Dumy
character*16 ifile
character*70 itext(20)
integer*2 icmd, fw, fc, itrig

integer*4 inum, isize, iseg, ibdata, ibturb
integer*2 ibig[allocatable], huge(:)
integer*2 idata(20000), ii

```

```

integer item, outdat, port, icode, ichan, mm
integer ihva1, ihva2, ibbg
real period, initper
real ttime,itime, idelay, ica, ilpwr

write(*, '(/////)' )
print *, ' *****'
print *, ' * RECORDS4.FOR  Last Modified: MARCH 16, 1995*'
print *, ' *'
print *, ' *   This program uses an Analog To Digital   *'
print *, ' *   Converter to collect data from the laser *'
print *, ' *   receiver and store it on a file.         *'
print *, ' *'
print *, ' *   NOTE: Parentheses enclose default responce *'
print *, ' *****'
write(*, '(/////)' )
print *, ' Press <RETURN> to Continue.'
read(*,1003) Dmy

10  inum=0

C   *****
C   Allocate 64k element array in order to be sure
C   that some portion will be stored at the start of a new
C   page in physical memory and that at least 32k elements
C   will be in that page.

      isize = 64*1024

      allocate (ibig(isize), stat = ierr)
      if (ierr .ne. 0) then
          print *, 'bad ibig allocate status: ',ierr
          goto 980
      endif

200 write(*, '(/////)' )
print *, ' -----'
print *, ' |                MAIN MENU                |'
print *, ' |-----|'
print *, ' |      1. record data      |'
print *, ' |      2. view data        |'
print *, ' |      3. save on disk     |'
print *, ' |      4. load data file   |'
print *, ' |      5. DMA status       |'
print *, ' |      6. plot data        |'
print *, ' |      7. fft to data      |'
print *, ' |      8. exit              |'
print *, ' |-----|'
print *, ' -----'

write(*, '(/////)' )
print 1001, 'Enter the number', ' of your choice (1) --> '
read(*, 1010, err=200) icmd

if (icmd.eq.0) icmd=1
if(icmd .eq. 1) goto 300
if(icmd .eq. 2) goto 400
if(icmd .eq. 3) goto 500
if(icmd .eq. 4) goto 600
if(icmd .eq. 5) goto 800
if(icmd .eq. 6) goto 700
if(icmd .eq. 7) goto 850
if(icmd .eq. 8) goto 900
goto 200

C   -----***** Default Parameters *****-----
300  idnds = 100          ! default # of data sets in a file

C   determine and print physical address of ibig.
C   The values "index" and "iseg" are returned by caddr.
C   index is array index to element that is located at
C   the start of a physical memory page.
C   iseg is the segment for that page.

```

```

        call caddr(ibig(1), index, iseg)
c      write(*,'(1x,i6,2x,z8,a)')index, iseg, 'index and seg'

C      initialize a/d board

50     call adinit(ierr)
        if (ierr .ne. 0) then
            print *,'bad init a/d board status: ',ierr
            goto 980
        endif

1001    format(1x,2a,\)
1002    format(/1x, a)
1003    format(a1)
1004    format(1x, a)
1005    format(1x, a, \)
1006    format(1x,2a,i1,a,\)
1007    format(1x,a,i1,a,\)
1008    format(1x,2a,f7.3,a,\)
1010    format(i5)

C      initialize I/O register
        port=787
        outdat=139
        call outbyt(port, outdat)

C -----***** Main Loop For Creating Entire Files *****-----
c      read parameter file
40     open (9, file='records4.par', err=40, status='old')

C      laser power
41     print *
        read(9, *, err=41) ilpwr
        print 1008, 'The transmitted laser power ', '(in Milliwatts) (' , ilpwr ,)''

c      No. of channels, 2 channel data
42     print *
        read(9, *, err=42) ichan
        print 1007, 'The No. of Channels (' , ichan ,)''

43     print *
        read(9, *, err=43) ica
        print 1008, 'The two channel calibrating parameter ', '(Ifilter/Io) (' , ica, '))'

45     print *
        read(9,*,err=45) fw
        print 1006, 'The Campbell Unit CA-9 Range ', '[5, 10, 20] m/sec (' , fw, '))'

60     print *
        read(9,*,err=60) fc
        print 1006, 'The CA-9 Time Constant ', '[1, 10, 100] seconds (' ,fc, '))'

61     print *
        read(9,*,err=61) ibdata
        print 1006, 'The number of data per data set', 'for 2 channel data (' , ibdata, '))'

62     print *
        read(9,*,err=62) ibturb
        print 1006, 'The number of turbulence per data set', '( , ibturb, '))'

63     print *
        read(9,*,err=63) ibbg
        print 1006, 'The number of background data ', '( , ibbg, '))'

c      chose the delay time
        print *
65     read (9, *, err=65) idelay
68     read (9,*,err=68) icode
        write(*,'(a, f7.3, a, i3, a)') " The delay time is ",
*      idelay," (us). The corresponding code is (",icode,")"

        print *
        print *,'The High Voltage to the No1. PMT may be ', 'set from -300V to -1110V.'
238    read(9,*,err=238) ihval
        write(*,1120) "High Voltage (PMT1): ", -ihval, "V"

```

```

240   print *
      print *, 'The High Voltage to the No2. PMT may be ', 'set from -500V to -1110V.'
      read(9,*,err=240) ihva2
      write(*,1120) *High Voltage (PMT2): ', -ihva2, *V"
1120   format (1x,a,15,a\)

70   write(*,'(//1x,a)') "The sampling trigger type: "
      read(9,*, err=70) itrig
      write(*,'(1x, 2a, i2, a\)') "1. Internal 2. External", " [1 or 2] (' , itrig, *)"

80   write(*,'(//1x,a)') "Read the PRC signal type "
      read(9,*, err=80) iterm

72   if (itrig.eq.1) then
75     call periset(initper, ierr)
      if (ierr .ne. 0) then
          print *, 'bad a/d period set status: ',ierr
          goto 75
      endif

      else
c     set the trigger source and its period
      call trigset(initper, iterm)
      endif

      itime=initper*1.0e6
      print 1015, 'Sampling Period =',itime,' micro-sec; ',
*      'Sampling Frequency =',1.0/initper,' Hertz'
1015   format (1x,a,f12.3,a,a,f10.3,a)

      tpd = itime * 1.0e-3      ! time per data set (seconds)

      print 1002, 'The sampling rate will be:'
      print 1030, 1/tpd        !data sets per second
1030   format(2x,'or',16x,f8.2,' data sets/second')

      print 1035, tpd, tpd/60
1035   format(2x,'or',16x, f8.2, ' seconds/data set (' ,f5.3, ' minutes/data set)')

150   print 1002, 'How many data sets do you want recorded in this file?'
      print 1040, '[1 to 350] (' ,idnds,') --> '
1040   format (1x,a,i3,a\)
      read(*,1045,err=150)inds
1045   format(i3)
      if (inds .eq. 0) inds = idnds
      if ((inds .lt. 0).or.(inds .gt. 350)) then
          print 1005, char(7)
          print *, 'Your entry may not be < 1 or > 350; please try again!'
          goto 150
      endif
      idnds = inds

      inum=inds*10

      print *
      ttime = tpd*inds
      print 1050, 'Sampling will require: ', ttime, ttime/60
1050   format(1x,a,f7.2,' seconds or ',f6.2, ' minutes')

      close(9)

C     ----***** Open Data File *****----
2010   print *
      print 1005, 'Enter the Data File Name (dxxx.xx) --> '
      read(*, '(a16)') ifile

      open (10, file=ifile, err=2030, status='old')
2020   write(*,1005) "The File Exist, Overwrite It? [Y/N] "
      read(*,1003) YorN
      if ((YorN .eq. 'Y').or.(YorN .eq. 'y')) goto 2040
      if ((YorN .ne. 'N').and.(YorN .ne. 'n')) then
          print *, char(7)
          write(*, '(1x, a/)') "It should be Y or N! "
          goto 2020
      endif
      end if

```

```

        goto 2010

2030   open (10, file=ifile, err=2010, status='new')
c      write(*, '(1x,a,a16)') "ifile= ", ifile

C -----***** Read Comments Into ibuf As Part Of Header *****-----
2040   print 1002,'Enter text for comment block in file header.'
      print 1002,'      But no more than 20 lines'
      print *,' (Terminate with a blank line!)'
      print *,'-----'
      print *

      do 2050 n=1, 20
        read(*, '(a)') itext(n)
        if (itext(n).eq.' ') goto 350
        write(10,'(1x, a)') itext(n)
2050   continue

C -----***** Finished Reading Comments *****-----

C      Executive call to get current time
350    call getdat(iyr, imon, iday)
      call gettim(ihr, imin, isec, i100th)
      write(10,'(1x,i4.2,1h-,i2.2,1h-,i2.2,5x,i2.2,1h:,i2.2/)') iyr, imon, iday, ihr, imin

      write(10,'(a)') " ***** End of Comments *****"
      print *
      print *,'Do you need to change the parameters', ' or reenter the text?'
      print 1005,' [Y/N] -->'
      read(*,1003) YorN
      if ((YorN .eq. 'Y').or.(YorN .eq. 'y')) goto 40
      if ((YorN .ne. 'N').and.(YorN .ne. 'n')) then
        print 1005, char(7)
        goto 350
      endif

2015   open (11, file='temp', err=2015, status='unknown')

C *****
C      Write Header Block For Data File

      write(10, 104) "Laser power = ", ilpwr, " mW"
      write(10, '(a,i2,a)') " The wind range of Camp. = (", fw, ") m/s"
      write(10, 101) "High voltage of no.1 PMT = ", -ihva1, " Volts"
      write(10, 101) "High voltage of no.2 PMT [Io] = ", -ihva2, " Volts"
      write(10, '(a, f15.3, a)') " sampling period = ", itime, " us"
      write(10, 104) "The delay time = ", idelay, " us"
      write(10, 101) "Num. of data sets = ", inds, "."
      write(10, 101) "Num. of data per set for each channel = (", ibdata/2, ") ."
      write(10, 101) "Num. of turb. data per set = (", ibturb, ") ."
      write(10, 104) "The calibrating parameter = (", ica, ") ."

101    format(1x, a, i5, a )
102    format(1x, a, f15.5, a)
104    format(1x, a, f10.3, a)

      write(10, '(/a)') " @@@@@@ Beginning of Data File @@@@@@"

C -----***** Begin Recording Data *****-----
520   print 1002, ' Adjust spatial filter for MINIMUM signal.'
      print *, ' THEN press <RETURN> to continue.'
      read(*,1003) Dummy
      print *
      print *, ' Recording Data Now !'
      ibadds = 0                ! number of bad data sets
      ids = 0                   ! data set number
      port=784                  ! set the I/O

      print 1065, 'Time','Data Sets','Bad Blocks'
1065   format (/16x,a,26x,a,11x,a)
      print *, '-----'
      print *, ' minutes   seconds   tics(1/100)   in file', ' remaining   Total'
      print *

6000   ids = ids + 1                ! next data set

```

```

C      Executive call to get current time
      call gettim(ihr1, imin1, isec1, i100th1)

C      Recording Background( both channels)
      outdat = icode
      call outbyt(port, outdat)

578     do 578 ii=1, 1000000
          continue

C      Channel 0 and channel 1
      call chanset(0, 1, ierr)
580     call dstats(ibbg, ibig(index), iseg, bgmen, bgvar, 0, itrigr, ierr)
      if (ierr .ne. 0) then
          print *, ' error in sampling the data, try again'
          goto 580
      endif

      do 610 m=1, 2
          write(10, 604) bgmen(m)
          continue
610     format(1x, f15.5)
604

C      for 511us PRC
      outdat = icode + 128                ! open the shutter

C      for wavetek
      if (iterm .gt. 1) then
          outdat = icode + 8
      endif

      call outbyt(port, outdat)

1064    do 1064 ii=1, 1000000
          continue

C      set channel 2 & 3 to get ibturb wind readings from channel 2
C      and ibturb turbulence readings from channel 3
      call chanset(0, 3, ierr)
      mm=4*ibturb
      call takead(ibig(index), mm, idata, iseg, 1, itrigr, ierr)
      if (ierr .ne. 0) ibadds = ibadds + 1! count bad data sets
      do 630 m=1, mm
          write(10, 605) idata(m)
630     continue

C      set channel 0 and 1 to record ibdata/2 data

      call chanset(0, 1, ierr)
      mm=ibdata
      call takead(ibig(index), mm, idata, iseg, 1, itrigr, ierr)
      if (ierr .ne. 0) ibadds = ibadds + 1! count bad data sets
      do 631 m=1, mm
          write(10, 605) idata(m)
631     continue

C      set channel 2 & 3 to get ibturb wind readings from channel 2
C      and ibturb turbulence readings from channel 3
      call chanset(0, 3, ierr)
      mm=4*ibturb
      call takead(ibig(index), mm, idata, iseg, 1, itrigr, ierr)
      if (ierr .ne. 0) ibadds = ibadds + 1 ! count bad data sets
      do 632 m=1, mm
          write(10, 605) idata(m)
632     continue

605     format(1x, i5)

      print 1070, imin1, isec1, i100th1, ids, inds-ids, ibadds
1070    format (3(8x, i2), 9x, i6, 4x, i6, 9x, i6)

C      -----***** End Block Loop For This Data Set *****-----

C      Take next data set unless this was the last one in this file.
      if (ids .lt. inds) goto 6000
C      -----***** End Data Set Loop For This File *****-----

```

```

print 1005, char(7)
print *, 'Finished recording data file.'

820  print *, 'Would you like to record another file of data?'
      print 1005, ' [Y/N] -->'
      read(*,1003)YorN
      if ((YorN .eq. 'Y').or.(YorN .eq. 'y')) then
          goto 40
      elseif ((YorN .ne. 'N').and.(YorN .ne. 'n')) then
          print 1005, char(7)
          goto 820          ! ask again
      endif
      print *

      close(10)
      close(11)
      period = inltper          ! set period save
      call clearwindow
      goto 200

*****

400  call seedat(ibig(index), inum, idata(1) )
      goto 200

500  call save(idata(1), period)
      goto 200

600  call load(idata(1), period)
      goto 200

700  call setgr
      call plot(idata(5), period)
      read(*,*)                ! save screen until key pressed
      call clearwindow
      call closeSEgraphics
      goto 200

800  call statdma
      goto 200

850  call setgr
      call datfft(idata(5), period)
      call clearwindow
      call closeSEgraphics
      goto 200

*****

900  deallocate (ibig, stat = ierr)
      if (ierr .ne. 0) then
          print *, 'bad deallocate status: ',ierr
          goto 980
      endif

c    print * , 'deallocated ibig'

+++++*****
980  write(*, '(1x,a,\)') "Are you sure to quit? [Y/N] --> "
      read(*,1003) YorN
      if ((YorN .ne. 'Y').and.(YorN .ne. 'y')) then
          goto 10
      endif

990  call closeSEgraphics
      end

*****
*          statdma subroutine
*****

*          get dma status

subroutine statdma

```

```

implicit integer(A-Z)
integer*2 ic(16),mode,flag
character*1 Dmy

mode = 8
call fdasg(mode, ic(1), Flag)
if (flag .NE. 0) then
print *, 'Mode = ', mode, ' Error # ', flag
goto 990
endif

print *
print *, ic(1), ' = operation      1 = DMA, 2 = Interrupt'
print *, ic(2), ' = status        0 = done, 1 = active '
print *, ic(3), ' conversions so far'

990  print 1020, 'Press <Return> to exit'
1020 format( /1x, a)
read( *, '(a1)') Dmy

return
end

```

C.1.3.2 records4.par

```

35.0  laser power
2     Channel No.
161.28 Calibrating factor
5     campbell unit range
10    campbell unit time constant
1000  No. of data /set (2 channels )
10    No. of turbulence data
1000  No. of background data/set
2.0   delay time
1     delay code
640   high voltage for PMT1
800   high voltage for PMT2
2     trig type 2. e 1. i
3     type of PRC, 1:9 2:10 3:15 4:20 5:other

```

C.1.4 Subroutines

C.1.4.1 highv.for

```

C *****
C
C           subroutine highv(ihvs,ihva)
C
C   Input & Calculation Of High Voltage Used For PMT #1.
C   ihvs = the default high voltage setting
C   ihva = the actual high voltage (calculated)
C   compile with "fl /c /Fohi highv.for"
C *****-----*****

idhvs = ihvs
240  print *
print *, 'The High Voltage to the No1. PMT may be ', 'set from -500V to -1110V.'
1120 format (1x,a,i5,a\

```

```

1125     print 1120, 'Enter the voltage setting. (', -idhvs, ' V) -->'
        format(i5)
        read(*, 1125, err=240) ihvs
        if (ihvs .eq. 0) then
            ihvs = idhvs
        else
            ihvs = abs(ihvs)
            idhvs = ihvs
        endif
C       For our power supply the measured V differs from the V setting.
        ihva = nint(1.0244 * ihvs - 0.75) ! calc actual H.V.
1130     format (1x, a, i5, a, i5, a)
        print 1130, 'High Voltage:  setting =', -ihvs, ' V      actual value =', -ihva, ' V'

900     return
999     end

```

C.1.4.2 adin.for

```

C       The following programe named as "adin.for"
C       It is compiled by "fl /c /Foad adin.for"
C
*****
*           phys subroutine
*****
*
*       converts iad from locfar call to physical address
*       ipad16 (lower 16 bits) and ipage (upper 4 bits)
*
        subroutine phys(iad, ipage, ipad16)
*
            integer*4 iad, ipage, ipad16
            integer*4 iphi, iplo
            integer*4 ihi, ilo
            integer*4 ihi1, ilo1, ihi2, ilo2
*
            ilo = iand(iad, #ffff)
            shift upper 16 bits down to lower 16 bits
            ihi = ishft(iad, -16)
            ihi = iand(ihi, #ffff)
*
            ihi1 = iand(ihi, #f)
            ihi2 = ishft(ihi, -4)
            ihi2 = iand(ihi2, #fff)
*
            ilo1 = iand(ilo, #ff)
            ilo2 = ishft(ilo, -8)
            ilo2 = iand(ilo2, #ff)
*
            iplo = ilo1 + ishft(ihi1, 4)
*
            iphi = ihi2 + ilo2
            check for carry
            if (iplo .gt. #ff) iphi = iphi + 1
*
            mask any carry
            iplo = iand(iplo, #ff)
*
*       example of the variables used to hold the 20 bit physical address
*       12345 (hex):
*
            hex address:   123 45
*                          iphi iplo
*
*                          1 2345
*                          ipage ipad16
*
            ipage = ishft(iphi, -8)
            ipage = iand(ipage, #f)
*
            ipad16 = ishft(iphi, 8)

```

```

        ipad16 = land(ipad16, #ff00)
        ipad16 = ipad16 + iplo

        return
    end

C*****
C          adint subroutine
C*****

C          initialize a/d board

        subroutine adinit(istat)

            implicit integer(A-Z)
            integer*2 ic(16), mode, flag

C          Initialize Das-16G using Mode 0...
            mode=0
            ic(1)=768! board address
            ic(2)=2                                ! interrupt level (as set on card)
            ic(3)=1                                ! DMA level (as set on card)
            flag=0                                  ! error flag

            call fdasg(mode, ic(1), Flag)

            if (flag .NE. 0) then
                print *, 'Mode = ', mode, '      Error # ', flag
            endif

            istat = flag

            return
        end

*****
*          caddr subroutine
*****
*          In order for the DMA controller to store 32k readings,
*          the data array must start at the beginning of a
*          physical memory data page.
*          This routine calculates which element of the array
*          ibig is stored at the beginning of the page.
*          That element is returned in the value "index".
*
*          It also returns the segment value to be passed to the
*          a/d driver. This is the equivalent segment value for
*          the starting element address. Since this address is
*          at the beginning of a physical page, its offset is zero.

        subroutine caddr(jjdata, index, iseg)

            integer*4 iad
            integer*4 ioffset, index
            integer*4 iseg
            integer*2 jjdata [huge]
*          dummy array, but needs declaration anyway
            dimension jjdata(1)

            iad = locfar(jjdata(1))
            call phys(iad, ipage, ipad16)
            print *, 'locfar      page 16 bits'
            write(*, '(1x,z8,6x,z1,1x,z4,a)')
*          1 iad, ipage, ipad16

            ioffset = -ipad16
            ioffset = land(ioffset, #ffff)
            index = (ioffset/2) + 1
            write(*, '(1x,z8,2x,z8,a)')
*          1 ipad16, ioffset, ' ipad16, offset'
            print *, index, ' index for array held at start of page'

            iad = locfar(jjdata(index))
            call phys(iad, ipage, ipad16)
            print *, 'locfar      page 16 bits'
            write(*, '(1x,z8,6x,z1,1x,z4,a)')

```

```

*      1 iad, ipage, ipad16

*      Knowing the desired physical address for the start of
*      the offset array, we need to determine the equivalent
*      segment and offset values of the address.
*      These values are passed to the a/d driver which
*      recalculates the physical address and loads it into
*      the dma register and dma controller.

*      This is an easy calculation since we are at the beginning
*      of a page, the offset is zero and the lower 12 bits of
*      the segment are zero. The upper 4 bits of the segment are
*      just the page value.

*      shift page up 12 bits

      iseg = ishft(ipage, 12)
      iseg = iand(iseg, #f000)

c      write(*, '(1x,a,z4)') 'Using segment ', iseg

      return

      end

```

C.1.4.3 seedat.for

```

C      compile with "fl /c /Fose seedat.for"
*****
*      seedat subroutine
*****

      subroutine seedat(iraw, inum, idata)

      implicit integer(A-Z)
      integer*4 inum
      integer*2 iraw[huge]
*      dummy arrays, but they need declaration anyway
      dimension iraw(inum)
      integer*2 idata(2048)

100     print *, 'Enter CR for idata '
        print *, ' or 1 for raw'
        print *, ' or -1 to quit'
        read(*,900,err=100) jcmd
900     format(i5)
        if(jcmd .eq. 0) goto 200
        if(jcmd .eq. 1) goto 300
        if(jcmd .lt. 0) goto 990

200     jstart = 1
210     print *
        print *, inum, ' conversions'
        print *, 'j, idata(j), idata(j), idiff'

        do 250, j=jstart,jstart+19
            if(j.gt.32000) goto 100
            idiff= (idata(j))-(idata(j-1))
            if (j .eq. 1) idiff = 0
            write(*, '(1a, i5, 1x, z4, 5x, i5, 2x, i6)') ' ', j, idata(j), idata(j), idiff
250     continue

        jstart =jstart+20
260     print *, 'Enter CR for more, or new index value, or -1 to quit'
        read(*,960,err=260) jcmd
960     format(i5)
        if(jcmd .eq. 0) goto 210
        if(jcmd .lt. 0) goto 990

```

```

*      otherwise, set new index to display
      jstart = jcmd
      goto 210

300    jstart = 1
310    print *
      print *, inum, ' conversions'

      print *, ' j      iraw(j)      idiff'

      do 350, j=jstart,jstart+19
         if(j.gt.32000)goto 100
         idiff= (iraw(j))-(iraw(j-1))
         if (j .eq. 1) idiff = 0
         write(*,'(a1 ,i5, 5x, z4, 2x, i6)') ' ', j, iraw(j), idiff
350    continue

      jstart =jstart+20
360    print *, 'Enter CR for more, or new index value'
      print *, ' or -1 to quit'
      read(*,960,err=260) jcmd
      if(jcmd .eq. 0)goto 310
      if(jcmd .lt. 0)goto 990
*      otherwise, set new index to display
      jstart = jcmd
      goto 310

990    return
      end

```

C.1.4.4 set.for

```

      compile with `fl /c set.for`
*****
*      trigset subroutine
*****

*      set external trigger source

      subroutine trigset(period, item)

      real*4 period
      integer item, i

5      write(*,'(1x,a)') "Please Choose the External Trigger Source"
      write(*,*) "-----"
10     format( 5(1x, a/), a, i2, a\ )
      write(*,10) " 1. 2^9 - 1 PRC", " 2. 2^10 - 1 PRC",
+      " 3. 2^15 - 1 PRC", " 4. 2^20 - 1 PRC", " 5. other",
+      " Enter your choice (*, item, *) ---> "
20     read(*,'(i2)',err=20) i
      if (i. eq. 0) goto 30
      if ((i.gt.5) .or. (i.lt.0)) goto 5

      item = i

30     if(item .eq. 1) period = 511.0e-6
      if(item .eq. 2) period = 1.023e-3
      if(item .eq. 3) period = 32.767e-3
      if(item .eq. 4) period = 1.048575
      if(item. eq. 5) then
         write(*,*) "Enter the trigger source period (in sec.) --> "
         read(*,*) period
      endif

980    return
      end

*****
*      periset subroutine

```

```

*****
*      set pacer clock
      subroutine periset(period, istat)
      implicit integer(A-Z)
      integer*2 ic(16), mode, flag, upper, lower
      real freq, period
C      Clock source is 10 MHz, so 10*1000 divisor yields
C      1 kHz sampling rate.
C      print *, 'Enter sampling period in microsec (2 to 32000) : '
C      print *, '10 for 100 kHz, 1000 for 1 kHz'
      print *
100  write(*, '(1x,2a,\)') *Enter sampling freq. ( 30Hz ", "to 100kHz ) in KHz --> *
      read( *, *, err=100) freq
      if ( freq .eq. 0) then
        print *, ' Frequency can not be zero, try again '
        goto 100
      endif
C      freq = 1e7/(upper*lower)
      lower = 10
      upper = int(1.0e3/freq)
      period = 1.0*(upper*lower)/1.0e7
C      write(*, *) *upper=", upper
C      set pacer clock
      flag=0
      ic(1)=lower
      ic(2)=upper
      mode = 17
      call fdasg(mode, ic(1), flag)
      if (flag .NE. 0) then
        print *, 'Mode = 17 Error # ', flag
      endif
C      print *, 'divisor: ', upper, ' sampling freq: ', freq
      istat = flag
      return
      end
C*****
C      chanset subroutine
C*****
C      set the channel scan upper and lower limits
      subroutine chanset(ichlo, ichhi, istat)
      implicit integer(A-Z)
      integer*2 ic(16), mode, flag
      integer ichhi, ichlo
C      set upper and lower scan limits
C      select channel from ichhi to ichlo
      mode=1
      ic(1)=ichlo
      ic(2)=ichhi
      flag=0
      call fdasg(mode, ic(1), Flag)
      if (flag .NE. 0) then
        print *, 'Mode = ', mode, ' Error # ', flag
      endif
      istat = flag

```

```

return
end

```

C.1.4.5 plot.for

```

      compile with "fl /c /Fopl plot.for"
*****
*           setgr subroutine
*****
      subroutine setgr
*           setup for graphics

*           font directory for graphs
      CHARACTER * 30 defaultdirect
      PARAMETER (defaultdirect = 'C:\usr\fortran\lib\*.fon')

*           -3 is autodetect graphics board (or use 16 for EGA)
*           defaultdirect is font file directory
*           0 is plotmode (crt only)

      CALL InitSEGraphics(16, defaultdirect, 0)

      return
      end

*****
*           setplot subroutine
*****
      subroutine setplot(xttics, xmax, ymin, ymax)

      real xttics, xmax, ymin, ymax

      call setpercentwindow(0.0, 0.0, 1.0, 1.0, 1)
      call setwin2plotratio(1, 0.1, 0.05, 0.0, 0.05 )

      CALL SetCurrentWindow(1)
      CALL ClearWindow
!      CALL BorderCurrentWindow(6)

      CALL SetAxesType(0, 0) ! linear-linear scale
      CALL setxyintercepts(0.0, 0.0)
      CALL SelectColor(7) ! 7 = green
*      xmin,  ymin,  xmax,  ymax
      CALL ScalePlotArea( 0.0, ymin, xmax, ymax)

      CALL SetXYIntercepts(0.0,0.0)
      CALL DrawYAxis(1.0, 0) ! tic spacing

      CALL LabelYAxis(1, 0) ! tics per label
      CALL DrawXAxis(xttics, 0)

      CALL DrawGridX(1)
      CALL DrawGridY(1)

      return
      end

*****
*           plot subroutine
*****
c           Graph is plotted using setools subroutines.

      subroutine plot(jdata, period)

      REAL xdata(0:996), ydata(0:996)
      INTEGER i
      integer*2 jdata(0:2048)
      real period, tpd, xtics
      character*25 ctitle

```

```

character*7 cfactor

* transfer jdata array to real array for plotting
* also create x data array
* convert a/d counts to volts 5V/2047 counts = 2.44 mV / count

DO i = 0, 100
c ydata(i) = jdata(i) * 0.0024426-5.0! when choose -5 ~ 5 mode
  ydata(i) = jdata(i) * 0.0024426! when choose 0 ~ 10 mode
  xdata(i) = i
END DO

xtics=10.0
call setplot(xtics, 100.0, 0.0, 10.0)

c calculate time/division

tpd = period*xtics
if (tpd .ge. 1.0) then
  write(cfactor, '(f6.1)')tpd
  ctitle = cfactor // 'sec/div'

else if (tpd .ge. 1e-3) then
  tpd = tpd*1000
  write(cfactor, '(f6.1)')tpd
  ctitle = cfactor // 'ms/div'

else if (tpd .lt. 1e-3) then
  tpd = tpd*1e6
  write(cfactor, '(f7.1)')tpd
  ctitle = cfactor // 'microsec/div'
endif

call titlexaxis(ctitle, 0)

ipoints = 100 ! points to plot
CALL LinePlotData(xdata, ydata, ipoints, 10, 0)

return

end

```

C.1.4.6 takead.for

```

compile with "fl /c /Fota takead.for"
C *****
C
C          subroutine dstats(ipts, iraw1, iseg, mean, vary, ovflo, itrigr, lstat)
C
C          Use the ADC to measure inum data values from channel # ichan
C          Return mean and variance in the real variables: mean, vary
C *****-----*****
C
C          integer*4 ipts, ovflo, icnt, lsum(3), lstat, iseg
C          integer*2 i, j, k, itemp(3), itrigr
C          real*4 mean(3), vary(3)
C          real*8 ssum(3)
C          integer*2 iraw1(5096)
C          dimension iraw1(inum)
C          integer*2 idata(5096)
C
C          icnt = ipts
C          ovflo = 0
C
C          do 100 i=1, 3
C            lsum(i) = 0
C            ssum(i) = 0.0
C            itemp(i) = 0
100          continue

```

```

call takead(iraw1, icnt, idata, iseg, 0, itrig, istat)! take data
if( istat .ne. 0) then
  print *, 'data taking error'
  goto 900
endif

do 400 i = 1, icnt/2
  j=2*(i-1)+1
  k=2*i
  itemp(1)=idata(j)
  itemp(2)=idata(k)
C      --Check for gain (High Voltage) set too high
      if (itemp(1).ge.4095) ovflo = ovflo + 1
      if (itemp(2).ge.4095) ovflo = ovflo + 1
      lsum(1) = lsum(1) + itemp(1)
      lsum(2) = lsum(2) + itemp(2)
      ssum(1) = ssum(1) + float(itemp(1))** 2
      ssum(2) = ssum(2) + float(itemp(2))** 2
400  continue

do 500 i=1, 2
  mean(i) = float(lsum(i))*2.0/ipts
C      sample variance
      vary(i) = (ssum(i) - mean(i) * lsum(i))/ (ipts -1)
500  continue
c      mean = mean + 2048

900  return
999  end

C*****
C      takead subroutine
C*****
C      take a/d data

subroutine takead(iraw, inum, idata, iseg,ipri,itrig,istat)

C      The array iraw holds the raw a/d readings.
C      Note that iraw is a dummy array that overlays the array
C      ibig.
C      iraw(1) is the same as ibig(index). Index is calculated so that
C      iraw starts at the beginning of a physical memory page.

implicit integer(A-Z)
integer ipri
integer*2 ic(16), mode, flag
integer*2 ib(16), model, flag1
integer*4 iseg, istat, inum
c      integer*2 iraw[huge]
c      dummy arrays, but they need declaration anyway
c      dimension iraw(inum)
integer*2 iraw(5000)
integer*2 itrig, idata(5000)

C      initialize raw data set to be zero
do 100, j=1,inum
  iraw(j)= 0
  idata(j)=0
100  continue

irecyc = 0 ! non-recycle

ic(1) = inum
ic(2) = iseg ! segment to stuff data
if (itrig.eq.1) ic(3) = 1 ! use pacer clock for trigger
if (itrig.eq.2) ic(3) = 0 ! use external clock for trigger
ic(4) = irecyc
mode=6
flag=0

call fdasg(mode, ic(1), Flag)
if (flag .NE. 0) then
  print *, 'Mode = ',mode, ' Error # ',flag
  goto 990
endif

```

```

C      convert a/d word to signed integer
C      first shift out channel nibble

*      get dma status, out if the conversions done

130   continue
      model = 8
      call fdasg(model, ib(1), flag1)
      if (flag1 .NE. 0) then
        print *, 'Mode = ', mode, '      Error # ', flag
        goto 990
      endif

c      print *, ib(1), ' = operation      1 = DMA, 2 = Interrupt'
c      print *, ib(2), ' = status        0 = done, 1 = active '
c      print *, ib(3), ' conversions so far'

      if( ib(2). eq. 1) goto 130

      do 150 i=1, inum

        idata(i)=ishft(iraw(i), -4)

        if (ipri. eq. 0) then
          goto 150
        endif
c      write(20, *) "iraw(i)=", i, iraw(i)

c      write(20, 910) i, idata(i)-2048!when chose -5 - 5 mode
c910   format(1x,i5,2x,i5)

150   continue

990   istat = flag

      return
      end

```

C.1.4.7 fft.for

```

      compile with "fl /c fft.for"
*****
*      datfft subroutine
*****

C      data is processed by FFT

      subroutine datfft( sdata, period)

      REAL xdata(0:1024), ydata(0:1024)
      REAL zdata(0:1024)
      INTEGER i, i1, ic, nd, ipoints
      integer*2 sdata(0: 2048)
      real period, xtics, freq
      real tpd
      character*25 ctitle
      character*7 cfactor

      nd=1024
      ic=0

      do 150 i=1, 1024
        xdata(i-1) = sdata(i) * 0.0024426-5.0
        ydata(i-1) = 0.0
c      write(*,*) i, xdata(i-1), ydata(i-1)
150   continue

      xtics=100.0

```

```

call setplot(xtics, 1024.0, 0.0, 10.0)

C   FFT transformation
call FFTCalc(xdata, ydata, nd)

do 350 i=1, 1024
  i1=i-1
  zdata(i1)=sqrt(xdata(i1)*xdata(i1)+ydata(i1)*ydata(i1))/300.0

c   find the peak value and freq. of FFT
c   ic is peak number counter
  if(zdata(i1).gt.3) then
    freq=i1/(nd*period)
    if ( freq .gt. 0.5/period) then
      write(*,300) "peak",ic," frequency=", freq-1.0/period," Hz"
    else
      write(*,300) "peak",ic," frequency=", freq, " Hz"
    endif
    write(*,'(1x,a,i2,a,f7.3)') "peak",ic," value=", zdata(i1)
    ic=ic+1
  endif
300 format(1x, a,i2,a,f13.3, a)
c   write(*,*) i1, xdata(i1), ydata(i1), zdata(i1)
350 continue

do 450 i=1, 1024
  i1=i-1
  xdata(i1)=i1
450 continue

C   calculate frequency/division

tpd = 1.0/(1.024*period*xtics)
if (tpd .ge. 1.0e3) then
  tpd = tpd/1.0e3
  write(cfactor, '(f6.1)') tpd
  ctitle = cfactor // 'KHz/div'

else
  write(cfactor, '(f6.1)') tpd
  ctitle = cfactor // 'Hz/div'
endif

call titlexaxis(ctitle, 0)

ipoints = 1024          ! points to plot
CALL LinePlotData(xdata, zdata, ipoints, 10, 0)

read(*,*)

return
end

```

C.1.5 The PRC delay time versus digital code number for 511-PRC generator

<u>Delay Time (μs)</u>	<u>Digital code number</u>
0.31	7
0.51	0
0.71	1
0.91	2
1.11	3
1.31	4
1.51	5
1.71	6
1.91	10

2.11	11
2.31	12
2.5	13
2.71	14
2.91	18
3.11	19
3.31	20
3.51	21
3.71	22
3.91	26
4.11	27
4.31	28
4.51	29
4.71	30
4.91	34
5.11	35
5.31	36
5.51	37
5.71	38
5.91	42
6.11	43
6.31	44
6.51	45
6.71	46
6.91	50
7.11	51
7.31	52
7.51	53
7.71	54
7.91	58
8.11	59

C.1.6 Program for the data processing (p4.c)

```

/*****
 *
 *          p4.c --- Data Processing Program"records4.for"
 *          by Chunyan Zhou
 *
 *****/

#include <stdio.h>
#include <math.h>
#include <ctype.h>
#include <string.h>
main(int argc, char *argv[])
(
    /* main */
    int          file_no, para_no[4];
    int          i, i1, ichan, iext, auton;
    char         file[20], dfile[20];
    char         fout[20], y_n;
    double       ical;
    double       para[20], ica;
    double       data1[100000], data2[100000];
    double       dwind[100000], dturb[100000];
    double       mwind[200], cturb[200], mdata1[200],
    double       mdata2[200], ndata[200], bg1[200],
    double       bg2[200];
    char         filename[60], systemcom[600], _str[200];
    FILE         *fp2, *file_out1, *file_out2, *file_out3;
    printf("argc %d \n", argc);
    if (argc != 5) {
        printf("\n*****\n");
        printf("\nThis program processes data stored on Files name as 'dxxx.x'\n xxx in case name is
the date the data being token\n x in ext. name is the digit number standing for the \n sequence
of the file.\n\n");
        printf("This option produces files containing the mean & variance along \nwith the output of
the Campbell Unit Anemometer.\n\n");
        printf(" Comment: use symbolic link ln -s /eeap/ogi/student/chunyan/.par_files/prcss.xmgr\n");
    }

```

```

printf("*****\n\n");
printf("\n\nCommand format: %s 1 d830 2 y      Today is ", argv[0]);
sprintf(systemcom, "date \'+Date: %s%s%s%s\'", "%", "m", "%", "d");
system(systemcom);
exit(0);
}
/* get the number of files need to be processing */
/* printf("Please enter the number of files you want to
 * process -- > "); */
/* scanf(" %d", &file_no); */
file_no = atoi(argv[1]);
if (file_no == 0) {
    printf("No file needs to be processed, quit!\n");
    return;
}
printf("%d is the No. of file\n", file_no);

/* two channel data */
ichan = 2;

/* get the number of channels */
/* do ( printf("Please enter the number of channels ( 1
 * or 2) -- > "); fflush(stdin); scanf(" %d", &ichan); )
 * while ((ichan != 1) && (ichan != 2)); */

/* get the name of the data file */
/* printf("Please enter the data file case name (without
 * ext. name) --> "); */
sprintf(file, "%s", argv[2]);
/* scanf(" %s", &file); */

/* printf("Please enter the first data file ext. name --
 * > "); */
iext = atoi(argv[3]);
/* scanf(" %d", &iext); */

/* Name the output file for results */
do {
    /* printf("The results will save to the files, do you
     * want these files to be named \nautomatically?
     * [y/n] -- >"); */
    sprintf(_str, "%s", argv[4]);
    /* scanf(" %c", &y_n); */
    y_n = _str[0];
    y_n = toupper(y_n);
    fflush(stdin);
} while ((y_n != 'Y') && (y_n != 'N'));

if (y_n == 'Y') {
    auton = 1;
} else {
    auton = 0;
}

printf(" %d %s %d %c \n", file_no, file, iext, y_n);

for (i1 = 0; i1 < file_no; i1++) {
    sprintf(dfile, "%s.%d", file,
        i1 + iext);
    printf("\nThe data file is %s\n", dfile);
    file_out1 = fopen("chan1.xmgr", "w");
    file_out2 = fopen("chan2.xmgr", "w");
    file_out3 = fopen("turb.xmgr", "w");

    /* reading the data file */
    read_file(i1, ichan, iext, file, dfile, para, data1, data2, dwind, dturb, para_no, bg1, bg2);

    printf("\nFinishing reading the data file!!!\n\n");

    /* para_no[0] is the No. of parameter, para[1] is the
     * No. of data per dataset, para_no[1] is the number
     * of dataset */
    for (i = 0; i < para_no[0]; i++) {
        printf("the para is %lf\n",
            para[i]);
    }
}

```

```

)

/* for (i = 0; i < 2*para[1] * para_no[1]; i++) { if
 * (ichan == 2) { printf(" %lf %lf\n", data1[i],
 * data2[i]); } else { printf(" %lf\n", data1[i]); }
 * } */
/* open the output file */

outfile(file, fout, i1, iext, auton);
fp2 = fopen(fout, "w");

/* processing the data */
printf("\nData Processing Is In Progress! \n");

/* find the mean value of the wind speed */
/* ical = para[0] / 409.5; wind_mv(0, para[2],
 * para_no[1], ical, dwind, mwind); */

/* find the covariance of turbulence */
/* ical is 1/(409.5**2) */
ical = 5.96e-06;
wind_mv(1, para[2], para_no[1], ical, dturb, cturb);

/* Do Statistics on intensity data set */
data_mv(ichan, para[1], para_no[1], data1, data2, mdata1, mdata2);

for (i = 0; i < para_no[1]; i++) {

    /* 1/409.5 is d=>v converting to volts para[1] is
     * calibrating effect */
    /* ndata[i] = (mdata1[i] - bg1[i]) / 409.5 /
     * (para[3] * (mdata2[i] - bg2[i]) / 409.5); */

    /* write to the file */
    fprintf(file_out1, "%lf %lf\n", bg1[i]/409.5, (mdata1[i]-bg1[i])/409.5);
    fprintf(file_out2, "%lf %lf\n", bg2[i]/409.5, (mdata2[i]-bg2[i])/409.5);
    fprintf(file_out3, "%lf\n", log10(cturb[i]));
    ndata[i] = (mdata1[i] - bg1[i]) / para[3] / (mdata2[i] - bg2[i]);
    ndata[i] = log10(ndata[i]);
    fprintf(fp2, "%lf %lf \n", log10(cturb[i]), ndata[i]);
}

)

printf("\nEnd of the program !\n");
fclose(fp2);
fclose(file_out1);
fclose(file_out2);
fclose(file_out3);

printf("Generating file ==> %s \n", fout);
printf("          chan1.xmgr\n");
printf("          chan2.xmgr\n");
printf("          turb.xmgr\n");
/* sprintf(systemcom, "xmgr prcss.xmgr %s& ", fout);
 * system(systemcom); */
return;
} /* main */

read_file(int i1, int ichan, int iext, char file[20], char dfile[20], double para[20], double
data1[100000], double data2[100000], double dwind[100000], double dturb[100000], int para_no[4],
double bg1[200], double bg2[200])
{
    FILE          *fp1;
    char          ddfile[20], _string[10];
    char          q_string[2] = "q";
    int           i, j, k, in_char;
    double        a1, a2;

    /* open the file, if no such file, given the msg. */

    while ((fp1 = fopen(dfile, "r")) == NULL) {
        printf("No such data file !!!\n");
        printf("\nPlease enter the data file case name again\n ");
        printf(" (or Press 'q' to quit ) --- > ");
        scanf(" %s", &ddfile);
    }

```

```

    if ((strcmp(ddfile, q_string) == 0) {
        exit();
    }
    sprintf(dfile, "%s.%d", ddfile, i1 + iext);
    strcpy(file, ddfile);
    printf("\nThe file name is %s\n", dfile);
}

/* display the first two line */
for (i = 0; i < 2; i++) {
    do {
        in_char = fgetc(fp1);
        putchar(in_char);
    }
    while (in_char != '\n');
}

/* read the data file until read the '*' */
while ((in_char = fgetc(fp1)) != '*') {
    ;
}

/* read the 'end of comments' line */
do {
    in_char = fgetc(fp1);
} while (in_char != '\n');

/* read until get all the parameters */
i = 0;
while ((in_char = fgetc(fp1)) != '@') {

    /* the parameters is inside a brace ( ) */
    while ((in_char = fgetc(fp1)) != '(') {
    }

    /* para[ ] is the parameter, 1st _string is ')', 2nd
     * is unit */
    fscanf(fp1, " %lf %s %s \n", &para[i], &_string, &_string);
    i++;
}
printf("\n%d parameters have been read !\n", i);
para_no[0] = i;

/* read the 'beginning the data file' line */
do {
    in_char = fgetc(fp1);
} while (in_char != '\n');

/*
    printf("%lf %lf %lf %lf \n ", para[0], para[1], para[2], para[3]);
*/

k = 0;
while ((in_char = fgetc(fp1)) != EOF) {
    ungetc(in_char, fp1);
    /* reading the first 2 background data */
    fscanf(fp1, " %lf\n %lf\n", &bg1[k], &bg2[k]);

/*
    printf("bg1[%d] = %lf, bg2[%d] = %lf \n", k, bg1[k], k, bg2[k]);
*/

    /* read the first para[2] wind data and turb data */
    for (i = 0; i < para[2]; i++) {
        j = 2 * k * para[2] + i;
        fscanf(fp1, " %lf\n %lf\n %lf\n %lf\n", &a1, &a2, &dwind[j], &dturb[j]);
    }

    /* reading the para[1] data */
    for (i = 0; i < para[1]; i++) {
        /* read the two chanel data into two data array */
        j = k * para[1] + i;
        if (iCHAN == 2) {
            fscanf(fp1, " %lf\n %lf\n", &data1[j], &data2[j]);

/*
            printf("%d %lf %lf\n", j, data1[j], data2[j]);
*/
        }
    }
}

```

```

    } else {
        /* read the one chanel data into one data array */
        fscanf(fp1, "%lf\n", &data1[j]);
        data2[j] = 0;
    }
}

/* reading the last para[2] wind and turb data */
for (i = 0; i < para[2]; i++) {
    j = (2 * k + 1) * para[2] + i;
    fscanf(fp1, "%lf\n %lf\n %lf\n %lf\n", &a1, &a2, &dwind[j], &dturb[j]);
/*
    printf("%d %lf %lf\n", j, dwind[j], dturb[j]);
*/
}

k++;
)

para_no[1] = k;
printf("%d data sets have been read\n", k);

fclose(fp1);
return;
)

outfile(char file[20], char fout[20], int i1, int iext, int auton)
{
    char          y_n;
    FILE          *fp2;

    /* the results keep in the file automatically */
    if (auton == 1) {
        sprintf(fout, "%s%d.%s", file, i1 + iext, "dat");
    } else {
        /* name the file to keep the processing results */
        do {
            printf("Please enter output file name ( <20 char.) -- > ");
            scanf("%s", fout);
            if ((fp2 = fopen(fout, "r")) != NULL) {
                do {
                    printf("The file exist !!! Do you want to overwrite it ? [y/n] -- > ");
                    scanf("%c", &y_n);
                    y_n = toupper(y_n);
                    fflush(stdin);
                } while ((y_n != 'Y') && (y_n != 'N'));
            } else {
                y_n = 'Y';
            }
        } while (y_n == 'N');
        fclose(fp2);
    }

    printf("\nThe output file will be named as %s\n", fout);

    return;
}

wind_mv(int k, double npara, int inum, double ical, double data[20], double mdata[20])
{
    int          i, j, i1, i2;
    double       a;

    /* npara is the no of turb. data per dataset, inum is
     * the total data set , ical is the calibrating factor. */
    for (i = 0; i < inum; i++) {
        mdata[i] = 0.0;
        i1 = 2 * i * (int) npara;
        i2 = 2 * (i + 1) * (int) npara;
        for (j = i1; j < i2; j++) {
            mdata[i] += data[j];
        }
        if (k == 0) {

```

```

        /* remove the offset +1 for the wind speed data */
        a = (mdata[i] - 409.5 * npara * 2.0) * ical / (2.0 * npara);
        mdata[i] = a;
    ) else (
        /* gain 10 , dc 110.0 */
        a = pow((mdata[i] - 110.0 * npara * 2.0), 2.0) * ical / (400.0 * npara * npara);
        mdata[i] = a;
    )
}
return;
}

data_mv(int ichan, double npara, int inum, double data1[20], double data2[20], double mdata1[20],
double mdata2[20])
{
    int          i, j, i1, i2;
    double       ical;

    /* npara is the no of data per dataset, inum is the
    * total data set , ical is the calibrating factor. ical
    * = 1.0/409.6; */

    ical = 1.0;

    for (i = 0; i < inum; i++) (
        mdata1[i] = 0.0;
        if (ichan == 2) {
            mdata2[i] = 0.0;
        }
        i1 = i * npara;
        i2 = (i + 1) * npara;
        for (j = i1; j < i2; j++) (
            mdata1[i] += data1[j];
            if (ichan == 2) {
                mdata2[i] += data2[j];
            }
        )
        mdata1[i] = ical * mdata1[i] / npara;
        if (ichan == 2) {
            mdata2[i] = ical * mdata2[i] / npara;
        }
    )
    return;
}
/* get the data processing parameters para[0] ___ Range
* set for Campbell Unit para[1] ___ The number of each
* channel data in one data set para[2] ___ number of
* turbulence data per set para[3] ___ The calibrating
* coefficient of 2 channels If/IO para_no[0] ___ The No. of
* parameters para_no[1] ___ The No. of Data set in each
* file */

```

C.1.7 Program for numerical simulation (intensity.f)

```

* *****
* * f5.f -- 3-D integration with d01fbf1.f *
* *****

* .. Parameters ..
* integer ndim, lwamax
* parameter (ndim=3, lwamax=1000)

* .. Local Scalars ..
* real*8 a, b
* integer i, ifail, itype, iw, lwa

* .. Local Arrays ..
* real*8 abscis(lwamax), weight(lwamax)
* integer nptvec(ndim)

```

```

* .. External Functions ..
  double precision d01fbf1, fun1, fun2, fun3, fun4
  external d01fbf1, fun1, fun2, fun3, fun4
* .. External Subroutines ..
  external d01baz, d01bbf ! Gauss-Legendre
  real*8 sigma2, s, inte(70), inte1, inte2

* .. Data statements ..
  data nptvec/32,32,32/

c   open file
  open(10, file='f5.rst', status='unknown')

* .. Executable Statements ..
  lwa=0
  do 20 i=1, ndim
  lwa = lwa + nptvec(i)
20  continue

    itype=1
    iw=1
    a = 0.0d0
    b = 0.018d0
    ifail = 0
    ! r

*   call d01bbf(d01baz,a,b,itype,nptvec(1),weight(iw),abscis(iw),
+             ifail)
*
  iw = iw + nptvec(1)

  a = 0.0d0
  b = 0.5d-3
  ! u

*   call d01bbf(d01baz,a,b,itype,nptvec(2),weight(iw),abscis(iw),
+             ifail)
*
  iw = iw + nptvec(2)

*   a=689.5d-9
  b=690.5d-9
  ! lamd

*   call d01bbf(d01baz,a,b,itype,nptvec(3),weight(iw),abscis(iw),
+             ifail)
*
  iw = iw + nptvec(3)

  do 100 i=1,21
  s=-5.0d0+(i-1)*0.3d0
  sigma2=(10.0)**s
  inte1=0.0d0
  inte2=0.0d0

  ifail=0
  inte1 = d01fbf1(ndim,nptvec,lwa,weight,abscis,fun1,ifail,sigma2)

  ifail=0
  inte2 = d01fbf1(ndim,nptvec,lwa,weight,abscis,fun2,ifail,sigma2)

  inte(i)=inte2/inte1
  write(10,'(4f15.7)') s, log10(inte(i)), inte2, inte1
c   write(10,*) s, inte1, inte2
c   write(*,'(3d15.7)') s, inte1, inte2

100  call flush(10)
      continue

      close(10)

  stop
  end

c   double precision function fun1(ndim, sigma2, z)
  .. Scalar Arguments ..
  integer ndim, ifail
  real*8 z(ndim), sigma2, x, y, x1
  real*8 pi, k, lamd0, z1, F, q0, f1, p0, dlamd

```

```

real*8 Cn2, p1, d, delta, z10
C .. External Functions ..
real*8 s17aef
external s17aef

C parameters
pi=4.0d0*atan(1.0d0)
lamd0 = 690.0d-9
dlamd = 0.5d-9
C a0=7.0d-3 ! beam size
a0=15.0d-3 ! beam size
z10=2.4d2 ! path length
F=2.0d4 ! laser focal length
q0=1.016d-1 ! telescope radius
f1=0.9144 ! telescope focal length

k=2.0d0*pi/z(3)
z1=z10
d=f1*z1/(z1-f1) ! distance to the image plane

delta=1.0d0/a0/a0+(k*a0*(1-z1/F)/z1)**2+2.0d0/q0/q0+0.5d0*(k*q0*(1+z1/f1*(1-d/f1))/z1)**2

x1=delta*z(1)*z(1)/4.0d0

Cn2=1.24d-12*((500.0d0/z1)**(11.0d0/6.0d0))*sigma2
p1=0.545625d0*Cn2*z1*k*k
p0=(p1)**(-0.6)

C the value for bessell function
x=k*z(1)*z(2)/f1
y=s17aef(x, ifail)

C write(*,*) x, y, ifail
if(x1.gt.1.0d2) then
fun1=0.0
return
endif

C real function
fun1 = z(1)*z(2)*dexp(-2.0d0*(z(1)/p0)**(5.0/3.0))
+ *y*dexp(-x1)*(k**5)*1.0d-8
+ *exp(-((z(3)-lamd0)**2)/2.0d0/((dlamd)**2))
C write(*,*) *fun12= *, fun1

return
end

double precision function fun2(ndim, sigma2, z)
C .. Scalar Arguments ..
integer ndim, ifail
real*8 z(ndim), sigma2, x, y, x1
real*8 pi, k, lamd0, z1, F, q0, f1, p0
real*8 Cn2, p1, d, delta, z10
C .. External Functions ..
real*8 s17aef
external s17aef

C parameters
pi=4.0d0*atan(1.0d0)
lamd0 = 690.0d-9
dlamd = 0.5d-9
C a0=7.0d-3 ! beam size
a0=15.0d-3 ! beam size
u0=1.7d-4 ! filter radius
z10=2.4d2 ! path length
F=2.0d4 ! laser focal length
q0=1.016d-1 ! telescope radius
f1=0.9144 ! telescope focal length

k=2.0d0*pi/z(3)
z1=z10
d=f1*z1/(z1-f1) ! distance to the image plane

delta=1.0d0/a0/a0+(k*a0*(1-z1/F)/z1)**2+2.0d0/q0/q0+0.5d0*
+ (k*q0*(1+z1/f1*(1-d/f1))/z1)**2

```

```

x1=delta*z(1)*z(1)/4.0d0
Cn2=1.24d-12*((500.0d0/z1)**(11.0d0/6.0d0))
+ *sigma2
p1=0.545625d0*Cn2*z1*k*k
p0=(p1)**(-0.6)
C   the value for bessell function
x=k*z(1)*z(2)/f1
y=s17aef(x, ifail)
C   write(*,*) x, y, ifail
if(x1.gt.1.0d2) then
fun2=0.0
return
endif
c   real function
fun2 =z(1)*z(2)*dexp(-2.0d0*(z(1)/p0)**(5.0/3.0))*y*dexp(-x1)*(k**5)*1.0d-8
+ *exp(-(z(3)-lamd0)**2)/2.0d0/(dlamd**2))*(1-dexp(-z(2)*z(2)/u0/u0))**2)

return
end

```

Appendix D

D.1 Experimental procedure

I. Detection of target backscattering signal

1. Calibration system set-up

- a. Set the He-Ne laser close to the target
- b. Align the optical path between the He-Ne laser and the Campbell Unit.
- c. Adjust the Campbell Unit tilting angle to obtain the highest intensity reading from the meter.

2. Electronic system set-up

- a. Turn on the electronic system, which includes a Wavetek PRC generator, an analog data processor and two PMTs. Set both PMT powers around -500 volts.

In the analog data processor,

- b. Adjust the DC offset so that the outputs of the AD734 multipliers are zero.
- c. Adjust the DC offset of the integrators so that their outputs are several mV.

3. Optical system alignment

This can be done easily at night because the spot on the target is visible.

- a. Adjust the telescope direction so that the image of the target is at the center of the telescope image plane.
- b. Adjust the transmitter mirror, which is located at the center of the telescope, so that the laser beam hits the target.
- c. Set the PRC signal delay corresponding to the time that the laser beam transmitting to the target and reflecting back to the receiver. For instance, when the target distance is 800 meters, the corresponding PRC delay time is 5.6 μ s.

d. Adjust both receiving fibers to obtain the maximum output signals, which are monitored by the scope.

e. If the signals are weak, increase the gain of the multiplier, which ranges from 0.1 to 10. Another approach is to increase gain by raising the PMTs' voltage level.

f. Measure the background signal by blocking the outgoing laser signal. If the background signal is negative, increase the DC offset of the integrator

4. PRC delay time selection

Measure the intensity-range curve. Find out the exact delay time (T_d) for the maximum receiving intensity. Set the PRC delay time equals to T_d .

5. Two-channel calibration

Insert the receiving fiber (the one without optical filter) into the two PMTs respectively and record the corresponding receiving PMT signals. The calibrator factor of the two channel is the ratio of the two channel intensities multiplied by the reflecting-and-transmitting ratio of the beam splitter.

6. Data recording

a. Adjust one of the receiving fiber (the one with the optical filter) to obtain the minimum receiving intensity.

b. Adjust the other receiving fiber (without the optical filter) to obtain the maximum receiving intensity.

c. Execute the data recording program.

II. Measurements of aerosol backscattering signal

The optical system alignment and electronic system set-up have been described in the target backscattering measurement. After that

1. Move the whole telescope to transmit the laser beam into the atmosphere.

2. Measure the intensity-range curve and locate the maximum backscattering source. Set the delay time corresponding to this position. Then set the He-Ne laser of the calibration system near the maximum backscattering source.

3. Increase the system gain by increasing the PMT power.

Warning: the PMT anode current can not exceed the its limit. Otherwise, PMT damage may occur.

4. Execute the data recording program.

VITA

The author was born on the 10th of April, 1963, in Tianjin, P. R. China. In 1985, she finished her B. S. with honors from the Physics Department, Nankai University, P. R. China. In 1988, she completed her M. S. in Optics, at the Institute of Modern Optics, Nankai University, P. R. China. The author came to the United States in 1991 and began to pursue the Ph.D degree in electrical engineering at Oregon Graduate Institute of Science and Technology (OGI), where her research focused on measuring the atmospheric turbulence strength by laser remote sensing. In 1994, she got the Master of Science degree in Electrical Engineering at OGI. By the end of 1995, she completed all requirements for the Ph.D degree in Electrical Engineering. After her graduation, the author accepted a position with Intel Corporation at Hillsboro, Oregon. She is currently pursuing a career in the field of VLSI design.